J. Micropalaeontology, 40, 101–144, 2021
https://doi.org/10.5194/jm-40-101-2021

Journal of Micropalaeontology
Open Access

Revised taxonomy and early evolution of fasciculiths at the Danian–Selandian transition

Francesco Miniati[1], **Carlotta Cappelli**[2], **and Simonetta Monechi**[3]

[1]Dipartimento di Scienze della Terra "Ardito Desio", Università di Milano, Via Mangiagalli 34, 20133 Milan, Italy
[2]Dipartimento di Geoscienze, Università di Padova, Via Giovanni Gradenigo, 6, 35131 Padova, Italy
[3]Dipartimento di Scienze della Terra, Università di Firenze, Via La Pira 4, 50121 Florence, Italy

Correspondence: Francesco Miniati (francesco.miniati@unimi.it)

Received: 25 February 2021 – Revised: 16 July 2021 – Accepted: 24 July 2021 – Published: 13 September 2021

Abstract. We present a taxonomic revision of the family Fasciculithaceae focused on forms that characterize the early evolution of this family group, which are currently included within the genera *Gomphiolithus, Diantholitha, Lithoptychius* and *Fasciculithus*. The investigation approach is based on a combined light microscope (LM) and scanning electron microscope (SEM) analysis of specimens from well-preserved ODP–DSDP site material (ODP Site 1209; Site 1262; ODP Site 1267; DSDP Site 356; DSDP Site 119) and outcrops (Bottaccione and Contessa, Italy; Qreiya, Egypt) across the Danian–Selandian transition. The direct LM–SEM comparison of the same individual specimen provides clarification of several taxa that were previously described only with the LM. One new genus (*Tectulithus*), five new combinations (*Tectulithus janii, Tectulithus merloti*, *Tectulithus pileatus*, *Tectulithus stegastos* and *Tectulithus stonehengei*) and six new species are defined (*Diantholitha pilula*, *Diantholitha toquea*, *Lithoptychius galeottii, Lithoptychius maioranoae, Tectulithus pagodiformis* and *Fasciculithus realeae*). The main characteristics useful to identify fasciculiths with the LM are provided, together with a 3D–2D drawing showing the main structural features. The accurate taxonomic characterization grants the development of an evolutionary lineage that documents a great fasciculith diversification during the late Danian and early Selandian. Four different well-constrained events have been documented: the lowest occurrence (LO) of *Gomphiolithus*, the paracme of Fasciculithaceae at the top of Chron C27r (PTC27r), the radiation of *Diantholitha* (LO *Diantholitha*), the paracme of Fasciculithaceae at the base of Chron C26r (PBC26r), the radiation of *Lithoptychius* (LO *Lithoptychius*) and the radiation of *Tectulithus* (lowest common occurrence of *Tectulithus*) that shows the biostratigraphic relevance of this group across the Danian–Selandian transition.

1 Introduction

During the early Paleocene, radiation of planktonic communities took place and many new genera of calcareous nannofossils evolved, including the appearance of a new morphostructural group in the order Discoasterales (Hay, 1977) consisting of biantholiths, fasciculiths and sphenoliths. Studies to choose the Global Stratotype Section and Point (GSSP) for the base of the Selandian Stage (61.6 Myr) focused on a rapid diversification of fasciculiths, with the occurrence of a wide range of morphotypes in the late Danian–early Selandian (Bernaola et al., 2009; Schmitz et al., 2011). A renewed interest in biostratigraphy, taxonomy and evolution of fasciculiths led to the taxonomic revision of this group (Aubry et al., 2011, 2012; Monechi et al., 2012, 2013; Aubry, 2014). In addition to the emendation of the genus *Fasciculithus*, three new genera were introduced by Aubry et al. (2011): *Gomphiolithus, Diantholitha* and *Lithoptychius*. These new genera include new species as well as numerous forms that were previously classified as *Fasciculithus*, distinguished by the presence or absence of structural units such as the column, the collaret, the calyptra and the central body. The origin of these nannoliths remains uncertain and the postulated hypotheses suggested a phylogenetic relationship with either *Markalius inversus* (Perch-Nielsen, 1977,

1981) or *Biantholithus* (Prins, 1971; Aubry, 1998, Aubry et al., 2012). Fasciculiths characterized early Paleocene calcareous nannofossil assemblages up to the earliest Eocene, when the entire group went into decline and became extinct (Agnini et al., 2007; Angori and Monechi, 1996; Angori et al., 2007). The evolution of fasciculiths has been punctuated by intervals of rapid increase in the number of species in the stratigraphic record. These periods are labeled as radiation or diversification events (i.e., Romein, 1979; Bernaola et al., 2009; Monechi et al., 2013; Agnini et al., 2014). At least three major radiation–diversification events have been observed, and each of them was characterized by changes in the number of cycles and shape of structural elements. The cause of these radiation events and changes in structural features is still not well understood. Monechi et al. (2013) noted that at ODP Site 1262 the "first radiation event", as described by Steurbaut and Sztrákos (2008) and Bernaola et al. (2009), corresponded to the onset of the hyperthermal Latest Danian Event (LDE). According to Aubry et al. (2012), the increase in oceanic oligotrophy during the LDE led to a change in the morphology (structure) of fasciculiths with the occurrence of the collaret present in *Lithoptychius*. This new structure improved the capacity of fasciculiths to photosynthesize by increasing the volume and surface area of the nannolith.

Here we present new results obtained by the analysis of nannofossil assemblages of several successions spanning the Danian–Selandian transition in different paleoceanographic settings in the Tethyan, Atlantic Ocean and Pacific Ocean. In particular, a taxonomic revision of Fasciculithaceae (order Discoasterales Hay 1977, emended by Bown, 2010) is presented. According to the subdivision of Aubry et al. (2011) the recognized species belong to the genera *Gomphiolithus*, *Diantholitha*, *Lithoptychius* and *Fasciculithus*. Original descriptions of fasciculith species with a well-defined SEM holotype and optical counterpart are very rare. This has led to uncertainty and disagreement with regards to identification of species with the light microscope (LM). For example, compare the holotype of *Lithoptychius ulii* with *Lithoptychius janii*. Thus, this work aims to resolve these problems by using a combined analysis of LM and SEM images of different fasciculith taxa. The goals are: to describe the ultrastructure of the different morphotypes in detail, to identify the structural features that have been used to define each genus, to resolve existing taxonomic problems (Agnini et al., 2014), to document structural changes through time, and to improve our understanding of the fasciculith evolution.

The genera have been described following the stratigraphic order of appearance in the geological record. The investigated interval includes the oldest appearance of *Gomphiolithus*, the radiation of *Diantholitha* and *Lithoptychius* in the late Danian, and the radiation event of the new genus *Tectulithus* at the Danian–Selandian transition (Steurbaut and Sztrákos, 2008; Monechi et al., 2013).

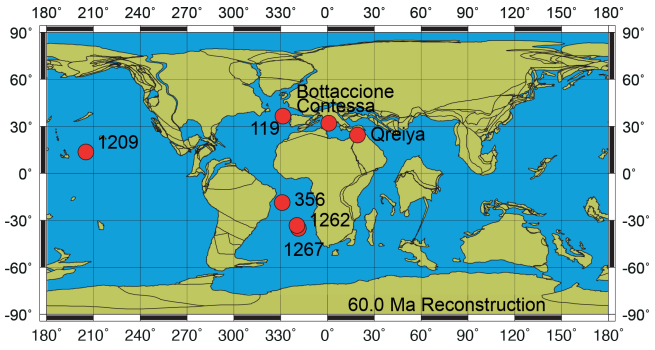

Figure 1. Paleoceanographic reconstruction at 60 Ma with the location of the studied sites and sections (http://www.odsn.de/odsn/services/paleomap/paleomap.html, last access: 25 February 2021; Hay et al., 1999).

2 Materials and methods

The samples analyzed in this study are from Danian–Selandian successions located in different paleogeographic settings in the Atlantic Ocean, the Pacific Ocean and the Tethyan realm (Fig. 1). DSDP and ODP sites include ODP Site 1209 (Shatsky Rise, western Pacific Ocean; 32°39′ N, 158°31′ E), ODP Site 1262 (Walvis Ridge, Atlantic Ocean; 27°15′ S, 1°62′ E), ODP Site 1267 (Angola Basin, Atlantic Ocean; 28°5.88′ S, 1°42.66′ E), DSDP Site 356 (San Pãulo Plateau, Atlantic Ocean; 28°22′ S, 41°28′ W) and DSDP Site 119 (Cantabria Seamount, Bay of Biscay; 45°90′ N, 7°49′ W). Outcrops examined include the Bottaccione and Contessa sections in the Gubbio area of central Italy (43°22′ N, 12°33′ E) and the Gebel Qreiya section in Egypt (26°21′ N, 33°01′ E). Most of these successions were previously analyzed for biostratigraphy and taxonomy and have abundant and well-preserved calcareous nannofossils across the Danian–Selandian interval (Fig. 2) (Perch-Nielsen, 1971, 1977; Fuqua et al., 2008; Youssef, 2009; Aubry et al., 2011, 2012; Monechi et al., 2012, 2013; Miniati et al., 2014).

In order to provide LM and scanning electron microscope (SEM) images of the same individual specimens, samples from DSDP and ODP were prepared following the technique proposed by Moshkovitz (1974). This method involves the use of a removable cover glass and a numbered grid placed on the slide. Slides were examined using a Zeiss Axioplan 2 at 1500× magnification using bright-field and cross-polarized light (XPL). The same sample was then observed in the SEM (Zeiss Evo Ma15 at M.E.M.A. laboratory, University of Florence). Due to preservation problems, outcrop samples were mainly scanned using the LM, and species photographs were then compared with similar specimens from the DSDP and ODP sites. Measurements for each illustrated specimen were taken using Fiji (Schindelin et al., 2012) software (see Tables S3–S7 in the Supplement). Lowest occurrence (LO) is used to describe the stratigraphic first occurrence of a taxon,

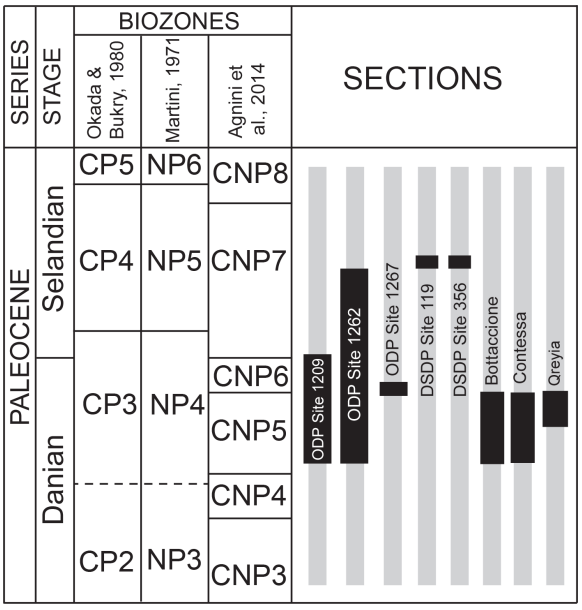

Figure 2. Stratigraphic intervals (in black) of the samples analyzed in this study correlated with the standard calcareous nannofossil zonations of Okada and Bukry (1980), Martini (1971), and Agnini et al. (2014).

and lowest common occurrence (LCO) is used to describe the stratigraphic level at which it becomes common.

3 Results

The taxonomic revision of early fasciculiths in Aubry et al. (2011) includes the description of three new genera (*Diantholitha, Gomphiolithus* and *Lithoptychius*) based on the identification of new structural units called the calyptra, collaret and central body. Herein, we provide a revision of the Romein (1979) and Aubry et al. (2011) fasciculith classification and terminology and include the definition of a new genus. We also provide a detailed description of the ultrastructure of each taxon. An explanation of the structures used for the description of taxa is shown in Fig. 3 and listed in Table 1.

3.1 *Gomphiolithus*

Gomphiolithus is a monocyclic fasciculith consisting of a cylindrical column that is formed from wedge-shaped, radially arranged elements. Monechi et al. (2012, 2013) described the proximal side of the column as characterized by a deeply concave depression (Fig. 4), whereas a reversed orientation of the column was proposed by several authors (Perch-Nielsen, 1977; Romein, 1979, Aubry, 2014). Following Monechi et al. (2012, 2013) the deeply concave side of *Gomphiolithus* is considered here to be a proximal face, as this orientation of the column is consistent with other Fasciculithaceae. Romein (1979) and Aubry et al. (2011) described a conical or diamond-shaped body, dark and visible only in XPL, in just a few specimens at the end of the proximal side. However, SEM photos of *Gomphiolithus magnus* in Perch-Nielsen (1977; pl. 11, figs. 5–6) show only the presence of several small crystals at the bottom of the proximal depression. We suggest that "the central body" (as defined by Romein, 1979) is an optical artifact visible only under LM due to the very deep depression and the presence of small crystals in the concave part of column. The new SEM analyses and photos do not show any peculiar or distinct features (see Figs. 8–9). The central body has been figured and drawn by MP Aubry (2014) as a rhombohedral and pyramidal crystals in *G. magnus* and *G. magnicordis*, respectively, but none of the SEM pictures have shown this structure. Therefore, we conclude that a central body inside the structure of the *Gomphiolithus* may not necessarily be present, but most likely it could be an optical artifact. Furthermore, according to us, the calyptra drawn by Aubry (2014) is not present in this genus and never observed with LM and SEM.

3.2 *Diantholitha*

Aubry et al. (2011) described the genus *Diantholitha* as being composed of two units: a column (proximal unit) and a monocyclic calyptra (distal unit). The new SEM images shown in this study clearly illustrate that the distal unit is composed of one (Fig. 11:7a, 11c) or two cycles, most often two.

The distal unit seems to be formed of only one cycle of elements in the LM; SEM photos reveal the presence of an outer cycle and an inner cycle of elements as shown in Fig. 3 (Figs. 8:2a, 3a; 12:9a; 13:2a, 3a, 4a). For this reason, the original description of *Diantholitha* of Aubry et al. (2011) is emended herein, and the distal unit of *Diantholitha* has been renamed as "biretta" (Fig. 3). Two new species, *D. pilula* and *D. toquea*, are described (see the "Systematic paleontology" section) (Figs. 5; 11:7–11).

3.3 *Lithoptychius*

Scanning electron microscope observations of taxa belonging to *Lithoptychius* document the distinctive arrangement of three cycles that characterize these forms (Fig. 3). Aubry et al. (2011) described *Lithoptychius* as formed by three superimposed structural units (column, collaret and calyptra) and a central body. In this study, we observe that the calyptra lies directly above the column with a collaret that encloses the distal part of the column and/or the proximal part of the calyptra. Thus, the collaret is an independent unit and cannot be considered an intermediate unit as defined by Aubry et al. (2011). Moreover, SEM and LM images (Figs. 16:5a; 17:4a, 5a, 7a, 8a) show the presence of two openings, one in the proximal side of the column and one in the distal end of the calyptra, respectively.

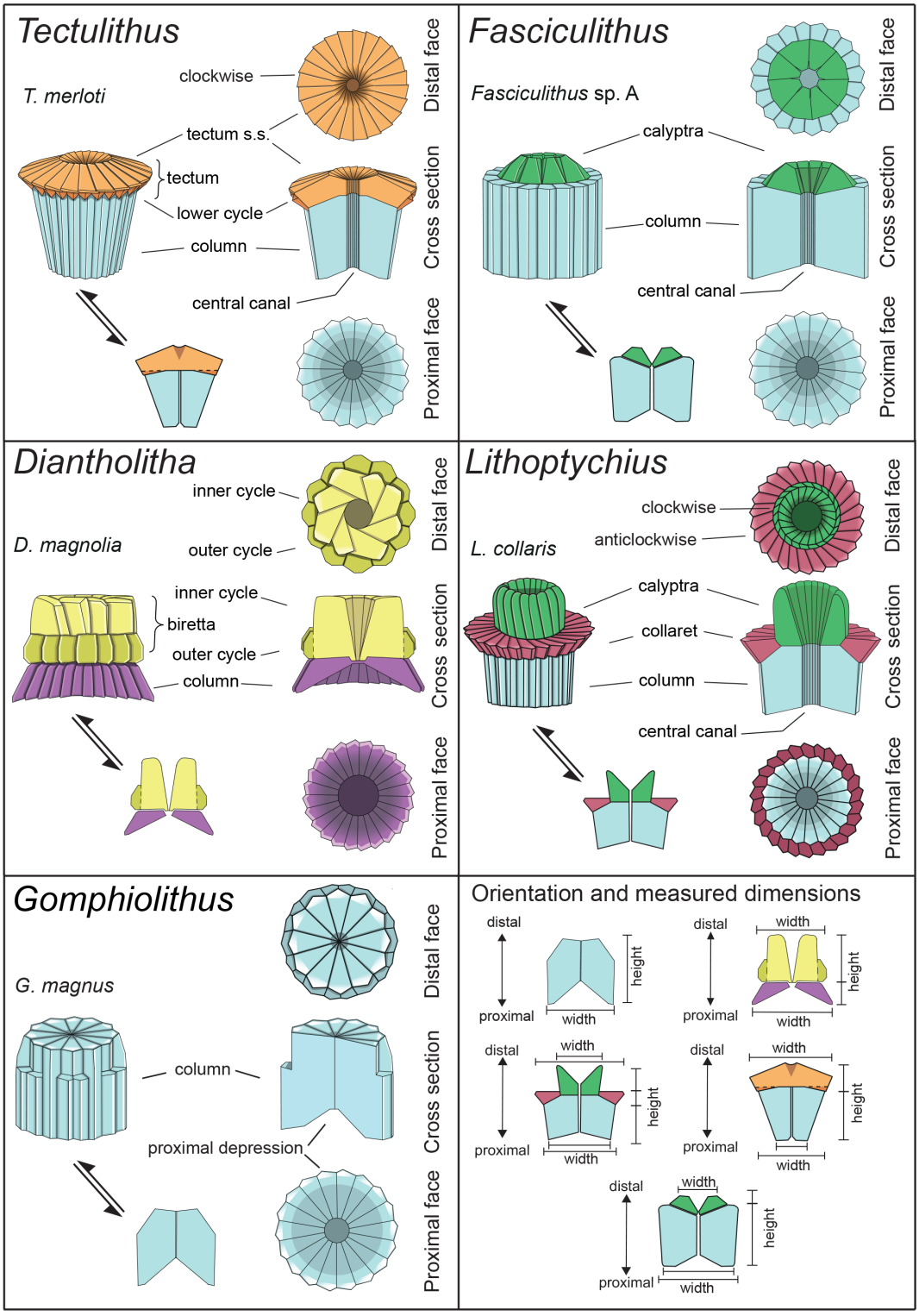

Figure 3. Explanation of the structural terms used for the description of taxa. For each genus a 3D schematic representation, a cross section, and a distal and proximal view of the type species are shown. *Tectulithus* is the new genus introduced in this work and described in the text. For measurement details refer to Tables S3–S7.

Table 1. Terminology used in the taxonomic descriptions.

Column – proximal cycle of fasciculith, cylindrical in shape. It consists of wedge-shaped, radially arranged elements with serrate outline. In plain view, the column is rosette-shaped and depressed in the center of the proximal surface in correspondence of the central canal opening (see below).
Central canal – axial opening that runs along the entire length of fasciculith. It is generated by the radial arrangement of the wedge elements of the column. In XPL the central canal appears as a distinct extinction line that bisects the fasciculith.
Collaret – disk of wedge-shaped, radially arranged elements that surround the distal part of the column and/or the lowermost part of the calyptra in the *Lithoptychius*. Elements of the collaret imbricate clockwise (rarely anticlockwise).
Corolla – (synonym of calyptra or distal unit according to Aubry et al., 2011) elements that flare distally, forming a corolla of variable height and shape.
Calyptra – distal cycle of *Lithoptychius* and *Fasciculithus*. It is made up of vertical or slightly tilted elements with clockwise imbrication. The general morphology can be variable between species with elements showing different orientations from the vertical direction. In LM flaring elements of the calyptra produce a crateriform appearance, whereas parallel or gently tapering elements give a dome- or mushroom-shaped appearance. The calyptra has a central opening that is always connected with the central canal.
Tectum – distal cycle of *Tectulithus* consisting of two superimposed cycles of elements. The tectum s.s. (upper cycle) is formed of wedge-shaped elements with radial arrangement and anticlockwise imbrication. In some species (e.g. *T. pagodiformis*), elements of the tectum s.s. intertwine towards the center. The tectum s.s. is supported by the thin lower cycle, which is made up of wedge-shaped elements. In LM, the tectum behaves like a single crystallographic unit to give an umbrella- or lens-shaped appearance.
Biretta – distal cycle of *Diantholitha* consisting of two concentric cycles of elements. The inner cycle is made up of massive elements with anticlockwise imbrication that make a central opening. The outer cycle consists of prismatic elements with a bossage ("bugnato") shape. Elements of the outer cycle are shorter and greater in number than those of the inner cycle. The biretta (Latin: *biretum, birretum*) is a square with three or four peaks or horns, sometimes surmounted by a tuft. Traditionally, the three-peaked biretta is worn by Roman Catholic clergy and some Anglican and Lutheran clergy. The four-peaked biretta is worn as academic dress by those holding a doctoral degree from a pontifical faculty or pontifical university.

This suggests the presence of a central canal that goes through the entire length of the fasciculith connecting the column with the calyptra. According to Monechi et al. (2012), the central canal is a cylindrical axial opening formed by the radial arrangement of the elements. In XPL the central canal is defined by a distinct extinction line that bisects the column. Thus, a central body between the column and the calyptra, as suggested by Aubry et al. (2011), does not exist. Most likely it could be an optical artifact, linked to the observation in side view of specimens with two overlapping empty cylindrical structures, like the central canal and the collaret, viewed at different focal planes. The central canal of *Lithoptychius* is clearly visible in XPL when focusing on the middle part of the nannolith. When focusing on the external part of the nannolith using a high focal distance, a portion of the collaret is visible in the distal part of the central canal. Based on previous observations, the original definition of *Lithoptychius* (Aubry et al., 2011) is emended herein. Furthermore, the identification of a specimen as the type species of *L. ulii* (Perch-Nielsen, 1971, for both SEM and LM; Fig. 18:4–7) allows us to clarify the characteristic features of this species under LM. Two new species (*L. galeottii* and *L. maioranoae*) are described (Figs. 16:1–4; 18:1–3).

3.4 *Tectulithus*

Forms that appear to have an umbrella- or lens-shaped distal structural unit, called a "tectum", are placed in the new genus *Tectulithus*. This distinctive structural unit behaves as a single crystallographic unit in the LM, but it appears to be made up of two superimposed cycles of elements in the SEM (Fig. 3). The lower cycle consists of wedge-shaped elements supporting the upper cycle (tectum s.s.). The latter consists of radial or slightly overlapping elements with clockwise imbrication. Several species previously classified within the genus *Lithoptychius* (*L. janii*, *L. merloti*, *L. pileatus*, *L. stegastos*, *L. stonehengei*) by Aubry et al. (2011, 2012) are included in *Tectulithus*, along with one new species (*T. pagodiformis*, Fig. 21:1–3).

3.5 *Fasciculithus*

The genus *Fasciculithus* is revised herein, and we provide detailed LM and SEM images of *F. billii*, *Fasciculithus* sp. A, *F. vertebratoides* and the new species *F. realeae* (Fig. 24:5–7). These early species of *Fasciculithus* are distinguished from those that appear in the late Paleocene by the absence of fenestrae on the column sides (Perch-Nielsen, 1971; Romein, 1979; Bown, 2010). The column is directly surmounted by

the calyptra, which is always narrower than the periphery of the column and is located in the distal depression of the column. A summary of the genera and the main features useful for the LM identification of the different species are listed in Figs. 4 and 5.

4 Evolutionary trend of early fasciculiths

Several lineages for the family Fasciculithaceae have been previously proposed (Prins, 1971; Romein, 1979; Perch-Nielsen, 1985; Aubry et al., 2012; Monechi et al., 2013). Recent biostratigraphic and taxonomic studies highlighted a complex evolutionary history across the Danian–Selandian transition in which species are often characterized by short stratigraphic ranges (Aubry et al., 2011, 2012; Monechi et al., 2012, 2013; Farouk and Faris, 2013; Kasem et al., 2017; Metwally, 2019; Mahanipour et al., 2021). In Fig. 6 we present an overview of the stratigraphic distribution of early fasciculiths correlated with the magnetostratigraphy and the Martini (1971), Varol (1989) and Agnini et al. (2014) standard calcareous nannofossil zonations. This scheme represents an improvement of the lineage proposed by Monechi et al. (2013) for ODP Site 1262.

Gomphiolithus magnus and *G. magnicordis* are the oldest representatives of Fasciculithaceae. These species have the same short stratigraphic distribution entirely contained in the middle part of Chron C27r (Monechi et al., 2013). Their first occurrence is documented by several studies (Bukry and Percival, 1971; Perch-Nielsen, 1977; Romein, 1979; Agnini et al., 2007; Steurbaut and Sztrákos, 2008; Monechi et al., 2013) in the lower part of zone NP4 (Martini, 1971), which corresponds to zones NTp5C–NTp6 (Varol, 1989) and to the top of zone CNP4 (Agnini et al., 2014). The origin of *Gomphiolithus* is still uncertain. *Gomphiolithus magnus* appears in the calcareous nannofossil assemblage without a clear ancestor, but, according to Perch-Nielsen (1977), it could be a possible descendent of *Markalius inversus*. Prins (1971), Aubry (1989), Aubry et al. (2011, 2012) and Monechi et al. (2013) postulate an evolution of *G. magnus* from *Biantholithus*. Unfortunately, none of these suggestions seem to be convincing because no transitional forms between *Gomphiolithus* and previously mentioned forms have been found. Therefore, the origin of this genus remains unclear.

Gomphiolithus has its last occurrence in the lower part of zone CNP5 (middle part of zone NP4, zones NTp5C–NTp6; Monechi et al., 2013). An interval characterized by the absence of forms ascribable to the family Fasciculithaceae follows the last occurrence of *Gomphiolithus* and has been documented by Monechi et al. (2013) from several cores and outcrops (ODP Site 1262, Gubbio area, Spain) This interval is defined as paracme PTC27r and occurs near the top of C27r.

The occurrence of *Diantholitha* in the lower part of Chron C27n (Fig. 6) marks the end of the paracme PTC27r. This level has been recorded in the middle part of zone NP4, top of zone NTp7A and middle part of zone CNP5 at ODP Site 1262, ODP Site 1209 (this study), and the Qreiya and Zumaia sections (Monechi et al., 2013; Criscione et al., 2017).

According to Monechi et al. (2013), the origin of *Diantholitha* is related to the addition of a distal structural unit (biretta in this study) to the column of *Gomphiolithus* (Figs. 3, 5). However, the absence of intermediate forms between *Gomphiolithus* and *Diantholitha* makes it difficult to establish a phylogenetic relationship between these two genera. Aubry et al. (2012) suggest that *Diantholitha* may have evolved from *Biantholithus*, without a link to *Gomphiolithus,* as the result of thickening of the distal and the proximal units. The SEM photos shown in this paper have made clear the structure of *Diantholitha*. The presence of a biretta with an inner and an outer cycle makes the relationship between *Biantholithus* and *Diantholitha* more difficult. Interestingly, the new observations on the construction of the biretta, which consists of two concentric cycles of elements, may suggest a link to *Cyclagelosphaera* or *Markalius*, in which the progressive thickening of the two shields and the lengthening of the inner tube may have originated the unusual structure of *Diantholitha*. The thin and concave shape of the column of *D. magnolia* provides support for this hypothesis (Figs. 3, 5). *Diantholitha alata* is the last species of the genus to evolve in the middle part of Chron C27n (Monechi et al., 2013; Criscione et al., 2017). Shortly thereafter, all *Diantholitha* species become extinct in the lower part of Chron C26r.

Lithoptychius appears in the middle part of Chron C27n (Monechi et al., 2013; Criscione et al., 2017), just above the first occurrence of *Diantholitha* from which it is distinguished by a more complex structure. Early *Lithoptychius* forms are *L. felis* and *L. collaris*, which are characterized by a thick collaret and a tall calyptra. Subsequently, *Lithoptychius* quickly undergoes radiation and two lineages are proposed: from *L. collaris* originated *L. galeottii* and *L. varolii* through a reduction of the collaret extension and calyptra height. *Lithoptychius chowii, L. maioranoae* and *L. ulii* originated from *L. galeottii*, whereas *L. felis* gave rise to *L. schmitzii* (Fig. 6).

During its stratigraphic range, *Lithoptychius* shows a gradual reduction in the extension and thickness of the collaret with a transition from a crown-shaped calyptra in the early forms to a more dome-shaped calyptra in the latter ones. The origin of *Lithoptychius* remains unclear, as no transitional forms were observed between this genus and *Gomphiolithus* or *Diantholitha*. Although a direct linkage between *Lithoptychius* and *Diantholitha* is not established yet, this latter can represent a possible ancestor of *Lithoptychius* (Monechi et al., 2013). In fact, the collaret and calyptra of *Lithopychius* may have respectively developed from the inner and the outer cycle of the biretta.

Alternatively, according to Aubry et al. (2012), *Lithoptychius* originated from *Biantholithus* with the addition of a collaret between the column and calyptra.

Tectulithus			COLUMN			COLLARET		CALYPTRA/ TECTUM/ BIRETTA			CENTRAL CANAL
			Shape/ Sides	Distal surface	Width (W)/ Height (H)	Width	Thickness	Shape	Width	Lower/ Outer cycl.	
T. janii			truncated cone - narrowed	flat	W less than H			boat profile or disc-shaped	extended	Not resolvable	narrow
T. merloti			truncated cone distally flearing	flat	W ≈ H			mushroom	extended	Not resolvable	narrow
T. pagodiformis	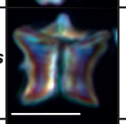		rectangular with a narrowing (vertebra?)	concave	W ≈ H			Pagoda	within the column	absent	narrow
T. pileatus	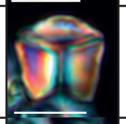		truncated cone distally flearing	concave	W less than H			convex lens	within the column	absent	narrow
T. stegastos	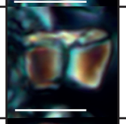		rectangular	flat	W greater than H			thin rectangle	within the column	absent	narrow
T. stonehengei	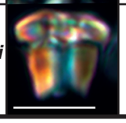		rectangular	flat	W less than H			rectangular	slightly convex	Not resolvable	wide
Fasciculithus			COLUMN			COLLARET		CALYPTRA/ TECTUM/ BIRETTA			CENTRAL CANAL
			Shape/ Sides	Distal surface	Width (W)/ Height (H)	Width	Thickness	Shape	Width	Lower/ Outer cycl.	
F. billii	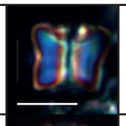		cotton reel (slightly constricted sides)	slightly concave flat	W less than H			small triangular protrusions	within the column		narrow
***Fasciculithus* sp.A**	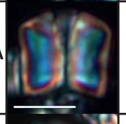		rectangular with slightly flaring sides	Not resolvable	W less than H			small convex	within the column		narrow
F. realeae	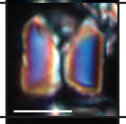		rectangular with parallel or slightly flaring sides	deeply concave	W less than H			small triangular protrusions	within the column		narrow
F. tympaniphormis	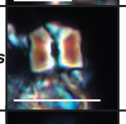		rectangular	Not resolvable	W ≈ H			small knob	within the column		narrow
F. vertebratoides	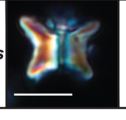		vertebra (constricted sides)	deeply concave	W ≈ H			ring	within the column		narrow
Gomphiolithus			COLUMN			COLLARET		CALYPTRA/TECTUM			CENTRAL CANAL
			Shape/ Sides	Distal surface	Width (W)/ Height (H)	Width	Thickness	Shape	Width	Lower cycle	
G. magnus	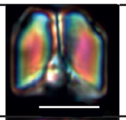		Parallel gets narrower	Flat of slightly concave	W less than H						
G. magnicordis	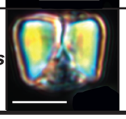		Slightly flaring parallel	Slightly concave / Flat	W ≈ H						

Figure 4. Scheme of the main characteristics to identify *Tectulithus, Fasciculithus* and *Gomphiolithus*. Scale bar 5 µm.

Lithoptychius			COLUMN			COLLARET		CALYPTRA/ TECTUM/ BIRETTA			CENTRAL CANAL
			Shape/ Sides	Distal surface	Width (W)/ Height (H)	Width	Thickness	Shape	Width	Lower/ Outer cycl.	
L. chowii	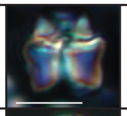		flaring or with a narrowing	flat	W less than H	restricted visible at 45°	thin	dome ≈ half of column	within the column		narrow
L. collaris	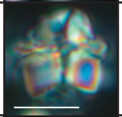		parallel to flearing	convex	W less than H	strong extended	prominent	dome	within the column		narrow
L. felis	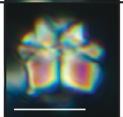		parallel to slightly flaring	convex	W greater than H	slightly extended	prominent	truncated cone	within the column		narrow
L. galeottii	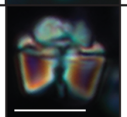		slightly flaring	flat	W less than H	slightly extended visible at 45°	thin	dome	within the column		narrow
L. schmitzii			slightly flaring	convex	W greater than H	strong extended	prominent	low and open cylinder	within the column		wide 1/3 of the column
L. maioranoae	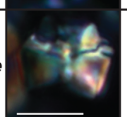		slightly flaring	flat	W greater than H	slightly extended	thin	wide and open cylinder	within the column		wide
L. ulii			parallel	flat	W less than H	restricted / Not resolvable	thin	dome	within the column		narrow
L. varoli	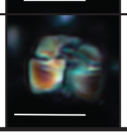	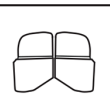	parallel	flat	W greater than H	restricted	thin	dome	column ≈ calyptra		narrow
Diantholitha			COLUMN			COLLARET		CALYPTRA/ TECTUM/ BIRETTA			CENTRAL CANAL
			Shape/ Sides	Distal surface	Width (W)/ Height (H)	Width	Thickness	Shape	Height	Lower/ Outer cycl.	
D. alata		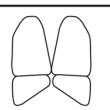	vertical	flat	W greater than H			rectangular	biretta twice of column	Not resolvable	
D. magnolia	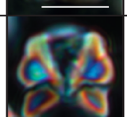	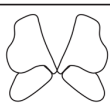	slighty bowed sides	flat	W greater than H			flower	biretta 1/2 to twice of column	Not resolvable	
D. mariposa	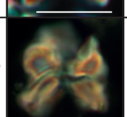	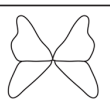	vertical	flat	W greater than H			butterfly	biretta = column	Not resolvable	
D. pilula	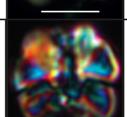		vertical	flat	W greater than H			rosebud	biretta ≈ twice of column	Not resolvable	
D. toquea			vertical	flat	W greater than H			round - oval	biretta around twice the column	Absent	

Figure 5. Scheme of the main characteristics to identify of *Lithoptychius* and *Diantholitha*. Scale bar 5 µm.

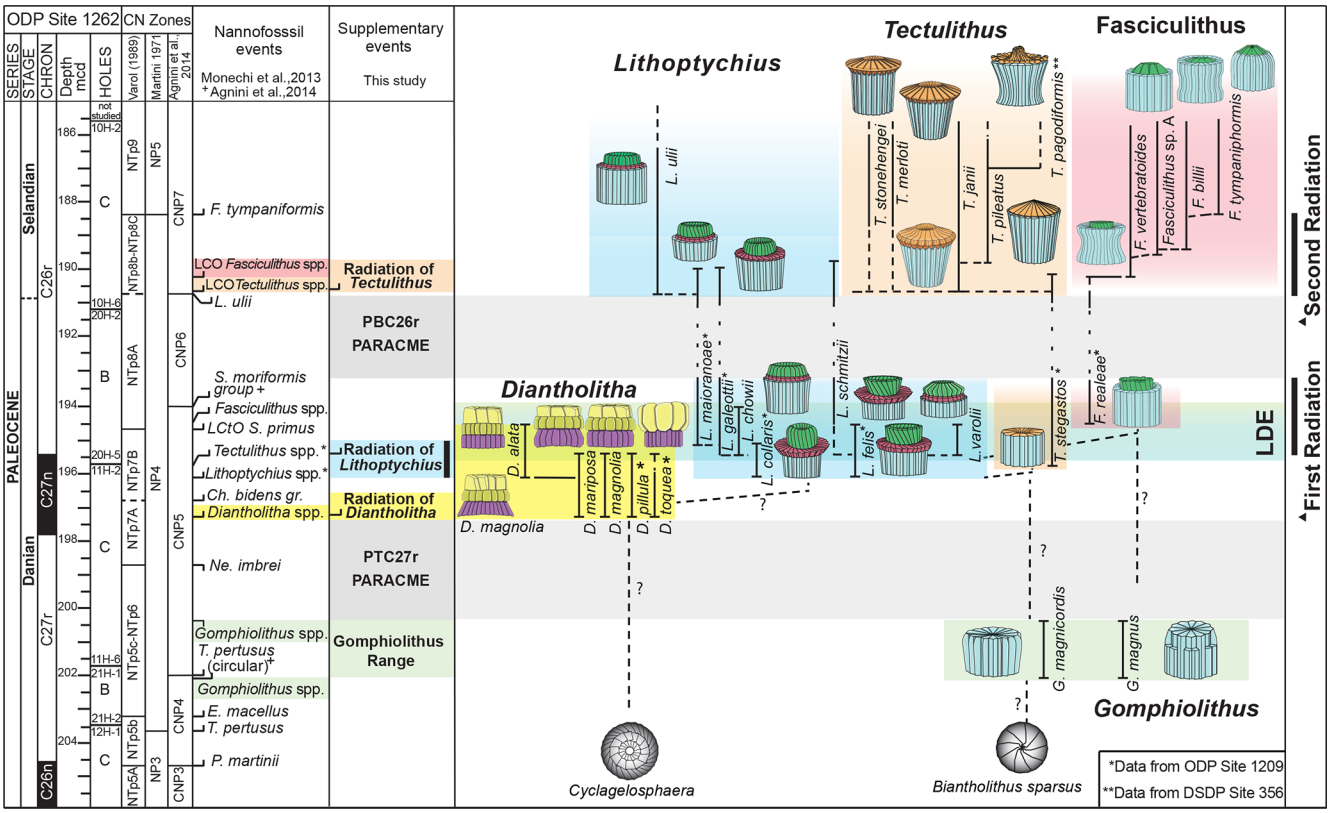

Figure 6. Stratigraphic distribution of early fasciculith genera and species based on ODP Site 1262 (Monechi et al., 2013) and new data introduced by this study. Biostratigraphy after Monechi et al. (2013) and Agnini et al. (2014). Magnetostratigraphy after Westerhold et al. (2008, 2011). Events marked with an asterisk are from ODP Site 1209, whereas events marked with two asterisks are from DSDP Site 356. LCO: lowest common occurrence; LCtO: lowest continuous occurrence. The triangle refers to the first and second radiation of fasciculith according to Monechi et al. (2013). LDE: Latest Danian Event. For biostratigraphic details refer to Table S2.

The first species of *Tectulithus* observed in this study was *T. stegastos* (Fig. 6) that first occurs in the upper part of zone CNP5 (middle part of zone NP4, zones NTp7B; Monechi et al., 2013).*Tectulithus stegastos* gave rise to a large number of species (*T. janii*, *T. pileatus*, *T. stonehengei* and *T. merloti*) in zone CNP7 (upper part of zone NP4–NP5, zones NTp8b–c–NTp9; Monechi et al., 2013). *Tectulithus* probably originated from *Lithoptychius*, after the gradual change in calyptra and collaret in the tectum and the acquisition of a conical column. Another possible ancestor of *Tectulithus* is *G. magnicordis* after the development of a simple tectum such as that of *T. stegastos* (Fig. 22:7–8). The evolutionary trend of *Tectulithus* is characterized by an increase in the complexity of the tectum pattern from *T. stegastos*, *T. pileatus*, *T. merloti* and *T. stonehengei* to *T. janii* and *T. pagodiformis* that show a tectum composed of curved intertwined elements.

The oldest species of *Fasciculithus* recognized in this study is *F. realeae* (Fig. 6) that occurs in the uppermost zone CNP5 (zone NP4, zones NTp8A; Monechi et al., 2013). As well as *Tectulithus*, *Fasciculithus* starts to differentiate only from zone CNP7 (upper part of zone NP4–NP5, zones NTp8b–c–NTp9; Monechi et al., 2013) with *F. realae*. *Fasciculithus* may have originated from *Lithoptychius* following the loss of collaret of species characterized by an open calyptra such as *L. felis* and *L. schmitzii*. Otherwise, *Fasciculithus* may have evolved directly from *Gomphiolithus* with the development of a calyptra. The specimens of *Fasciculithus* observed in this study show a gradual change in the orientation of the calyptra elements from vertical in *F. realeae* and *F. vertebratoides* (Figs. 24:5b; 26:3a) to more tilted in *F. billii, Fasciculithus* sp. A and *F. tympaniformis* (Figs. 23:6a; 24:1a), giving a more rounded shape to the fasciculiths.

4.1 The radiation of fasciculiths (characterization and comparison with first and second radiation)

The distribution of early fasciculiths is characterized by different episodes of rapid proliferation of morphotypes over short stratigraphic intervals, which are termed radiation–diversification events. At least two distinct radiation events (first and second radiation of fasciculiths) were recognized across the Danian–Selandian. Fasciculith radiation has been documented in different areas (e.g., Steurbaut and Sztrákos, 2008; Bernaola et al., 2009; Dinarès-Turell et al., 2010;

Aubry et al., 2012; Monechi et al., 2013; Miniati et al., 2014) and therefore represent an important biostratigraphic tools for this time interval.

Romein (1979) introduced the term "first radiation of *Fasciculithus*" to distinguish the gradual evolution of fasciculiths from the ancestor form *G. magnus* in the *E. macellus–F. tympaniformis* zones. A more detailed definition of this event was proposed by Steurbaut and Sztrákos (2008), Bernaola et al. (2009), and Aubry et al. (2012), who identified the onset of the first fasciculith radiation–diversification event, with the lowest occurrences of *Diantholitha* and *Lithoptychius*. Recent data from Monechi et al. (2013), however, show that the appearance of *Diantholitha* precedes *Lithoptychius*. Moreover, these authors point out the biostratigraphic relevance of the biohorizon corresponding to the lowest occurrence of *Diantholitha* and define the onset of the first radiation of fasciculiths in correspondence of the appearance of *Lithoptychius* (LOs of *L. chowii* and *L. varolii*). The first radiation of fasciculiths (sensu Monechi et al., 2013) has been recognized in different sections, including at ODP Sites 1262 and 1209 (Monechi et al., 2013; Miniati et al., 2014), and correlates with the Latest Danian Event (LDE). At present, the different definitions of the first radiation of *Fasciculithus* have resulted in a vague and ambiguous use of this term. In order to avoid misinterpretation, we suggest using "radiation of *Diantholitha*" and "radiation of *Lithoptychius*" to describe the appearance and rapid diversification of *Diantholitha* and *Lithoptychius*, respectively. This avoids the ambiguity between the first radiation–diversification of *Fasciculithus* (Steurbaut and Sztrákos, 2008; Bernaola et al., 2009; Dinarès-Turell et al., 2010) and the original definition of the first radiation of *Fasciculithus* defined by Romein (1979).

At ODP Site 1209, the first representative of *Tectulithus* (*T. stegastos*) and *Fasciculithus* (*F. realeae*, new species) appears just above the base of *Lithoptychius* (Fig. 6). These two genera are rare in their lowermost ranges and increase in abundance above paracme PBC26r. Unfortunately, due to the imprecise magnetostratigraphic record at Site 1209 (Dinarès-Turrel et al., 2014), the lowermost occurrences of *Tectulithus* and *Fasciculithus* are difficult to place. In Fig. 6, they have been tentatively correlated with the top of Chron C27n and the lower part of Chron C26r, respectively.

4.2 Second radiation of fasciculiths

A second paracme of fasciculiths has been recognized at the base of Chron C26r (PBC26r), and it comprises the upper part of zone NP4, zone NTp8A and zone CNP6 (Monechi et al., 2013). This interval is characterized by the absence of *Lithoptychius, Tectulithus* and *Fasciculithus* in the nannofossil assemblages. The end of paracme PBC26r is marked by the lowest occurrence of *L. ulii*. This event has been used by Varol (1989) and Agnini et al. (2014) to define the base of zone NTp8B and zone CNP7, respectively. Within early *Lithoptychius* species, only *L. schmitzii*, *L. maioranoae* and *L. galeottii* are recorded above paracme PBC26r, and they rapidly disappear just above the lowest occurrence of *L. ulii* (Fig. 6). At ODP Site 1262, Agnini et al. (2007) defined the "LO of *Fasciculithus*, coincident with the LOs of *Fasciculithus ulii* and *Fasciculithus pileatus*".

The Danian–Selandian boundary interval is characterized by the radiation of the genera *Tectulithus* and *Fasciculithus* with the occurrence of many species previously included within *Fasciculithus* and *Lithoptychius* (*T. stonehengei*; *T. merloti*; *T. janii*; *T. pileatus* and *T. pagodiformis*). *Tectulithus* is easily distinguished under LM, having a flat or conical distal cycle that covers like a roof the column. Unfortunately, the same term (second radiation) has been used to indicate two different and temporally distinct events and time intervals. The term "second radiation of fasciculiths" was used by Bernaola et al. (2009) to approximate the Danian–Selandian boundary at the Zumaia section, and it has also been documented at the Qreiya section (Monechi et al., 2013), Loubieng section (Steurbaut and Sztrákos, 2008) and Bjala section (Dinarès-Turell et al., 2010). The term "second radiation of *Fasciculithus*" was also used to indicate the differentiation of *Fasciculithus* occurring in the upper Paleocene (NP9) *Discoaster multiradiatus* zone (Romein, 1979; Perch-Nielsen, 1985; Aubry, 1989; Agnini et al., 2007; Aubry et al., 2012).

To avoid misunderstandings, we suggest using the term "radiation of *Tectulithus*" for the lowest common occurrence of *Tectulithus*, *L. ulii* and *Fasciculithus* (Fig. 6) instead of "second radiation of *Fasciculithus*" to describe the rapid differentiation of fasciculiths at the Danian–Selandian transition. The previous taxa appear close to each other but are always a minor component of the calcareous nannofossil assemblage. According to this subdivision, the Danian–Selandian boundary radiation differs from the "radiation of *Fasciculithus*" and "second radiation of *Fasciculithus*" sensu Romein (1979) and Aubry (1989) in the upper Paleocene.

5 Conclusions

The evolution of the family Fasciculithaceae in the upper Danian–lower Selandian resulted in a wide range of morphologies as a result of successive and rapid diversification events through time. Our study provides detailed morphologic descriptions of existing species and the establishment of the following: a new genus, *Tectulithus*; five new combinations, *Tectulithus janii, Tectulithus merloti*, *Tectulithus pileatus*, *Tectulithus stegastos* and *Tectulithus stonehengei*; and six new species, *Diantholitha pilula*, *Diantholitha toquea*, *Lithoptychius galeottii, Lithoptychius maioranoae, Tectulithus pagodiformis* and *Fasciculithus realeae*. These are new fasciculith morphotypes and combinations. Combined LM–SEM analyses provided an effective tool for documenting the shape of the fasciculith structural units (i.e., column, calyptra, collaret) that are currently used for the

generic assignments to *Gomphiolithus*, *Diantholitha*, *Lithoptychius* and *Fasciculithus*. It also allowed us to report new structural units (biretta and tectum) that led to the description of a new genus (*Tectulithus*). The complex evolutionary history of the early fasciculiths explained the successive occurrence of five genera, which are typically associated with a radiation of forms. This rapid diversification, characterized by distinctive morphostructural features, allowed for the definition of several radiation and/or events within the Danian–Selandian transition: the lowest occurrence of *Gomphiolithus* at the top of zone CNP4, the radiation of *Diantholitha* in the middle part of zone CNP5, the radiation of *Lithoptychius* in upper zone CNP5 and the radiation of *Tectulithus* at the base of zone CNP7. The early evolution of fasciculiths is also marked by two paracme intervals (PTC27r and PBC26r) that were documented at the top of C27r and at the base of Chron C26r, respectively. Moreover, new data from several ODP sites and outcrop sections prove that these new taxa had a wide geographical distribution in different paleoceanographic settings.

Confusion in the consistent use of the terms "first and second radiation" of fasciculiths is resolved in this study with the definition of four well-constrained events in terms of both the genera and/or species involved and in terms of stratigraphic position. Thus, the "radiation events" defined in this study can be used for a greater biostratigraphic subdivision of the Danian and lower Selandian sediments, confirming their relevant potential in improving the biostratigraphy of this time interval.

6 Systematic paleontology

Order Discoasterales Hay, 1977 emend. Bown 2010

Family Fasciculithaceae Hay and Mohler, 1967

Gomphiolithus Aubry in Aubry et al. (2011), emend.

Type species

Gomphiolithus magnus (Bukry and Percival, 1971) Aubry in Aubry et al. 2011.

Remarks

According to Aubry et al. (2011), the genus *Gomphiolithus* consists of a tall and compact cylindrical structural unit, the column, which is formed of "radially arranged elongated wedge-shaped elements" of different heights (Fig. 7). One end of the column is deeply concave, whereas the other is slightly concave to flat. We follow Monechi et al. (2012, 2013) in calling the deeply concave end of the column the proximal side. This interpretation correlates well with the classic orientation of *Fasciculithus* (Young et al., 1997), which likely derives from *Gomphiolithus*. On the proximal side, the elements of the column slope steeply toward the central axis, forming a wide conical depression. In proximal view, the elements of the column are radially arranged with slightly anticlockwise imbrication (Figs. 8:1d; 9:2a, 6f). Romein (1979) suggested the presence of a central body on the deeply concave side of this species. He described this structure as a conical or diamond-shaped body that shows an "equilateral-triangular cross section (very large in *G. magnicordis*)" and becomes dark in XPL. The central body was not imaged in our study, although a triangular shape (which is not distinct in XPL) is visible in bright field in well-preserved specimens at the end of the depression. Interestingly, Perch-Nielsen (1977) figured specimens with a mesh-like (porous) plug at the bottom of the depression (plate 11, figs. 5, 6). Thus, the central body of Romein (1979) is not a true structure, but it is related to the deep conical shape of the proximal depression and the presence of the mesh on which crystals can collect or grow. The mesh-like plug and the accumulated crystals can be observed at different focus in side view. With the LM, the elements of the column appear to be contiguous along the vertical axis, which is visible as a straight dark extinction line that bisects the column. SEM images of the distal side of *Gomphiolithus* show that the wedge-shaped elements of the column converge at the center of the fasciculith (Figs. 8:10b–11a; 9:6f), confirming the absence of a central canal. Given the absence of a central body, *Gomphiolithus* consists of one structural unit, the column, and differs from *Fasciculithus*, which is characterized by the presence of both a column and a calyptra (Aubry et al., 2011).

Gomphiolithus magnicordis (Romein, 1979) Aubry in Aubry et al., 2011

(Fig. 9:3–7)

1979 *Fasciculithus magnicordis* Romein: p. 149, pl. 9, figs. 12–13.
2012 *Gomphiolithus magnicordis* (Romein, 1979) Aubry in Aubry et al., 2011; Monechi et al.: pl. 1, figs. 13–25.

Measured dimensions

Height: 5.2–11.3 µm; width: 6.5–12.9 µm.

Biozone occurrence of the studied specimens

Lower zone NP4, lower zone CNP5.

Remarks

SEM photos of *G. magnicordis* show a column with a flat or slightly concave distal face and lateral sides that run parallel or flare slightly in the distal direction (Fig. 9:6e–g). The number of elements does not vary for the entire height of the column (Fig. 9:2e, 6e–g). The proximal side is characterized by a deep conical depression that is often filled by crystals (Fig. 9:3–7). *Gomphiolithus magnicordis* differs from *G.*

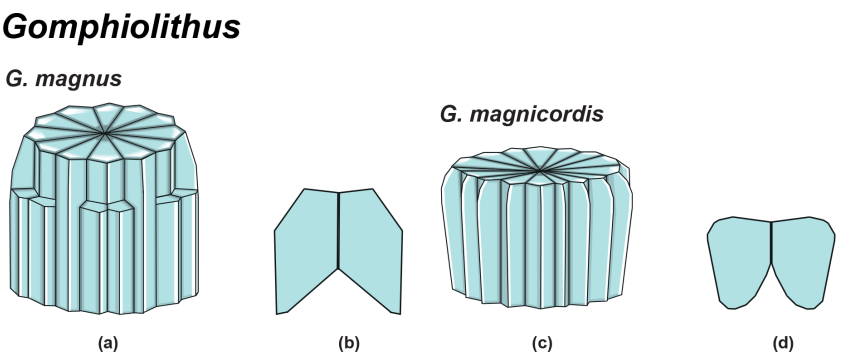

Figure 7. Overview of *Gomphiolithus*. **(a)** Schematic drawing of *G. magnus* showing elongated wedge-shaped elements of different heights forming the column. **(b)** Schematic cross section of *G. magnus*. **(d)** Schematic drawing of *G. magnicordis* with elongated wedge-shaped elements of the same length forming the column. **(g)** Schematic cross section of *G. magnicordis*.

magnus in having a smaller size and slightly flaring sides in the distal direction and by the absence of narrowing in the distal direction.

Gomphiolithus magnus (Bukry and Percival 1971) Aubry in Aubry et al. 2011.

(Figs. 8:1–11; 9:1–2)

1971 *Fasciculithus magnus* Bukry and Percival: p. 131, pl. 4, figs. 9–12.
1977 *Fasciculithus magnus* Bukry and Percival 1971; Perch-Nielsen: p. 747, pl. 11, figs. 4–11; pl. 49, figs. 10, 16, 22.
2012 *Gomphiolithus magnus* (Bukry and Percival 1971) Aubry in Aubry et al., 2011; Monechi et al.: pl. 1, figs. 1–12.
2019 *Gomphiolithus magnus* (Bukry and Percival 1971) Aubry in Aubry et al., 2011; Metwally: pl. I, fig. 13.

Measured dimensions

Height: 6.5–8 µm; width: 8.1–10.1 µm.

Biozone occurrence of the studied specimens

Lower zone NP4, lower zone CNP 5.

Remarks

The cylindrical body of *G. magnus* shows a narrowing toward the distal end of the column (Fig. 8). SEM images show that the column consists of about 20–30 elements in the lower part, decreasing to 10–12 in the distal part. The elements of the column have differing heights, narrowing in the upper part of the column (Fig. 8:1c, 2c, 7a–9a). The morphology of *G. magnus* has great variability. Narrowing of the body generally occurs in the upper part of the column, but it may also occur at about half the height of the column. The narrowing can be abrupt, giving rise to a sub-horizontal surface from which only about half of the elements continue more or less vertically to make up the distal end (Fig. 8:3, 10). However, specimens with gently tapering lateral sides are more common (Fig. 8:1, 2, 7–9).

Diantholitha Aubry in Aubry et al., 2011 emend.

(Figs. 9:11–12; 12–13)

Type species

Diantholitha mariposa Rodriguez and Aubry in Aubry et al. (2011).

Emended description

Forms consisting of two structural units: a column and a biretta (corolla or distal unit of Aubry) (Fig. 10). The column is the proximal unit, and it is made up of vertical, tightly arranged wedge-shaped elements. According to Aubry et al. (2011): "The periphery is smooth and the proximal edge is weakly to strongly scalloped". The column is shorter than the biretta, which is usually composed of two concentric cycles of elements, rarely one cycle (*D. toquea*) and unknown for *D. mariposa*. The outer cycle consists of a set of prismatic elements with an irregular outline that produce a bossage or "bugnato-shaped" appearance. The inner cycle is made up of massive elements standing almost vertically on the column, creating a deep central opening of variable size. Elements of the outer cycle are generally shorter and greater in number than those of the inner cycle. The number of elements usually varies from six to eight (Figs. 11:6a–e, 8a; 12:12a–d, 13a, 14a; 13:8a–f). The central body is absent.

Remarks

Based on SEM micrographs, the distal unit of *Diantholitha* is shown to be composed of two concentric cycles of elements (Miniati et al., 2015), as also suggested by Bown (2016), and the distal unit of *Diantholitha* (calyptra in Aubry et al., 2011)

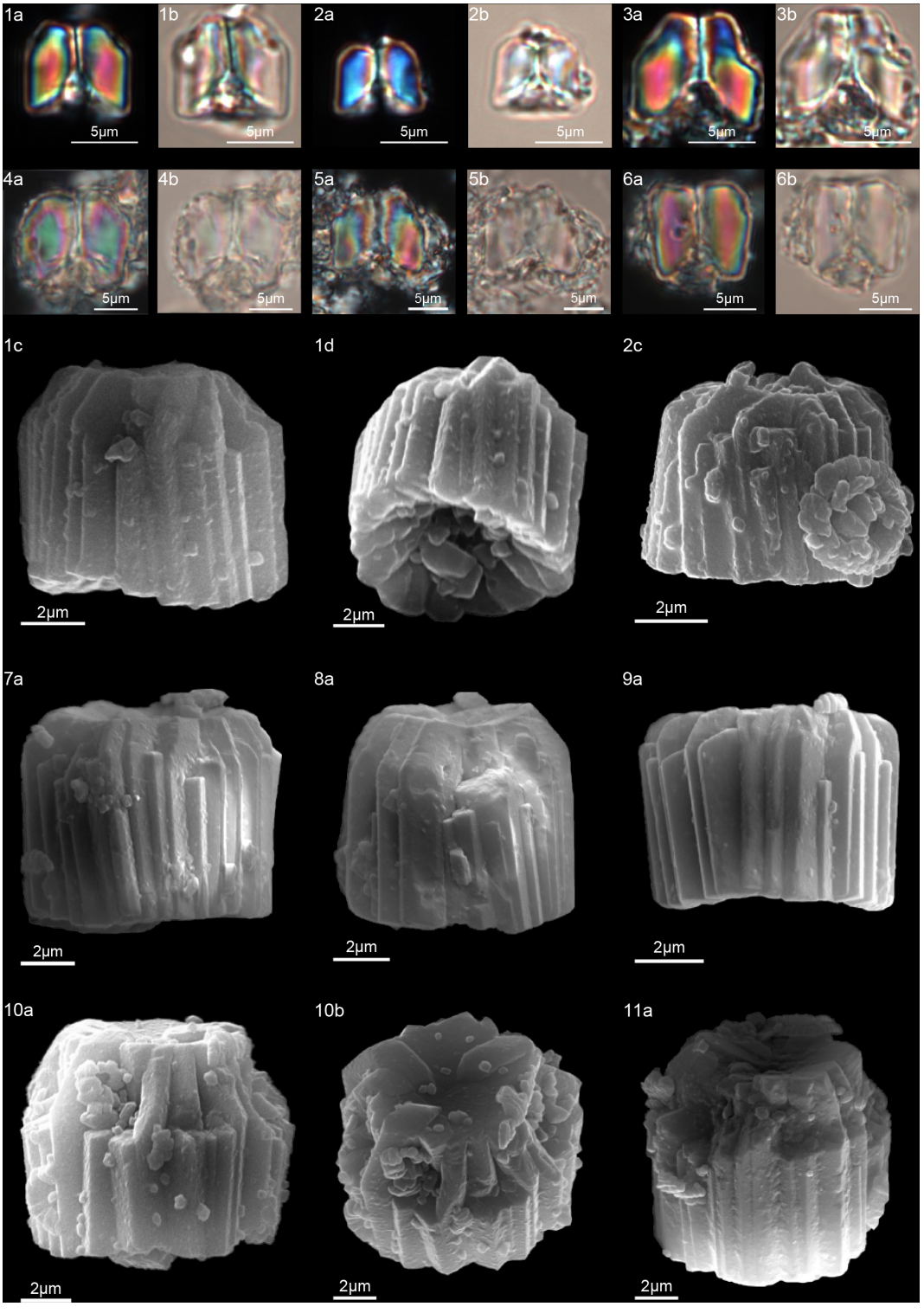

Figure 8. *Gomphiolithus magnus*. **(1)** Sample: 1209B 25-1, 142–143. **(1a)** Cross-polarized light (XPL). **(1b)** Plane-polarized light (PPL). **(1c–d)** Scanning electron microscope (SEM) images showing lateral **(1c)** and proximal view **(1d)**. **(2)** Sample: 1209B 25-1, 142–143. **(2a)** XPL, **(2b)** PPL, **(2c)** SEM. **(3)** Sample: 1209B 25-1, 142–143. **(3a)** XPL, **(3b)** PPL. **(4)** Sample: Contessa Highway 10.79 m (above the K–Pg boundary). **(4a)** XPL, **(4b)** PPL. **(5)** Sample: Bottaccione 10.60 m (above the K–Pg boundary). **(5a)** XPL, **(5b)** PPL. **(6)** Sample: Bottaccione 11.38 m. **(6a)** XPL, **(6b)** PPL. **(7)** Sample: 1262C 11-5, 131–132. **(7a)** SEM. **(8)** Sample: 1262C 11-5, 131–132. **(7a)** SEM. **(9)** Sample: 1262C 11-5, 131–132 (201.34 mcd). **(7a)** SEM. **(10)** Sample: 1209B 25-1, 142–143; SEM images showing lateral **(10c)** and distal view **(10d)**. **(11)** Sample: 1262C 11-5, 131–132. **(11a)** SEM. See Table S1 for sample details.

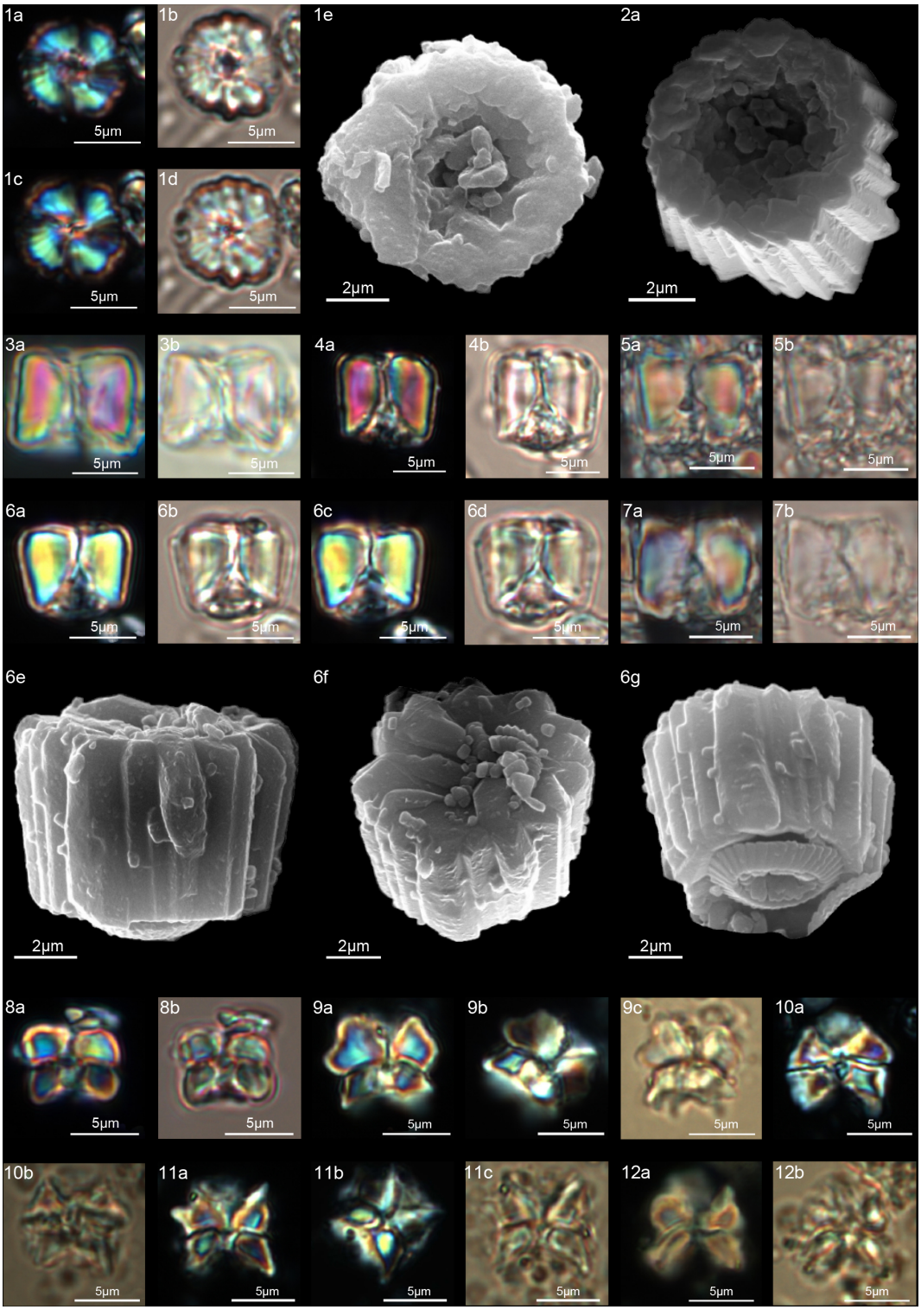

Figure 9. *Gomphiolithus magnus*. **(1)** Sample: 1209B 25-1, 142–143; views of proximal side. **(1a–c)** XPL, **(1b, d)** PPL, **(1e)** SEM. **(2)** Sample: 1262C 11-5, 131–132. **(2a)** SEM view of proximal side. *Gomphiolithus magnicordis*. **(3)** Sample: 1209B 25-2, 20–21. **(3a)** XPL, **(3b)** PPL. **(4)** Sample: 1209B 25-1, 142–143. **(4a)** XPL, **(4b)** PPL. **(5)** Sample: Bottaccione 11.14 m. **(5a)** XPL, **(5b)** PPL. **(6)** Sample: 1209B 25-1, 142–143. **(6a, c)** XPL, **(6b, d)** PPL, **(6e)** SEM side view, **(6f)** SEM distal view, **(6g)** SEM proximal view. **(7)** Sample: Contessa Highway 10.07 m (above the K–Pg boundary). **(7a)** XPL, **(7b)** PPL. *Diantholitha* cf. D. mariposa. **(8)** Sample: 1209C 14-1, 116–117. **(8a)** XPL, **(8b)** PPL. **(9)** Sample: Qreiya + 7.1 m. **(9a, b)** XPL, **(9c)** PPL. **(10)** Sample: Qreiya + 7.1 m. **(10a)** XPL, **(10b)** PPL. *Diantholitha mariposa*. **(11)** Sample: Qreiya + 7.7 m. **(11a, b)** XPL. **(11c)** PPL. **(12)** Sample: Qreiya + 9.42 m. **(12a)** XPL, **(12b)** PPL. See Table S1 for sample details.

has a different structure from the typically monocyclic calyptra of *Lithoptychius*. The presence of two cycles in the distal unit of *Diantholitha* conflicts with the original description of the genus (Aubry et al., 2011). Thus, the description of *Diantholitha* is emended herein and the distal unit, with two cycles, is defined as a biretta (see Table 1). According to us *Diantholitha magnolia* is the species that better characterizes the genus.

In the LM in side view, specimens are birefringent, and the column and biretta appear to have a deep concavity on the proximal side and a deep opening on the distal side (Fig. 9:10–12). No extinction line is observable between the outer and the inner biretta, and therefore the two cycles are difficult to identify with the LM, especially in poorly preserved material.

Diantholitha alata (Aubry and Rodriguez in Aubry et al., 2011) emend.

(Fig. 11:1–6)

2009 *Fasciculithus* sp.1 Bernaola et al.: fig. 4P.
2011 *Diantholitha alata* Aubry and Rodriguez in Aubry et al., 2011; Aubry et al.: pl. 1, fig. 3; pl. 3, figs. 1–3, not fig. 4, figs. 5a–d.
2012 *Diantholitha magnolia* Rodriguez and Aubry in Aubry et al., 2011; Monechi et al.: pl. 2, figs. 12–14.

Emended description

In the SEM, *D. alata* appears to have a column of hexagonal, radially arranged elements forming a wide concave depression on the proximal end (Fig. 11:2–3). The biretta is composed of two cycles: an inner cycle of thick, tall elements and a lower outer cycle with the same number of elements as the column. The inner cycle is composed of six vertical elements with anticlockwise imbrication that make up the central opening (Fig. 11:6a–e). The biretta is twice the height of the column. The column and the biretta have comparable width and vertical lateral sides.

In the LM, *D. alata* appears to have a rectangular outline (Fig. 11:1b–e, 4, 5), which differs from other species of *Diantholitha* that have more rounded outlines.

Measured dimensions

Total height 5.6–7.7 µm; column height 1.5–2.6 µm, width 4.2–8.5 µm; biretta height 3.7–5.1 µm, width 2.2–8.2 µm.

Biozone occurrence of the studied specimens

Middle zone NP4; zone CNP 5.

Remarks

Diantholitha alata differs from *D. magnolia* in having vertical lateral sides, a higher biretta and a straight extinction line between the column and the biretta.

Diantholitha magnolia (Rodriguez and Aubry, in Aubry et al., 2011) emend.

(Fig. 12:1–14)

2008 *Fasciculithus* sp. A Fuqua et al.: p. 189 fig. 10.
2009 *Fasciculithus* sp.1 Bernaola et al.: fig. 4Q.
2010 *Fasciculithus* sp.1 Dinarès-Turrel et al.: pl. 2, fig. 16.
2011 *Diantholitha magnolia* Aubry and Rodriguez in Aubry et al., 2011; Aubry et al.: p. 270, pl. 2, figs. 1–5.
2012 *Diantholitha hemisphaerica* Aubry et al., 2011: p. 32, fig. 3.
2012 *Diantholitha alata* Aubry and Rodriguez in Aubry et al., 2011; Monechi et al.: pl. 2, figs. 18–20, 23–25.
2019 *Diantholitha alata* Aubry and Rodriguez in Aubry et al., 2011; Metwally: pl. I, fig. 15.

Emended description

The column is formed of thin, radially arranged elements that flare in the distal direction, producing a wide concave proximal surface (Fig. 12:9a–11a). The biretta consists of two cycles; the inner cycle is taller than the outer cycle, and it is composed of massive elements with anticlockwise imbrication that form a central opening (Fig. 12:12–14). The outer cycle is composed of short and trihedral elements. In the LM, (Fig. 12:1–8), the column appears with slightly bowed with tapering sides. A wavy extinction line separates the column from the biretta. The biretta appears to be rounded downward due to the presence of the outer cycle and is thinner upward. The central opening is clearly visible along the central axis of the biretta for almost its entire length.

Measured dimensions

Total height 4.4–6.8 µm; column height 1.3–2 µm, width 4.7–7.6 µm; biretta height 3–4.6 µm, width 5.2–7 µm.

Biozone occurrence of the studied specimens

Middle zone NP4; zone CNP 5.

Remarks

The original description is emended because new SEM and LM images document a structural unit, the biretta in this study, that is composed of two different cycles.

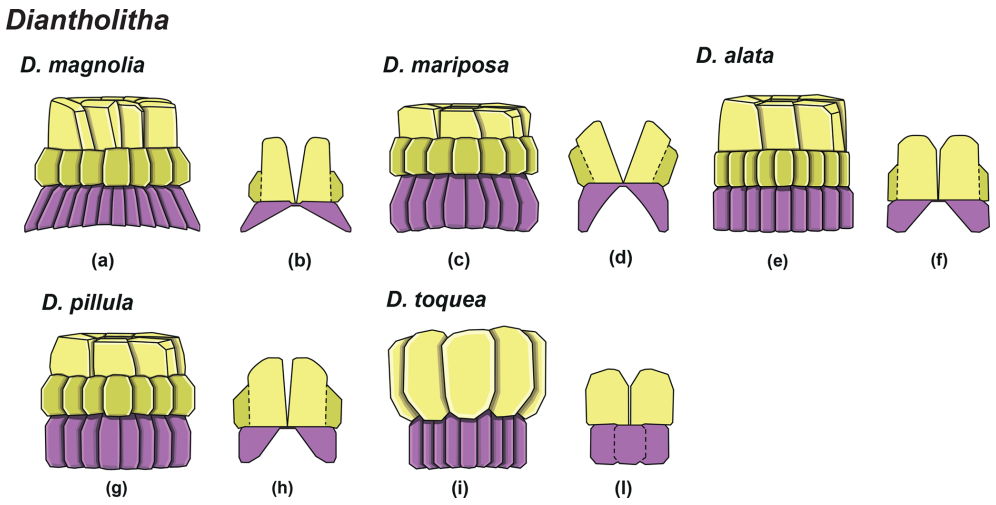

Figure 10. Overview of *Diantholitha*. **(a)** Schematic drawing of *D. magnolia* under SEM showing the position of the column (purple) and biretta (yellow and light green). **(b)** Schematic cross section of *D. magnolia*. **(c)** Schematic drawing of *D. mariposa*. **(d)** Schematic cross section of *D. mariposa*. **(e)** Schematic drawing of *D. alata*. **(f)** Schematic cross section of *D. alata.* **(g)** Schematic drawing of *D. pilula*. **(h)** Schematic cross section of *D. pilula*. **(i)** Schematic drawing of *D. toquea* showing the characteristic monocyclic biretta. **(l)** Schematic cross section of *D. toquea.*

Diantholitha mariposa (Rodriguez and Aubry in Aubry et al., 2011)

(Fig. 9:11–12)

2011 *Diantholitha mariposa* Rodriguez and Aubry in Aubry et al., 2011; Aubry et al.: p. 270, pl. 1, figs. 1–2.
2012 *Diantholitha magnolia* Rodriguez and Aubry in Aubry et al., 2011; Monechi et al.: p. 356, pl. 2, figs. 8–9, 10–11.
2017 *Diantholitha* cf. *D. mariposa* Rodriguez and Aubry in Aubry et al., 2011; Criscione et al.: p. 5, pl. 2, figs. 1, 4.

Measured dimensions

Total height: 6.8–7.4 µm; column height 3–3.3 µm, width 6.8–6.9 µm; biretta height 3.8–4.1 µm, width 6.6–7.7 µm.

Biozone occurrence of the studied specimens

Middle zone NP4; CNP 5 zone.

Remarks

At ODP Sites 1209 and 1262, *D. mariposa* is very rare, and specimens "reminiscent of a butterfly" with an open biretta (corolla) as described by Aubry et al. (2011, 2012) can hardly be recognized (Fig. 9:11–12). Only short, stocky specimens with a massive biretta are documented; these forms are assigned to *Diantholitha* cf. *D. mariposa* for having a slightly flaring corolla (biretta) with a height similar to the column height (Fig. 9:8a–b, 9a–c, 10a–b). Specimens with these characteristics and reminiscent of a butterfly shape were documented at Qreiya, but the poorly preserved material prevented detailed characterization of the structure of *D. mariposa* with the SEM. The structure of *D. mariposa* in Fig. 3 is inferred on the basis of the structures of *D. pilula* and *D. magnolia*.

Diantholitha pilula n. sp.

(Fig. 13:1–8)

2011 *Diantholitha mariposa* Rodriguez and Aubry in Aubry et al., 2011; Aubry et al.: p. 270, pl. 1, figs. 4–5.
2012 *Diantholitha magnolia* Aubry and Rodriguez in Aubry et al., 2011; Monechi et al.: pl. 2, figs. 3–8, 15–17.
2017 *Diantholitha magnolia* Aubry and Rodriguez in Aubry et al., 2011; Criscione et al.: p. 5, pl. 2, fig. 2.

Derivation of name

From the Latin *pilula* for small ball or balloon, referring to the spherical shape of the nannolith in side view.

Holotype

Figure 13:1e (SEM) (Fig. 13:1a–d; LM).

Paratype

Figure 13:3e (SEM) (Fig. 13:3a–d; LM).

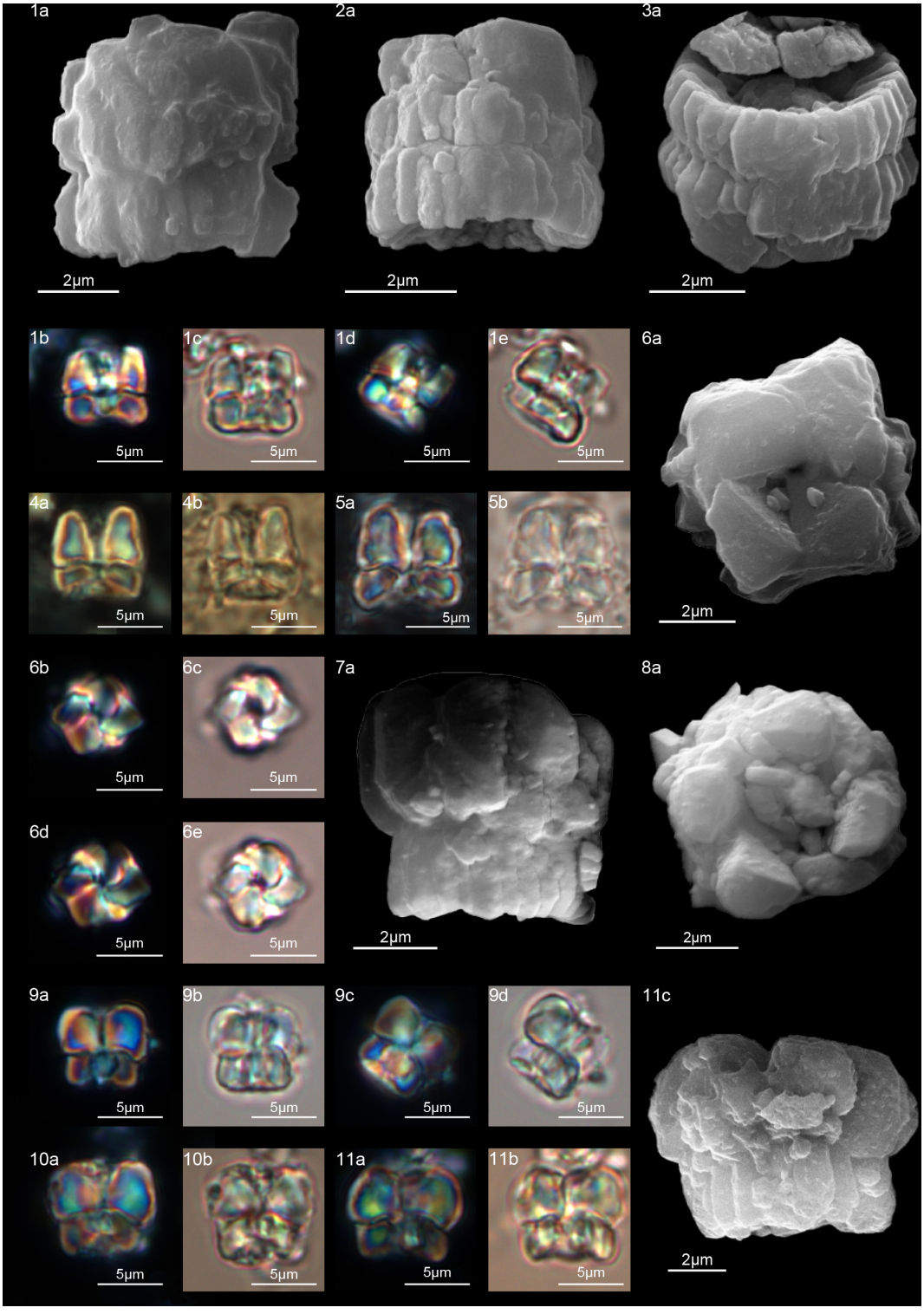

Figure 11. *Diantholitha alata*. **(1)** Sample: 1209C 14-1, 116–117. **(1a)** SEM, **(1b, d)** XPL, **(1c, e)** PPL. **(2)** Sample: 1262C 11-2, 56–57. **(2a)** SEM. **(3)** Sample:1262C 11-2, 56–57. **(3a)** SEM, proximal view. **(4)** Sample: 1262B 20-5, 2–3. **(4a)** XPL, **(4b)** PPL. **(5)** Sample: 1262B 20-5, 5–6. **(5a)** XPL, **(5b)** PPL. **(6)** Sample: 1209C 14-1, 84–85. **(6a–e)** Distal view. **(6a)** SEM, **(6b, d)** XPL, **(6c, e)** PPL. *Diantholitha toquea*. **(7)** Holotype (IGF 104720). Sample: 1262 11-2, 56–57. **(7a)** SEM. **(8)** Sample: 1262C 11-2, 56–57. **(8a)** SEM, distal side. **(9)** Paratype (IGF 104721). Sample 1209C 14-2, 50–51. **(9a, c)** XPL, **(9b, d)** PPL. **(10)** Sample: 1209 14-2, 50–51. **(10a)** XPL, **(10b)** PPL. **(11)** Sample: 1209 14-2, 50–51. **(11a)** XPL, **(11b)** PPL, **(11c)** SEM. See Table S1 for sample details.

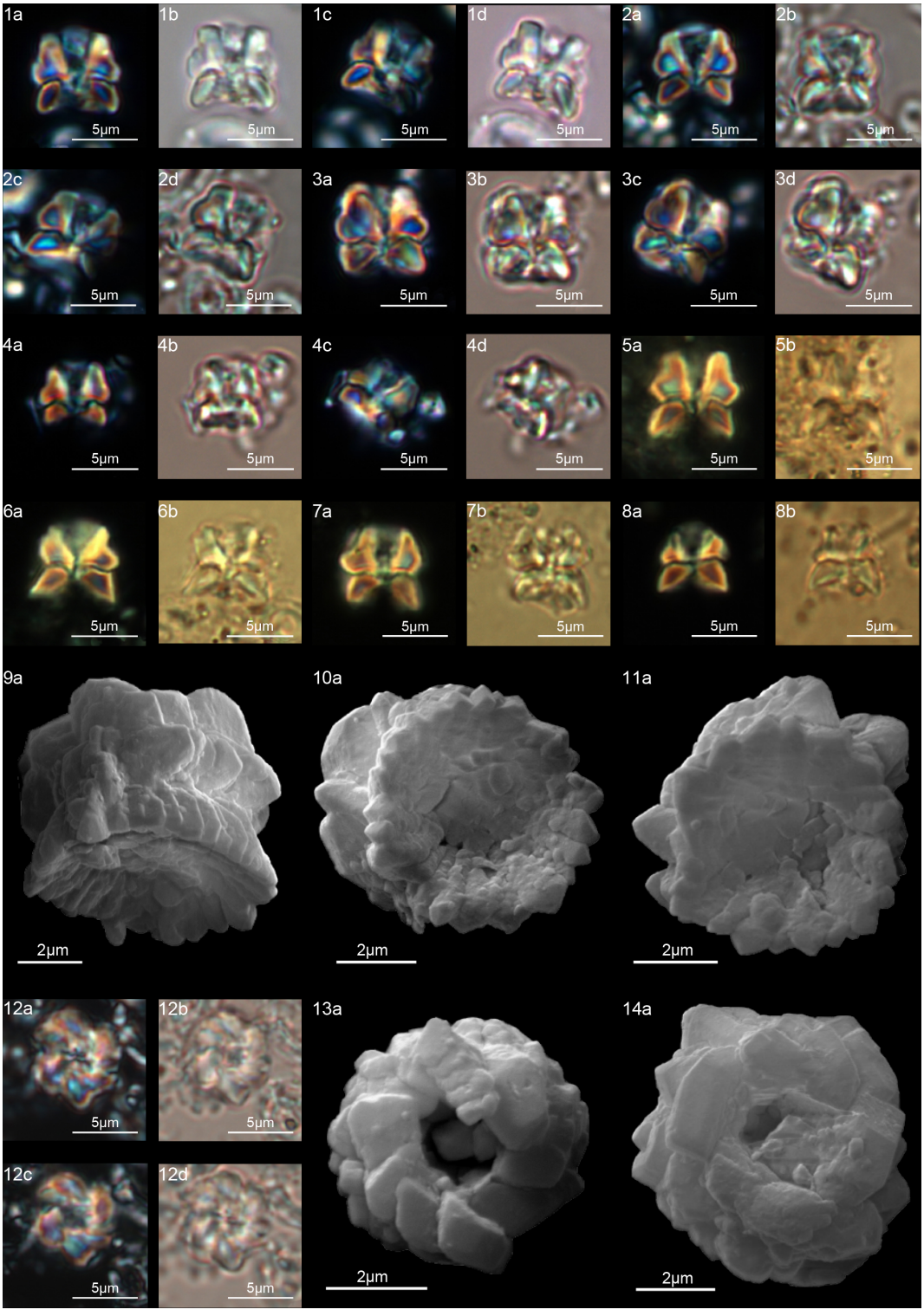

Figure 12. *Diantholitha magnolia*. **(1)** Sample: 1262C 11-2, 56–57. **(1a, c)** XPL, **(1b, d)** PPL. **(2)** Sample: 1262C 11-2, 56–57. **(2a, c)** XPL, **(2b, d)** PPL. **(3)** Sample: 1209C 14-1, 116–117. **(3a, c)** XPL, **(3b, d)** PPL. **(4)** Sample: 1209C 14-1, 116–117. **(4a, c)** XPL, **(4b, d)** PPL. **(5)** Sample: Qreiya + 8.3. **(5a)** XPL, **(5b)** PPL. **(6)** Sample: Qreiya + 8.6. **(6a)** XPL, **(6b)** PPL. **(7)** Sample: Qreiya + 8.3. **(7a)** XPL, **(7b)** PPL. **(8)** Sample: Qreiya + 8.3. **(8a)** XPL, **(8b)** PPL. **(9)** Sample: 1262C 11-2, 56–57. **(9a)** SEM lateral and proximal view. **(10)** Sample: 1262C 11-2, 56–57. **(10a)** SEM proximal view. **(11)** Sample: 1262C 11-2, 56–57. **(11a)** SEM, proximal view. **(12)** Sample: 1262C 11-2, 56–57. LM, distal view. **(12a, c)** XPL, **(12b, d)** PPL. **(13)** Sample: 1262C 10-6, 23–24. **(13a)** SEM, distal view. **(14)** Sample: 1262C 11-2, 56–57. **(14a)** SEM, distal view. See Table S1 for sample details.

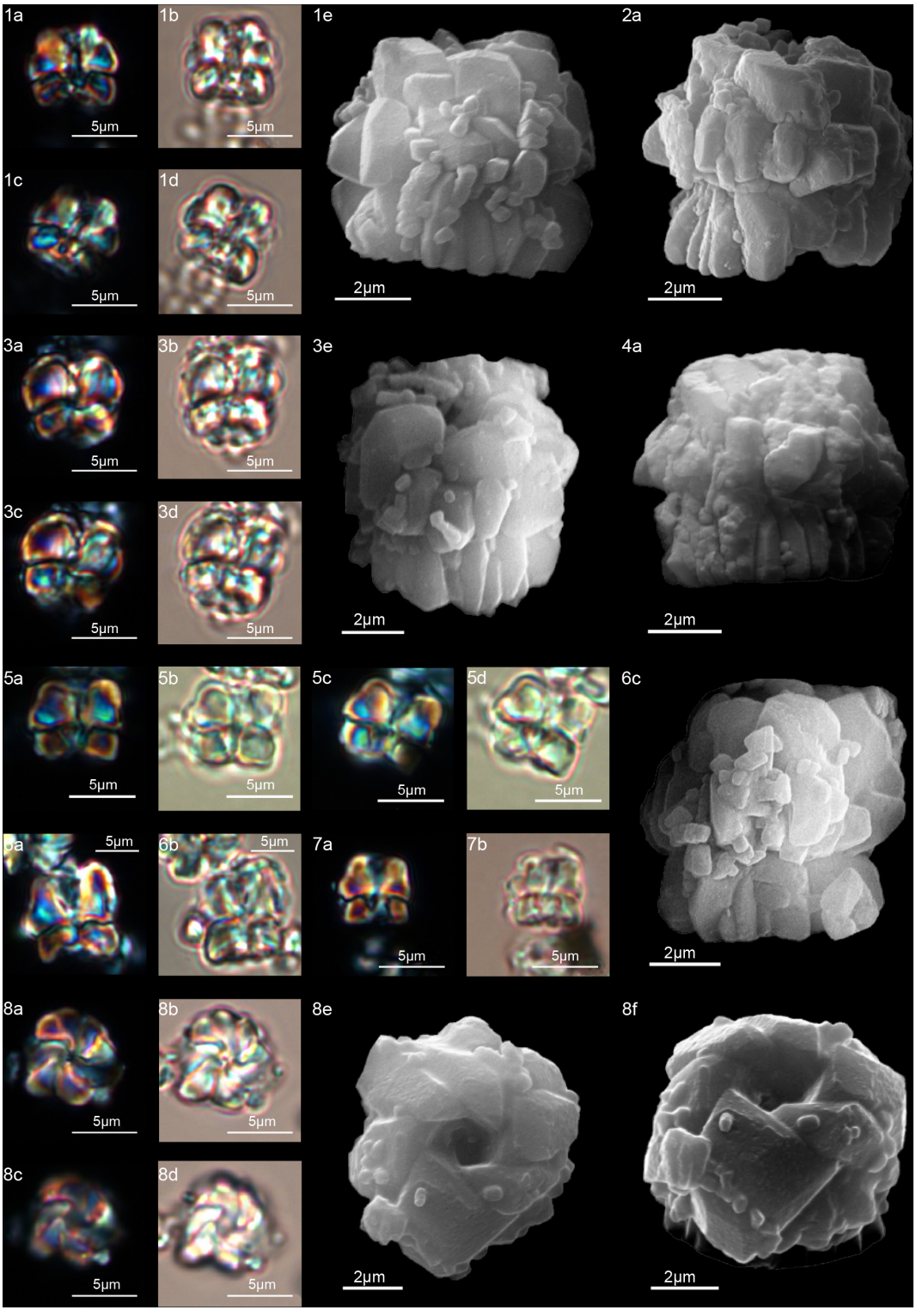

Figure 13. *Diantholitha pilula*. **(1)** Holotype (IGF 104335). Sample: 1209C 14-1, 116–117. **(1a, c)** XPL, **(1b, d)** PPL, **(1e)** SEM. **(2)** Sample: 1262C 11-2, 56–57. **(2a)** SEM. **(3)** Sample: 1209C 14-1, 116–117. **(3a, c)** XPL, **(3b, d)** PPL, **(3e)** SEM. **(4)** Paratype (IGF 104719). Sample: 1262C 11-2, 56–57. **(4a)** SEM. **(5)** Sample: 1209C 14-2, 50–51. **(5a)** XPL, **(5b)** PPL. **(6)** Sample: 1209 14-1, 116–117. **(6a)** XPL, **(6b)** PPL, **(6c)** SEM. **(7)** Sample: 1209C 14-2, 50–51. **(7a)** XPL, **(7b)** PPL. **(8)** Sample: 1209 14-1, 116–117. Distal view. **(8a, c)** XPL, **(8b, d)** PPL, **(8e)** SEM, **(8f)** SEM rotated 40°. See Table S1 for sample details.

Repository

Geological and Paleontological Museum, University of Florence. Holotype number: IGF 104335; sample IGF 104820-1. Paratype inventory number: IGF 104719; sample IGF 104719-1.

Type locality

ODP Site 1209 (Shatsky Rise, central Pacific).

Type level

Sample ODP 1209C-14-1, 116–117.

Age

Late Danian.

Description

Form composed of a solid column with vertical and closely arranged elements (Fig. 13:1–4). The column is smaller than the biretta, with vertical sides and a closed or narrow concavity in the proximal surface. The biretta consists of two cycles (inner and outer). The inner cycle is made up of massive vertical elements with anticlockwise imbrication that form the central opening (Fig. 13:8a–f). The outer cycle is composed of massive trihedral elements that are slightly wedge-shaped in the lower part of the inner cycle (Fig. 13:1–4). In the LM, *D. pilula* has a rounded outline (Fig. 13:1a–d, 3a–d) reminiscent of a hot-air balloon.

Dimensions of the holotype

Total height: 6.5 µm; column height 2.5 µm, width 6 µm; biretta height 4 µm, width 7 µm.

Occurrence of the holotype

Middle zone NP4; CNP 5 zone.

Remarks

Diantholitha pilula differs from *D. mariposa* in having a rounded corolla instead of a butterfly corolla and the biretta about twice the column.

Diantholitha pilula differs from *D. magnolia* in having a column with vertical sides and a biretta with the inner cycle slightly taller than the outer cycle.

Diantholitha toquea n. sp. (Fig. 11:7–11)

Derivation of name

From the Breton word "toque" meaning hat, a reference to the outline of this nannolith that is similar to the "toque blanche" (white hat) worn by chefs.

Diagnosis

Form composed of a column with vertical elements and a massive and rounded biretta.

Holotype

Figure 11:7a.

Paratype

Figure 11:9.

Repository

Geological and Paleontological Museum, University of Florence. Holotype number: IGF 104720; sample IGF 104720-1. Paratype number: IGF 104721; sample IGF 104721-1.

Type locality

ODP Site 1262C (Walvis Ridge, Atlantic Ocean; 27°15′ S, 1°62′ E).

Type level

Sample ODP 1262C-11-2, 56–57.

Age

Late Danian.

Description

The column is composed of vertical and tightly arranged elements with vertical lateral sides and a wide concavity on the proximal face. The biretta is monocyclic, composed of approximately eight massive vertical elements and shaped like a clove of garlic. The biretta has a rounded outline with a height 1.5 or 2 times that of the column, and it extends well beyond the perimeter of the column (Fig. 11:7a–11c).

In side view, the column and the tall rounded biretta resemble a chef's hat. Viewed from the distal side, the elements form a broad central opening (Fig. 11:8a).

In the LM (Fig. 11:9–11b), the vertical sides of the column and the prominent, round biretta with a narrow central canal are easily identifiable.

Dimensions of the holotype

Total height 6 µm; column height 2 µm, width 5 µm; biretta height 4 µm, width: 6 µm.

Occurrence of the holotype

Middle zone NP4; zone CNP 5.

Remarks

Diantholitha toquea differs from *D. pilula* in having a monocyclic biretta with a height twice that of the column and a less rounded outline. *Diantholitha toquea* differs from *D. alata* in having a more massive and more rounded monocyclic biretta.

Lithoptychius (Aubry in Aubry et al., 2011) emend.

(Figs. 15–19)

Type species

Lithoptychius ulii (Perch-Nielsen, 1971) Aubry et al., 2011.

Emended definition

Lithoptychius is composed of three structural units: column, collaret and calyptra (Fig. 14). The cylindrical column is the proximal unit and consists of 20–24 vertical wedge-shaped elements. The sides of the column are parallel or flare slightly in the distal direction. The proximal face is concave, whereas the distal surface is flat or convex. The crown-shaped calyptra overlies the column and consists of vertical elements with a clockwise imbrication. The calyptra can be narrower than the column or it can be similar in width. In XPL, the calyptra can be domed, mushroom-shaped or crater-shaped (Fig. 14). A central canal is always present, and it is generally broad. The central canal runs through both the calyptra and the column.

The collaret consists of a disk or "collar" of radially arranged elements that enclose as a ring the distal part of the column and/or the lowermost part of the calyptra. The collaret typically consists of a cycle of elements with an anticlockwise or rarely clockwise imbrication. It can sometimes have a shelf-and-bracket shape.

In the LM, the collaret is generally thicker laterally than centrally. The height of the collaret can be the same as or lower than that of the calyptra. In the SEM, the collaret is visually prominent and extends beyond the periphery of both the column and the calyptra, but it can also be narrower than the column (e.g., *L. ulii, L. varolii*; Figs. 18:4; 19:1). The lateral sides of the collaret can be vertical or flare markedly in the distal direction. It is composed of overlapping wedge-shaped elements with low-angle oblique sutures and anticlockwise imbrication or of small contiguous "parallelepipeds". The collaret can show a shelf-angle bracket shape or a squared cycle; the number of the elements is usually the same as that of the column.

Remarks

A well-developed collaret is typically observed in forms with tapering column sides (i.e., *L. collaris*, *L. felis*, *L. schmitzii*), whereas a thin collaret (that surrounds only the lower part of the calyptra) is generally present in forms with parallel column sides (i.e., *L. ulii*, *L. varolii*). In the LM, a central canal that goes through both the column and calyptra when focus is on the axial part of the column is clearly seen. The collaret appears as two separated segments placed laterally on the distal end of the column (Figs. 15:4b, d; 16:7a, 9a; 17:2b, 10a–10c, 11a). This is due to the disk and/or ring shape of the collaret. Focusing upwards, the central canal decreases in width and the collaret appears to be continuous between the column and calyptra (Figs. 15:6a–c; 16:5a–e, 8b–d; 17:1b–e, 11a–b; 18:3b–e). The arrangement of the column, calyptra and enclosing collaret is also evident in SEM photos. In particular, specimens with a partially removed collaret clearly illustrate that the elements of the calyptra lie proximally on the column (Fig. 16:1a). As a consequence of the newly described structural arrangements, the original definition of *Lithoptychius* (Aubry et al., 2011) is emended herein. The collaret is the main feature that distinguishes *Lithoptychius* from other fasciculiths.

Lithoptychius collaris (Aubry and Rodriguez in Aubry et al., 2011) emend.

(Fig. 15:4–6)

2009 *Fasciculithus* sp. 2 Bernaola et al.: fig. 4, figs. S–U.
2011 *Lithoptychius collaris* Aubry and Rodriguez in Aubry et al., 2011; Aubry et al.: pl. 4, figs. 1a–2d.
2017 *Lithoptychius collaris* Aubry and Rodriguez in Aubry et al., 2011; Criscione et al.: p. 5, pl. 2, figs. 8, 10, 11.

Emended description

The column, composed of approximately 20 tightly vertical wedge-shaped elements, is slightly taller than the calyptra (Fig. 14). The sides of the column vary from vertical to flaring in the distal direction; they are gently concave proximally and convex on the distal face. The collaret is prominent, extending beyond the periphery of both the column and the calyptra, and it is made up of elongated, radially arranged elements with anticlockwise imbrication (Fig. 15:4a). The collaret has a shelf-angle bracket shape. The number of elements equals that of the column. The sides of the collaret markedly flare in distal direction but the collaret has a flat distal surface (Fig. 15:4a, 5a, 6a). The collaret, together with the column, has the shape of a doric column. In SEM, a few specimens show a (lower) cycle of scattered elements around the base of the calyptra (Fig. 15:5a, 6a). It is difficult to assess if this is real or linked to recrystallization, and it is not detectable with the SEM. The calyptra has vertical sides and its diameter can be as large as the column. The elements of the calyptra show a clockwise imbrication (Fig. 15).

Measured dimensions

Total height 4.9–5.7 µm; column height 2–2.2 µm, proximal width 3.9–4.7 µm, distal width 4.3–5 µm; collaret height 1–1.5 µm, width 4.3-5 µm; calyptra height 1.8–2–2 µm, width: 3.4–4.5 µm.

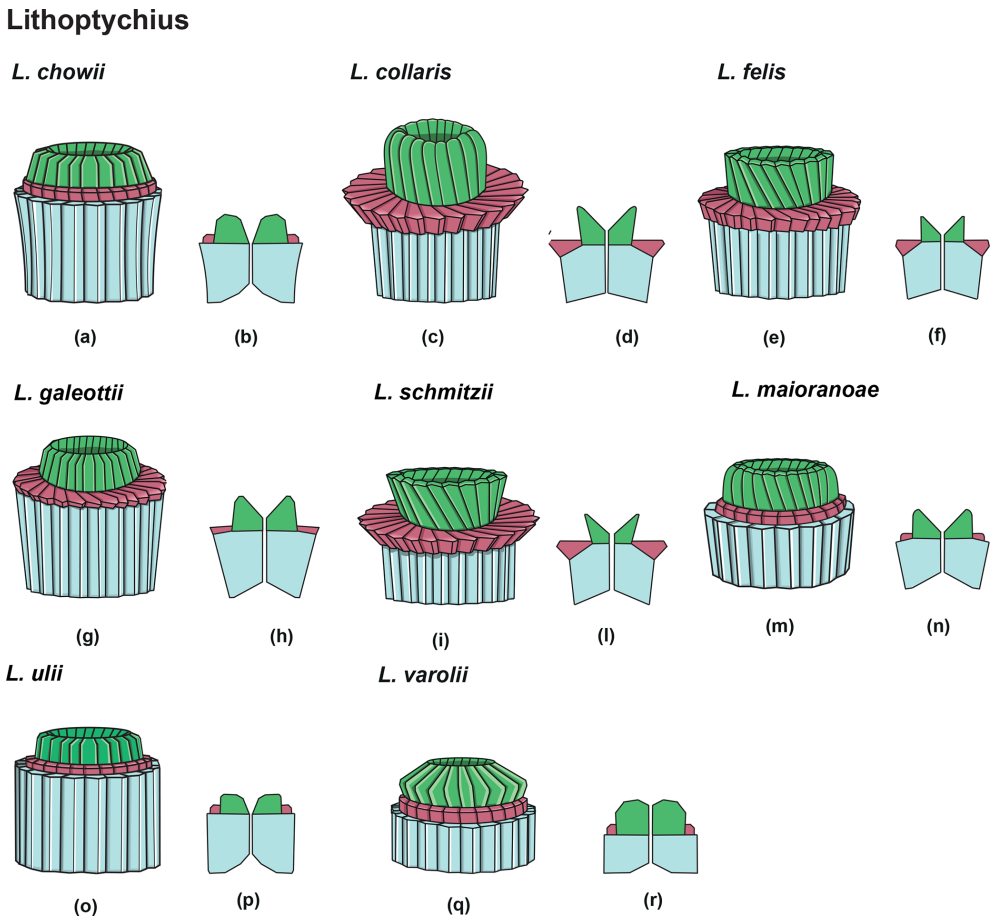

Figure 14. Overview of *Lithoptychius*: column (light blue), collaret (red) and calyptra (green). **(a)** Schematic drawing of the type species *L. chowii*. **(b)** Schematic cross section of *L. chowii*. **(c)** Schematic drawing of *L. collaris*. **(d)** Schematic cross section of *L. collaris*. **(e)** Schematic drawing of *L. felis*. **(f)** Schematic cross section of *L. felis*. **(g)** Schematic drawing of *L. galeottii*. h) Schematic cross section of *L. galeottii*. **(i)** Schematic drawing of *L. schmitzii*. **(l)** Schematic cross section of *L. schmitzii*. **(m)** Schematic drawing of *L. maioranoae*. **(n)** Schematic cross section of *L. maioranoae*. **(o)** Schematic drawing of *L. ulii*. **(p)** Schematic cross section of *L. ulii*. **(q)** Schematic drawing of *L. varolii*. **(r)** Schematic cross section of *L. varolii*.

Biozone occurrence of the studied specimens

Middle part of zone NP4; upper zone CNP5.

Remarks

Lithoptychius collaris differs from *L. felis* in having a shorter column, a wider concave proximal face, a wider collaret, a taller calyptra and a narrower central canal.

Lithoptychius chowii (Varol, 1989) Aubry in Aubry et al., 2011.

(Fig. 15:1–3)

1989 *Fasciculithus chowii* Varol: p. 297, pl. 12.5, figs. 11–13.
2008 *Fasciculithus ulii* Perch-Nielsen, 1971; Steurbaut and Sztrákos: p. 20, pl. II, figs. 19, 20.
2010 *Fasciculithus vertebratoides* Steurbaut and Sztrákos, 2008; Dinarès-Turrel et al.: pl. II, figs. 9, 10.
2010 *Fasciculithus ulii* Perch-Nielsen, 1971; Dinarès-Turrel et al.: pl. II, fig. 12 ; pl. III, fig.1.
2010 *Fasciculithus* transitional Dinarès-Turrel et al.: pl. II, fig. 15.
2010 *Fasciculithus* sp. 2 Dinarès-Turrel et al.: pl. II, fig. 17.
2010 *Fasciculithus* sp. Dinarès-Turrel et al.: pl. II, figs. 19, 20.
2010 *Fasciculithus ulii minor* Perch-Nielsen, 1971; Dinarès-Turrel et al.: pl. III, figs. 2–5.
2011 *Lithoptychius ulii* (Perch-Nielsen, 1971) Aubry in Aubry et al., 2011; Aubry et al.: pl. 8, figs. 4a–d.
2012 *Lithoptychius chowii* (Varol, 1989) Aubry in Aubry et al., 2011; Monechi et al.: pl. 4, figs. 1, 2.

Measured dimensions

Total height 4.3–6.5 µm; column height 2.5–4.2 µm, proximal width 3.8–5.3 µm, distal width 4.3–6.6 µm; collaret

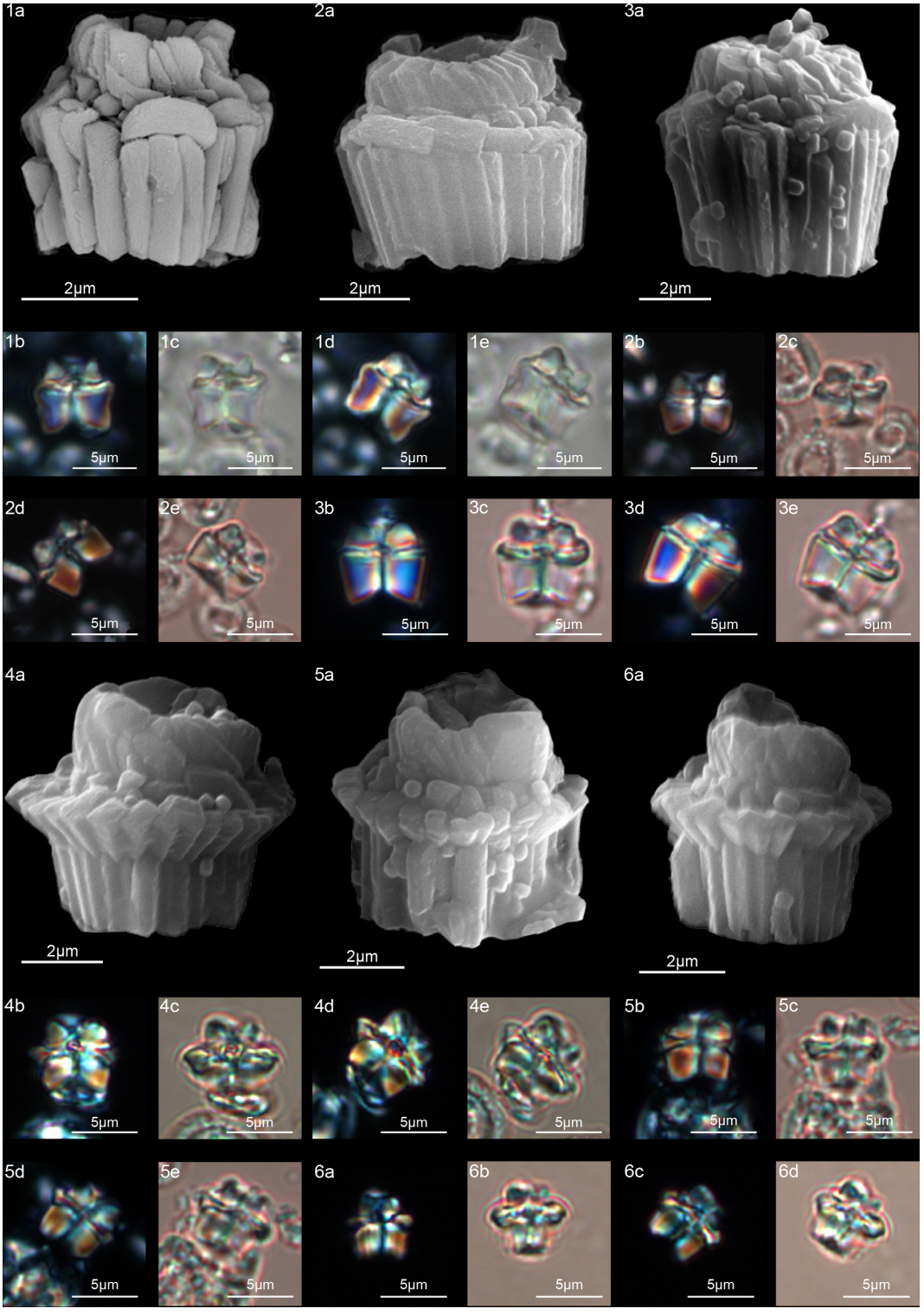

Figure 15. *Lithoptychius chowii.* **(1)** Sample: 1209C 14-1, 56–57. **(1a)** SEM, **(1b, d)** XPL, **(1c, e)** PPL. **(2)** Sample: 1209C 14-1, 56–57. **(2a)** SEM, **(2b, d)** XPL, **(2c, e)** PPL. **(3)** Sample: 1209C 14-1, 84–85. **(3a)** SEM, **(3b, d)** XPL, **(3c, e)** PPL. *Lithoptychius collaris*. **(4)** Sample: 1209C 14-1, 116–117. **(4a)** SEM, **(4b, d)** XPL, **(4c, e)** PPL. **(5)** Sample: 1209C 14-1, 1160–117. **(5a)** SEM, **(5b, d)** XPL, **(5c, e)** PPL. **(6)** Sample: 1209C 14-1, 116–117. **(6a)** SEM, **(6b, d)** XPL, **(6c, e)** PPL. See Table S1 for sample details.

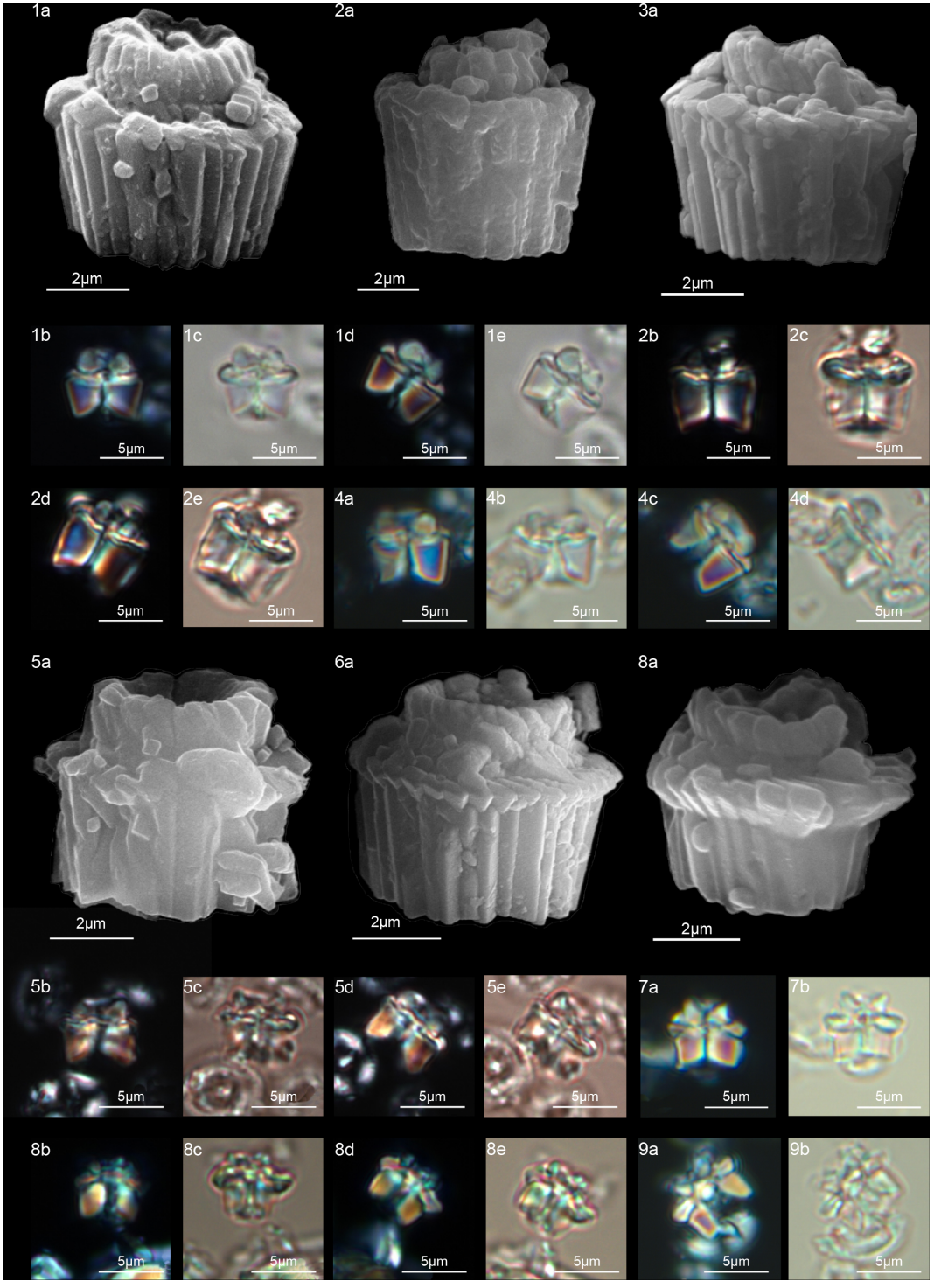

Figure 16. *Lithoptychius galeottii*. **(1)** Holotype (IGF 104722). Sample: 1209C 14-1, 56–57. **(1a)** SEM, **(1b, d)** XPL, **(1c, e)** PPL. **(2)** Paratype (IGF 104723). Sample: 1209B-24-5, 8–9. **(2a)** SEM, **(2b, d)** XPL, **(2c, e)** PPL. **(3)** Sample: 1267B 29-5, 84–85. SEM. **(4)** Sample: 1267 B 29-5, 84–85. **(4a, c)** XPL, **(4b, d)** PPL. *Lithoptychius felis*. **(5)** Sample: 1209C 14-1, 56–57. **(5a)** SEM, **(5b, d)** XPL, **(5c, e)** PPL. **(6)** 1262C 10-6, 23–24. SEM. **(7)** Sample: 1209C 14-1, 116–117. **(7a)** XPL, **(7b)** PPL. *Lithoptychius schmitzii*. **(8)** Sample: 1209C 14-1, 84–85. **(8a)** SEM, **(8b, d)** XPL, **(8c, e)** PPL. **(9)** Sample: 1209C 14-1, 80–81. **(9a)** XPL, **(9b)** PPL. See Table S1 for sample details.

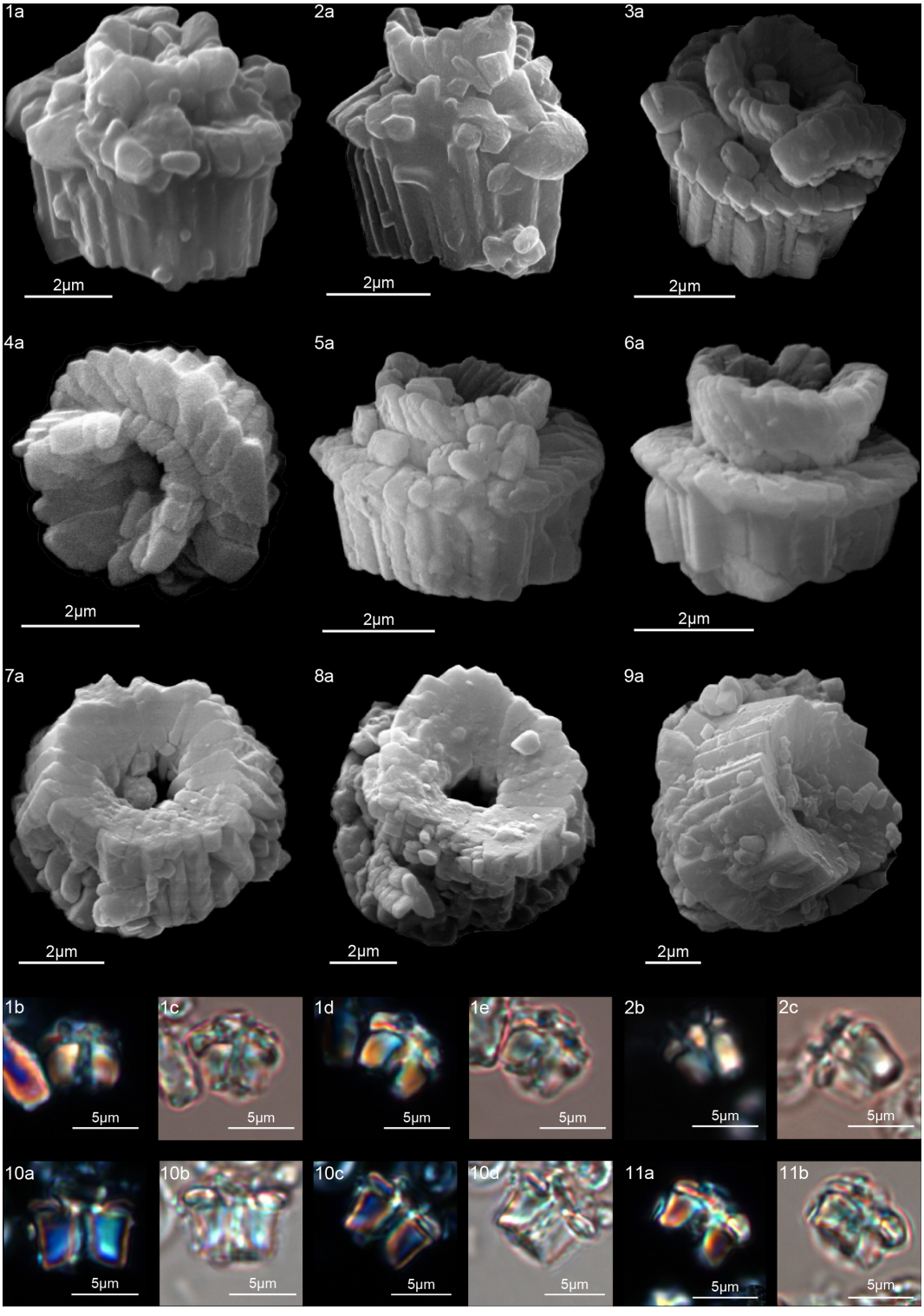

Figure 17. *Lithoptychius schmitzii*. **(1)** Sample: 1209C 14-1, 84–85. **(1a)** SEM, **(1b, d)** XPL, **(1c, e)** PPL. **(2)** Sample 1209C 14-1, 56–57. **(2a)** SEM, **(2b)** XPL, **(2c)** PPL. **(3)** Sample: 1267B 29-5, 84–85. **(3a)** SEM, distal view. **(4)** Sample: 1209C 14-1, 84–85. **(4a)** SEM, distal view. **(5)** Sample: 1262C 10-6, 23–24. **(5a)** SEM. **(6)** Sample: 1262C 10-6, 23–24. **(6a)** SEM. **(7)** Sample: 1267B 29-5, 84–85. **(7a)** SEM, proximal view. **(8)** Sample: 1267B 29-5, 84–85. **(8a)** SEM, proximal view. **(9)** Sample: 1262C 10-6, 23–24. **(9a)** SEM, proximal view. **(10)** Sample: 1262C 10-6, 23–24. **(10a, c)** XPL, **(10b, d)** PPL. **(11)** Sample: 1262C 10-6, 23–24. **(11a)** XPL, **(11b)** PPL. See Table S1 for sample details.

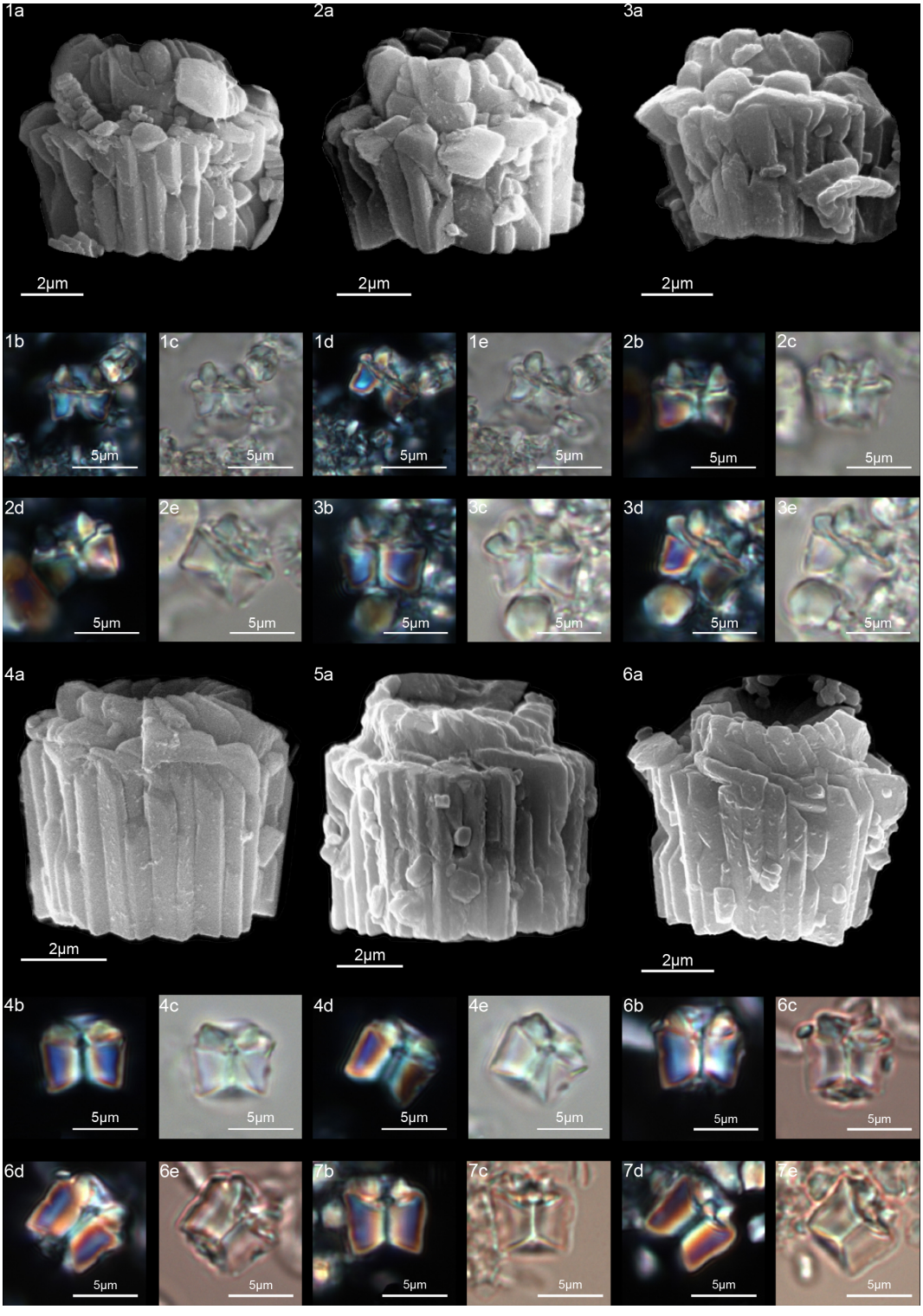

Figure 18. *Lithoptychius maioranoae*. **(1)** Paratype (IGF 104725). Sample: 1209C 14-1, 56–57. **(1a)** SEM, **(1b, d)** XPL, **(1c, e)** PPL. **(2)** Holotype (IGF 104724). Sample: 1209C 14-1, 56–57. **(2a)** SEM, **(2b, d)** XPL, **(2c, e)** PPL. **(3)** Sample: 1209C-14-1, 56–57. **(3a)** SEM, **(3b, d)** XPL, **(3c, e)** PPL. *Lithoptychius ulii*. **(4)** Sample: 1209C 14-1, 56–57. **(4a)** SEM, **(4b, d)** XPL, **(4c, e)** PPL. **(5)** Sample: 1267A 29-1, 60–61. **(5a)** SEM. **(6)** Sample: 1209C 14-1, 56–57. **(6a)** SEM, **(6b, d)** XPL, **(6c, e)** PPL. **(7)** Sample: 119 37-4, 135–136. **(7a, c)** XPL, **(7b, d)** PPL. See Table S1 for sample details.

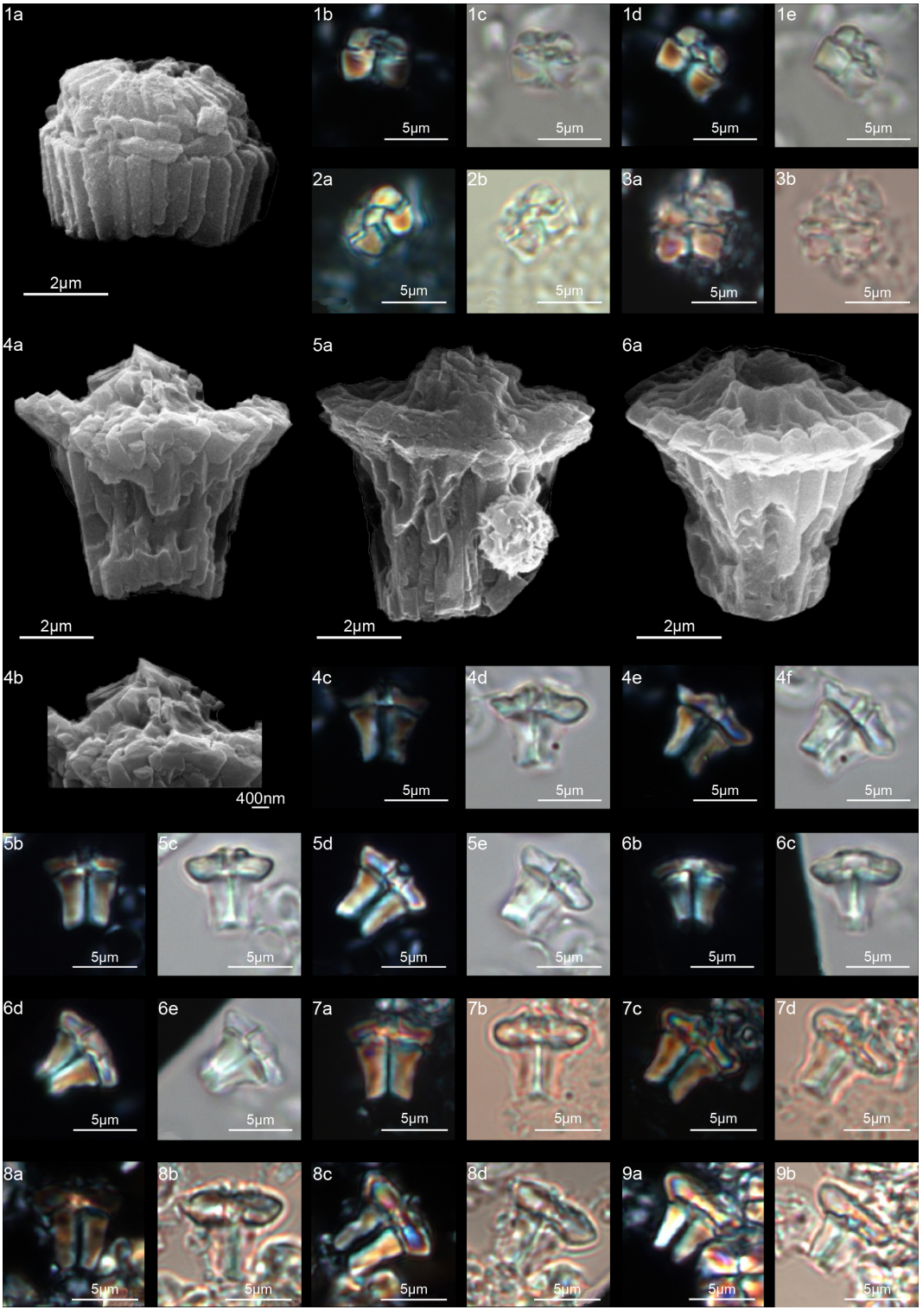

Figure 19. *Lithoptychius varolii*. **(1)** Sample: 1209C 14-1, 56–57. **(1a)** SEM, **(1b, d)** XPL, **(1c, e)** PPL. **(2)** Sample: 1209C 14-1, 56–57. **(2a)** XPL, **(2b)** PPL. **(3)** Sample: Contessa Road 9.50 m (above the K–Pg boundary). **(3a)** XPL, **(3b)** PPL. *Tectulithus janii*. **(4)** Sample: 356Z 23R-1W, 70–71. **(4a)** SEM, **(4b)** SEM, detail of tectum. **(4c, e)** XPL, **(4d, f)** PPL. **(5)** Sample: 356Z 23R-1W, 70–71. **(5a)** SEM, **(5b, d)** XPL, **(5c, e)** PPL. **(6)** Sample: 356Z 23R-1W, 70–71. **(6a)** SEM, **(6b, d)** XPL, **(6c, e)** PPL. **(7)** Sample: 356Z 23R-1W, 70–71. **(7a, c)** XPL, **(7b, d)** PPL. **(8)** Sample: 1209B 24-5, 8–9. **(8a, c)** XPL, **(8b, d)** PPL. **(9)** Sample: 1209B 24-5, 8–9. **(9a)** XPL, **(9b)** PPL. See Table S1 for sample details.

height 0.7–0.9 µm, width: 3.8–5.8 µm; calyptra height 1.1–1.7 µm, width 4.3–5.1 µm.

Biozone occurrence of the studied specimens

Middle part of zone NP4; upper zone CNP5.

Remarks

In SEM, *L. chowii* shows a column with slightly flaring lateral sides that narrow towards the base of the column (Fig. 15:1–3). The column has a thin collaret narrower than the column periphery. The calyptra is composed of elements with a slightly clockwise imbrication that forms a central opening. The calyptra is tall and narrower than the column and collaret. According to the original description of Varol (1989) the calyptra has a height almost equal to half of the column. In the LM, a thin extinction line divides the collaret from the column, and the collaret is easily recognizable in XPL when the specimen is oriented at 45° (Monechi et al., 2012). Varol (1989) concluded that "a straight contact between column and cone" was a main feature of *L. chowii*. This characteristic is clearly visible in Fig. 15:2b and 3b, but depending on the focus length the straight contact line can become curved (Fig. 15:1d, 2d, 3c). A central canal is present and runs through the column and calyptra. The central body does not exist.

Lithoptychius chowii differs from *L. varolii* in having a shorter calyptra and from *L. maioranoae* in having a column that is taller than it is wide, with a calyptra having a narrow central opening.

Lithoptychius felis Aubry and Bord in Aubry et al., 2011

(Fig. 16:5–7)

2010 *Fasciculithus* sp. 2/sp. 3 or sp. 4 Dinarès-Turrel et al.: pl. V, figs. 9–16.
2011 *Lithoptychius felis* Aubry and Bord in Aubry et al., 2011; Aubry et al.: pl. 5, figs. 1a–4d, not 5a–d.
2019 *Lithoptychius felis* Aubry and Bord in Aubry et al., 2011; Aubry et al.: pl. I, 18.

Measured dimensions

Total height 5.2–5.5 µm; column height: 2.4–2.8 µm, proximal width 4.9–5.5 µm, distal width 5–5.6; collaret height: 0.7–1.1 µm, width 6.1–6.3 µm; calyptra height 1.7–2 µm; calyptra width 3.9–4.7 µm.

Biozone occurrence of the studied specimens

Middle part of zone NP4; upper zone CNP5.

Remarks

The column has parallel or slightly flaring sides. The collaret is broader than the column, and it is made up of radially arranged elements with anticlockwise imbrication. The sides of the collaret vary from vertical to rounded, and the distal surface is mainly flat. In SEM, the collaret shows the same number of elements as that of the column. In the LM, the collaret appears as a disk-shaped cycle. The calyptra has the shape of an open corolla, and it is half as high as the column, with a wide central opening. According to the holotype photos (Aubry et al., 2011, pl. 5, figs. 1a–1d), *L. felis* has a calyptra narrower than the collaret and the column, which is in contrast with the original description of the species (Aubry et al., 2011) that the calyptra has the same diameter as the column. The column has an easily recognizable central canal (Fig. 16:5b–e); a central body is absent.

Lithoptychius felis , differs from *L. collaris* , in having a thinner collaret that extends only slightly past the column and a more open calyptra. *Lithoptychius schmitzii* , differs from *L. felis* in having a wider central canal and a reduced calyptra.

Lithoptychius galeottii n. sp.

(Fig. 16:1–4)

1977 *Fasciculithus ulii* Perch-Nielsen, 1971: pl. 14, figs. 17–18

Derivation of name

Named after Simone Galeotti (Università degli Studi di Urbino Carlo Bo, Italy), stratigrapher.

Holotype

Figure 16:1.

Paratype

Figure 16:2.

Repository

Geological and Paleontological Museum, University of Florence. Holotype number: IGF 104722; sample IGF 104724-1. Paratype number: IGF 104723; sample IGF 104723-1.

Type locality

ODP Site 1209 (Shatsky Rise, central Pacific).

Type level

Sample 1209C 14-1, 56–57.

Age

Late Danian.

Description

Lithoptychius composed of a compact column taller than both the collaret and calyptra (Fig. 16:1–4). The column sides are gently flaring in the distal direction. The thin collaret overlies the distal face of the column. The collaret consists of low elements extending laterally just beyond the periphery of the column and showing anticlockwise imbrication. In XPL, the collaret is easily recognizable when the specimen is oriented at 45° (Fig. 16:1d, 2d, 4c). The calyptra is cylindrical, extended and narrower than both the collaret and the column. The sides of the calyptra are typically parallel. A central canal runs through the entire length of the column and the calyptra. The new observations under both LM and SEM show that the specimen of *L. ulii* shown in pl. 14, figs. 17–18 by Perch-Nielsen (1977) cannot be assigned to *L. ulii*, but it can be related to *L. galeottii* for the flaring sides of the column and the well-extended calyptra.

Dimensions of the holotype

Total height 5.5 µm; column height, proximal width 5 µm, distal width 6 µm; collaret height: 0.5 µm, width 6.5 µm; calyptra height 2.5 µm, width 4.3 µm.

Occurrence of the holotype

Upper part of zone NP4; upper zone CNP5.

Remarks

Lithoptychius galeottii differs from *L. felis* in having a thinner and less extended collaret. It differs from *L. ulii* in having a collaret wider than the column and a cylindrical and extended calyptra. It differs from *L. schmitzii* in having a thinner and less prominent collaret and a narrower axial canal.

Lithoptychius maioranoae n. sp.

(Fig. 18:1–3)

2010 *Fasciculithus* sp. 3 Dinarès-Turrel et al.: pl. II, fig. 11.

Derivation of name

Named after Patrizia Maiorano (Università degli Studi di Bari, Italy), nannopaleontologist.

Diagnosis

Lithoptychius with a thin collaret and a wide calyptra overlapping a wide column.

Holotype

Figure 18:2a.

Paratype

Figure 18:1.

Repository

Geological and Paleontological Museum, University of Florence holotype number: IGF 104724; sample IGF 104724-1; paratype number: IGF 104725; sample IGF 104724-1.

Type locality

ODP Site 1209 (Shatsky Rise, western Pacific; 32°39′ N, 158°31′ E).

Type level

Sample ODP 1209C 14-1, 56–57.

Age

Late Danian.

Description

Lithoptychius maioranoae has a column that is wider than it is tall with sides that slightly flare in the distal direction. The proximal face is deeply concave and has a well-developed central canal. The column is surmounted by a thin collaret, often slightly larger than the column periphery. The calyptra consists of vertical to slightly imbricated elements, and its height is about half that of the column. The elements form a wide central opening (Fig. 18:1). In the LM, the collaret is difficult to see (Fig. 18:1b–e, 2b–e, 3b–e), and the extinction line between the collaret and calyptra varies from straight to slightly concave.

Dimensions of the holotype

Total height 5.5 µm; column height 3 µm, proximal width 6 µm, distal width 6.8 µm; collaret height 0.5 µm, width 7 µm; calyptra height 1.5 µm, width 4.3 µm.

Occurrence of the holotype

Middle zone NP4; upper zone CNP5.

Remarks

Lithoptychius maioranoae differs from *L. felis* in having a thin collaret, slightly larger than the column, and a wider calyptra. It differs from *L. ulii* in having a shorter and wider column. Unfortunately, the preservation of the observed specimens is not very good due to recrystallization.

Lithoptychius schmitzii Monechi et al., 2012

(Figs. 16:8–9; 17:1–11)

2009 *Fasciculithus* sp. 3 – Bernaola et al.: figs. 5/A–D.
2011 *Lithoptychius* sp. 1 – Aubry et al.: pl. 7, figs. 1a–d, 2a–d, 3a–d, 4a, b, 5a–c, 6a–c.
2011 *Lithoptychius* sp. 2 – Aubry et al.: pl. 8, figs. 1a–d.
2012 *Lithoptychius schmitzii* Monechi et al., 2012; Monechi et al.: pl. 3, figs. 3–5.
2013 *Lithoptychius schmitzii* Monechi et al., 2012; Monechi et al.: pl. 1, figs. 8–9, 11–14.
2016 *Lithoptychius schmitzii* Monechi et al., 2012; Bown: p. 23, pl. 8, figs. 38–40.
2019 *Lithoptychius schmitzii* Monechi et al., 2012; Metwally: pl. I, figs. 21–22.

Measured dimensions

Total height 3.5–8 µm; column height 1.2–4.4 µm, proximal width 3.9–6.3 µm, distal width 4.3–7.1; collaret height 0.9–2 µm, width 4.9–8.1 µm; calyptra height 1.1–2, width 3–4.4 µm.

Biozone occurrence of the studied specimens

Middle zone NP4; upper zone CNP5.

Remarks

The SEM photos show a column composed of vertical wedge-shaped, radially arranged elements with lateral sides slightly flaring in the distal direction. The proximal face is concave with a wide central opening (Fig. 17:7a, 8a, 9a). The collaret consists of a prominent cycle of sub-horizontal elements with anticlockwise imbrication extending beyond the periphery of the column. The sides of the collaret can vary from flaring laterally to sub-vertical. Its distal surface is almost flat (Fig. 17:5a, 6a), but some specimens with downward-tilted elements can occur (Fig. 17:2). The low and open calyptra has a broad central canal, and the sides flare gently in the distal direction. The elements of the calyptra show anticlockwise imbrication (Fig. 17:3a). In the LM, in lateral view, the column is slightly flaring in the distal direction and is surmounted by a well-developed collaret. A wide central canal passes through the column and calyptra.

Lithoptychius schmitzii differs from *L. collaris* in having a less prominent collaret and a lower and more flaring calyptra.

Lithoptychius ulii (Perch-Nielsen, 1971) Aubry in Aubry et al., 2011

(Fig. 18:4–7)

1971 *Fasciculithus ulii* Perch-Nielsen: pl. 2, fig. 3.
2009 *Fasciculithus ulii* Perch-Nielsen, 1971; Bernaola et al.: fig. 4, fig. R; fig. 5, fig. L.
2012 *Lithoptychius ulii* (Perch-Nielsen, 1971) Aubry in Aubry et al., 2011; Monechi et al.: pl. 3, figs. 16–19.

Measured dimensions

Total height 6.2–7.7 µm; column height 4.3–5.3 µm, proximal width 5.5–7.6 µm, distal width 6.2–8 µm; collaret height 0.7–0.8 µm, width 5.7–6.8 µm; calyptra height 1–1.5 µm, width 3.6–5.7 µm.

Biozone occurrence of the studied specimens

Middle zone NP4; upper zone CNP5.

Remarks

According to Perch-Nielsen (1971), the holotype of *L. ulii* is characterized by a column with parallel sides (her pl. 2, fig. 3). A low and lateral reduced collaret surmounts the column. It is made up of a cycle of low elements that tightly surrounds the calyptra. In SEM, the collaret shows the same number of elements as that of the column (Perch-Nielsen, 1971, pl. 2, fig. 3). In this study, only very rare specimens similar to the holotype (Perch-Nielsen, 1971) have been found. Indeed, our specimens usually show vertical column sides (Fig. 18:4a, 5a) and only rarely slightly flaring sides (Fig. 18:6a). The calyptra is low and narrower than the column with an almost flat distal surface. The elements of the calyptra show clockwise imbrication, and an easily recognizable central opening is present. Due to its reduced height, the collaret can be difficult to distinguish in the LM and SEM. Furthermore, in poorly preserved material the collaret is recrystallized or absent. Thus, the calyptra and the collaret can appear as a single cone showing a rounded shape in the LM compared to what is observed in the SEM. The collaret and calyptra together have a height about one-third of the column height. A central canal is present and passes through the column and the calyptra. *Lithoptychius ulii* differs from *L. chowii* in having a column with parallel sides and a lower and flatter calyptra ("height almost equal to half of the column").

Lithoptychius varolii (Steurbaut and Sztrákos, 2008) Aubry in Aubry et al., 2011

(Fig. 19:1–3)

2008 Steurbaut and Sztrákos: pl. II, figs. 17, 18.
2010 *Fasciculithus* sp. 2 or sp. 3 Dinarès-Turrel et al.: pl. V, figs. 17–19.
2011 *Lithoptychius varolii* Aubry in Aubry et al., 2011; Aubry et al.: p. 273, pl. 9, figs. 1–4.

Measured dimensions

Total height 4.1–5.9 µm; column height 1.8–2.5, proximal width 3.7–4.9 µm, distal width 5–5.5 µm; collaret height 0.7–1 µm; calyptra height 1.2–2.3 µm, width: 4.4–5.4 µm.

Biozone occurrence of the studied specimens

Lithoptychius varolii is rare. It occurs in middle zone NP4 and upper zone CNP5.

Remarks

In SEM, *L. varolii* shows a wider than tall column with a thick collaret narrower than the column. The calyptra is composed of polygonal tilted elements with a clockwise imbrication (Fig. 19:1a). The contact between the calyptra and the collaret is a sharp angle, giving specimens an overall mushroom-like appearance in the LM (Fig. 19:1b, 2a). A wide central canal passes through the calyptra and the column.

Lithoptychius varolii differs from *L. maioranoae* in having a collaret narrower than the column and a more rounded calyptra with a smaller central opening.

Tectulithus new gen.

(Figs. 19–23)

Type species

Tectulithus merloti (Pavšic, 1977) n. comb.

Descriptions

Cylindrical forms made up of a column and a tectum (Fig. 20). The column is cylindrical and can have a narrow waist or can flare distally. It is composed of wedge-shaped, radially arranged elements. Its proximal surface is always concave, while the distal surface can be convex or slightly concave. A narrow central canal runs through the vertical axis. The tectum can be composed of one or two cycles. The lower thin cycle of the tectum, if present, lies on the upper end of the column and usually consists of wedge-shaped elements supporting the upper cycle of the tectum (tectum s.s.) (Fig. 20d). The upper cycle is always present, and it is composed of either radial elements with a clockwise arrangement (Fig. 20b) that sometimes form a central opening or of wedge-shaped elements that spiral towards the center to form a truncated cone with a central opening (*T. janii*). The tectum, flat or conical, covers the top of the column like a roof, and it can be broader than, narrower than or as large as the periphery of the column. In the LM, the tectum behaves as a single crystallographic unit. It is birefringent and has variable shapes similar to an umbrella, lens or shitake mushroom. In XPL, *Tectulithus* in side view is birefringent with a straight thick dark line bisecting the column. The column and tectum are separated by a curved black line.

Remarks

Tectulithus merloti has been chosen as a type species because of the clear distinction between the column and the flat-cone tectum, which is composed of both an upper tectum s.s. and a lower cycle of wedge-shaped elements. The calyptra of *Lithoptychius* differs from the tectum in being crown-shaped and made up of vertical elements, whereas the tectum is conical or dome-shaped. The lower cycle of the tectum seems to occur only in species in which the tectum is wider than the perimeter of column. In the LM, *Tectulithus* differs from *Lithoptychius* in having two distinct crystallographic units (column and tectum), whereas in *Lithoptychius* three units (column, collaret and calyptra) are visible.

Tectulithus janii (Perch-Nielsen, 1971) n. comb.

(Fig. 19:4–9)

1971 *Fasciculithus janii* Perch-Nielsen: p. 352, pl. 5, figs. 1–4 (not pl. 14, figs. 37–39).
1977 *Fasciculithus janii* Perch-Nielsen, 1971; Perch-Nielsen: p. 748, pl. 12, figs. 2–5, 8–18, (not pl. 49, fig. 26).
1990 *Fasciculithus janii* Perch-Nielsen, 1971; Aubry, p. 132, figs 127-131 (not p. 131, figs. 124–126).
1990 *Fasciculithus bitectus* Romein, 1979; Aubry: p. 130, figs. 122–123 (not fig. 121).
2008 *Fasciculithus janii* Perch-Nielsen, 1971; Steurbaut and Sztrákos: pl. III, fig. 14 (not figs. 11, 13).
2010 *Fasciculithus janii* Perch-Nielsen, 1971; Dinarès-Turrel et al.: Pl. III, figs. 17, 18 (not fig. 16).
2011 *Lithoptichius janii* (Perch-Nielsen, 1971); Aubry in Aubry et al., 2011; Aubry et al.: pl. 8, figs. 2a–d

Measured dimensions

Total height 5.7–7.7 µm; column height 3.6–4.5 µm, proximal width 2.6–3.6 µm, distal width 4.3–5.4 µm; tectum height 2.1–3.2 µm, width: 6.7–7.8 µm.

Biozone occurrence of the studied specimens

Upper zone NP4 and lower zone NP5; zone CNP7.

Emended description

Tectulithus janii is composed of a distally flaring column which narrows slightly in the middle. The column supports the tectum. The lower cycle of the tectum consists of wedge-shaped elements that extend well beyond the column (Fig. 19:4a–b, 5a, 6a). The upper cycle of the tectum is composed of curved elements, and its sides taper distally. In overall morphology, the tectum has a thick external perimeter and

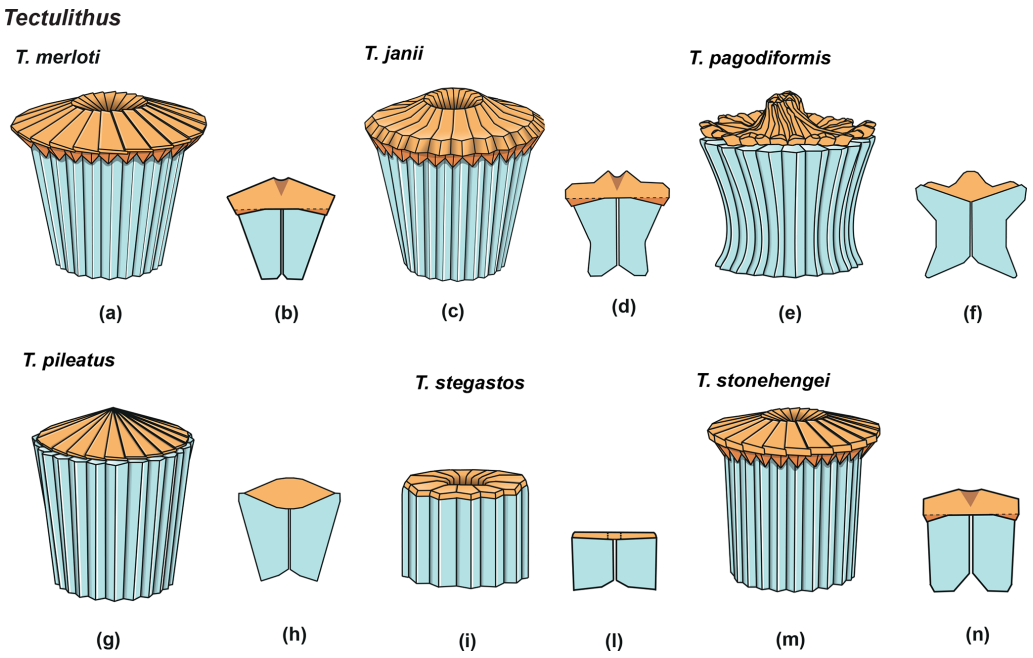

Figure 20. Overview of *Tectulithus* column (light blue) and tectum (orange). **(a)** Schematic drawing of the type species *T. merloti*. **(b)** Schematic cross section of *T. merloti*. **(c)** Schematic drawing of *T. janii*. **(d)** Schematic cross section of *T. janii*. **(e)** Schematic drawing of *T. pagodiformis*. **(f)** Schematic cross section of *T. pagodiformis*. **(g)** Schematic drawing of *T. pileatus*. **(h)** Schematic cross section of *T. pileatus*. **(i)** Schematic drawing of *T. stegastos*. **(l)** Schematic cross section of *T. stegastos*. **(m)** Schematic drawing of *T. stonehengei*. **(n)** Schematic cross section of *T. stonehengei*.

an elevated cone in the middle. The cone is truncated by a central opening (Fig. 19:6). In SEM, the tectum shows a characteristic boat profile. In the LM, the column shows a flared shape and the tectum covers it like a "sombrero" hat. *Tectulithus janii* differs from *T. merloti* in having a more flaring, longer, thinner column and a thinner tectum. In SEM *T. merloti* differs from *T. janii* in having a tectum s.s. with radial elements and a wider central opening.

Tectulithus merloti (Pavšic, 1977) n. comb.

(Fig. 21:3–6)

1977 *Fasciculithus merloti* Pavšic: p. 43, pl. 7, fig. 1; not pl. 7, figs. 2–3.
1979 *Fasciculithus pileatus* Bukry, 1973; Okada and Thierstein: pl. 6, fig. 3a–b.
1979 *Fasciculithus janii* Perch-Nielsen, 1971; Romein: pl. 5, fig. 1.
2008 *Fasciculithus janii* Perch-Nielsen, 1971; Steurbaut and Sztrákos: pl. III, figs. 12–15.
2008 *Fasciculithus pileatus* Bukry, 1973; Fuqua et al.: fig. 10.
2008 *Fasciculithus janii* Perch-Nielsen, 1971; Bernaola et al.: fig. 5, N.
2010 *Fasciculithus janii* Perch-Nielsen, 1971; Dinarès-Turrell et al.: pl. III, fig. 16.
2011 *Lithoptychius merloti* (Pavšic, 1977) Aubry in Aubry et al., 2011; Aubry et al.: p. 273.

Dimensions of the holotype

Total height 4.8–6.2 µm; column height 2.7–4 µm, proximal width 2.7–4.2 µm, distal width 4.2–5.5 µm; tectum height 1.9–2.3 µm, width 6.3–6.7 µm.

Biozone occurrence of the studied specimens

Upper zone NP4; zone CNP7.

Emended description

SEM images of *T. merloti* show a column with a truncated cone-shape and a deep depression in the proximal base (Pavšic, 1977). The column is of variable size and is surmounted by a tectum that extends slightly beyond the perimeter of the column (Fig. 21, figs. 3–6). The lower cycle of the tectum consists of wedge-shaped elements that support the protruding edge of the upper tectum s.s (Fig. 21, fig. 3a). The tectum s.s. is disk-shaped with radial elements showing a clockwise imbrication. The center of the tectum is characterized by a wide central opening. In the LM, the tectum looks like a mushroom cap. *Tectulithus merloti* differs from *T. pileatus* in having a tectum that extends slightly beyond the column perimeter and in having a central opening.

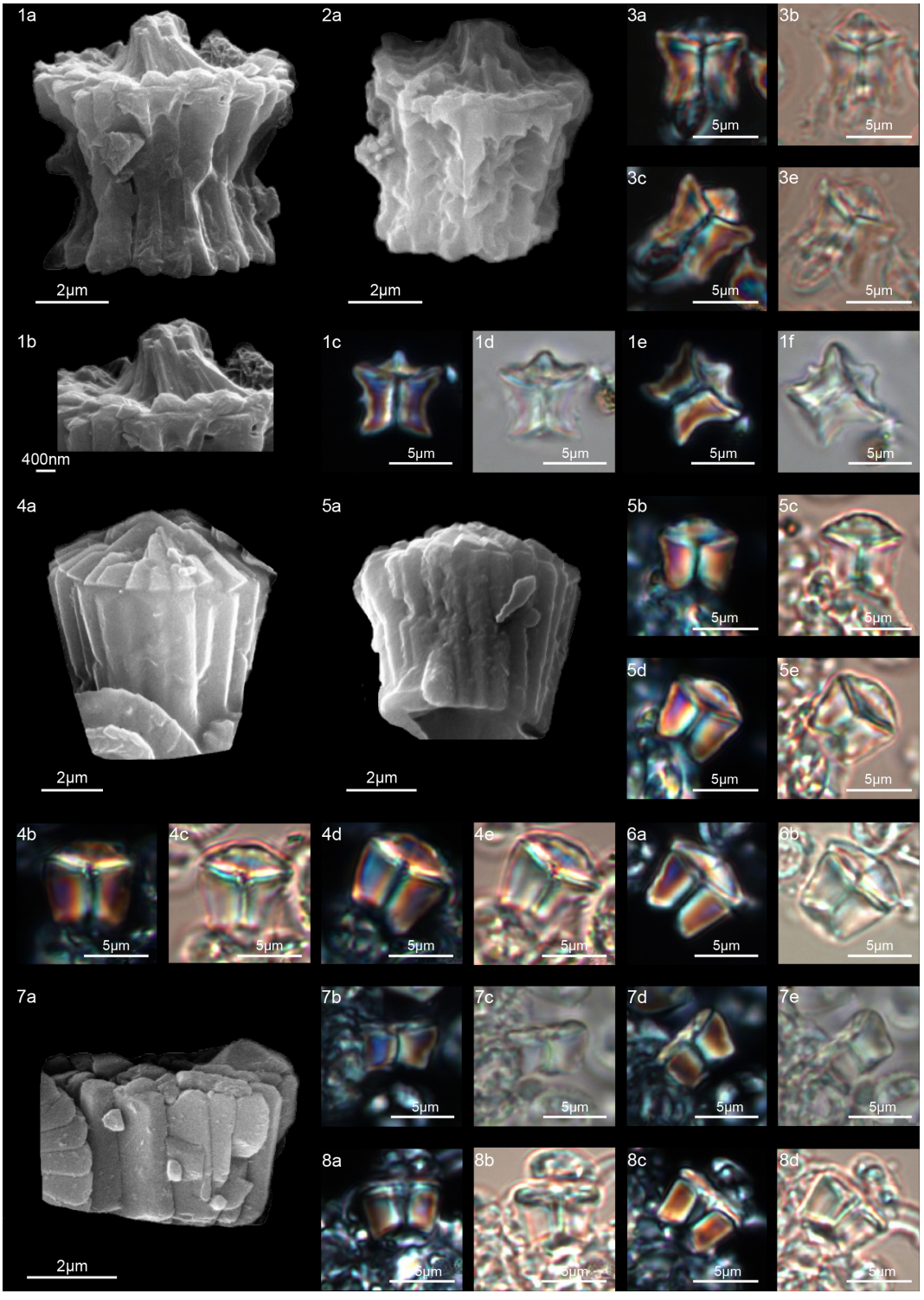

Figure 21. *Tectulithus pagodiformis.* **(1)** Holotype (IGF 104726). Sample: 356Z 23R-1, 70–71. **(1a)** SEM, **(1b)** SEM, detail of tectum; **(1c, e)** XPL, **(1d, f)** PPL. **(2)** Paratype (IGF 104727). Sample: 356Z 23R-1, 70–71. **(2a)** SEM. **(3)** Sample: 356Z 23R-1, 70–71. **(3a, c)** XPL, **(3b, d)** PPL. *Tectulithus pileatus*. **(4)** Sample: 1262C 10-4, 131–132. **(4a)** SEM, **(4b, d)** XPL, **(4c, e)** PPL. **(5)** Sample: 1262C 10-4, 131–132. **(5a)** SEM, **(5b, d)** XPL, **(5c, e)** PPL. **(6)** Sample: 1209B 24-5, 8–9. **(6a)** XPL, **(6b)** PPL. *Tectulithus stegastos*. **(7)** Sample: 1209C 14-1, 56–57. **(7a)** SEM, **(7b, d)** XPL, **(7c, e)** PPL. **(8)** Sample: 1209B 24-5, 8–9. **(8a, c)** XPL, **(8b, d)** PPL. See Table S1 for sample details.

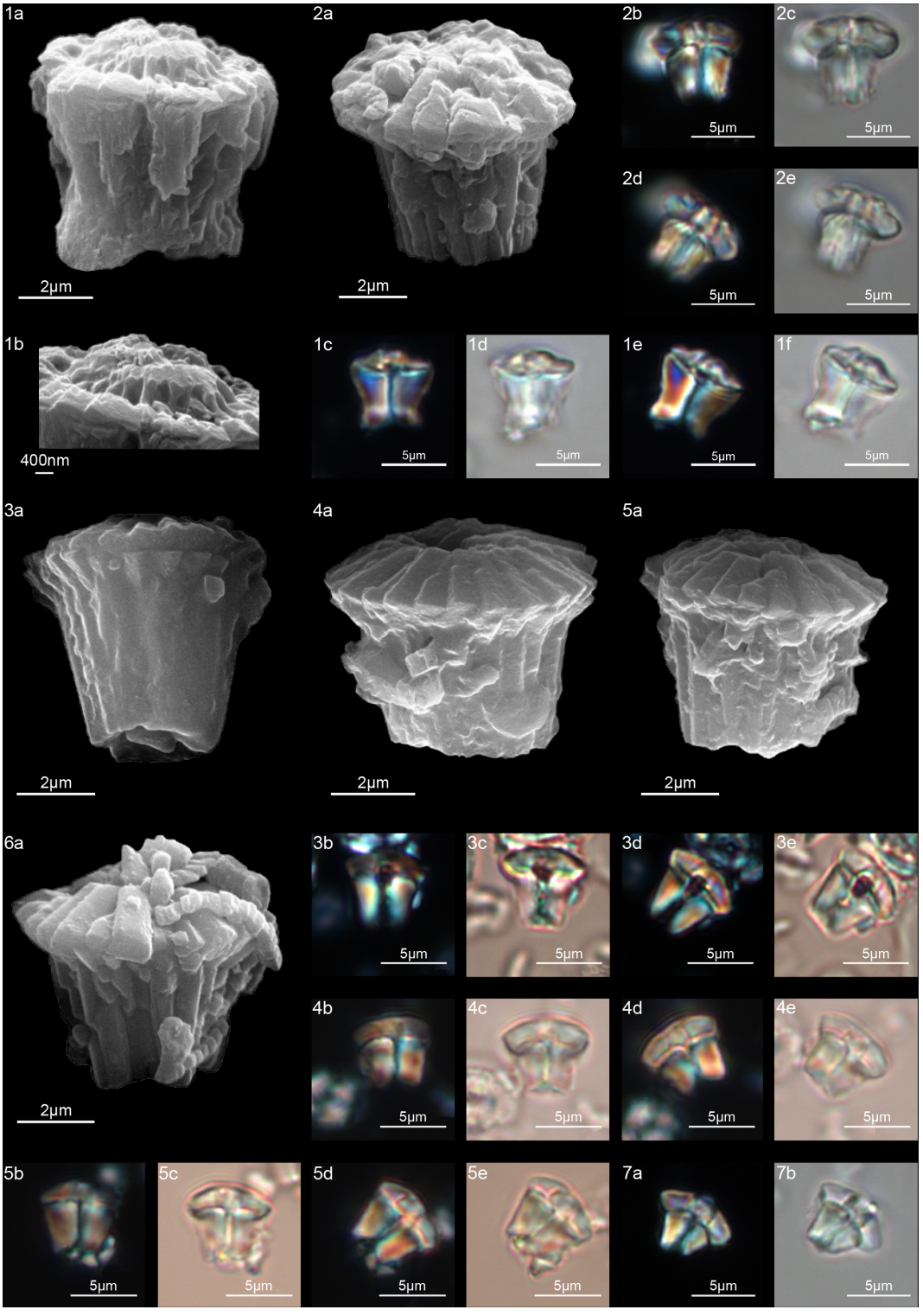

Figure 22. *Tectulithus* cf. *T. pagodiformis*. **(1)** Sample: 356Z 23R-1, 70–71. **(1a)** SEM, **(1b)** SEM, detail of the tectum; **(1c, e)** XPL, **(1d, f)** PPL. *Tectulithus* cf. *T. merloti*. **(2)** Sample: 119 37-4, 120–121. **(2a)** SEM, **(2b, d)** XPL, **(2c, e)** PPL. *Tectulithus merloti*. **(3)** Sample: 1262C 10-4, 131–132. **(3a)** SEM, **(3, d)** XPL, **(3, e)** PPL. **(4)** Sample: 1262C 10-3, 74–75. **(4a)** SEM, **(4b, d)** XPL, **(4c, e)** PPL. **(5)** Sample: 1262C 10-3, 74–75. **(5a)** SEM, **(5b, d)** XPL, **(5c, e)** PPL. **(6)** Sample: 1262C 10-3, 74–75. **(6a)** SEM. **(7)** Sample: 119 37-4, 120–121. **(7a)** SEM, **(7b)** XPL, **(7c)** PPL. See Table S1 for sample details.

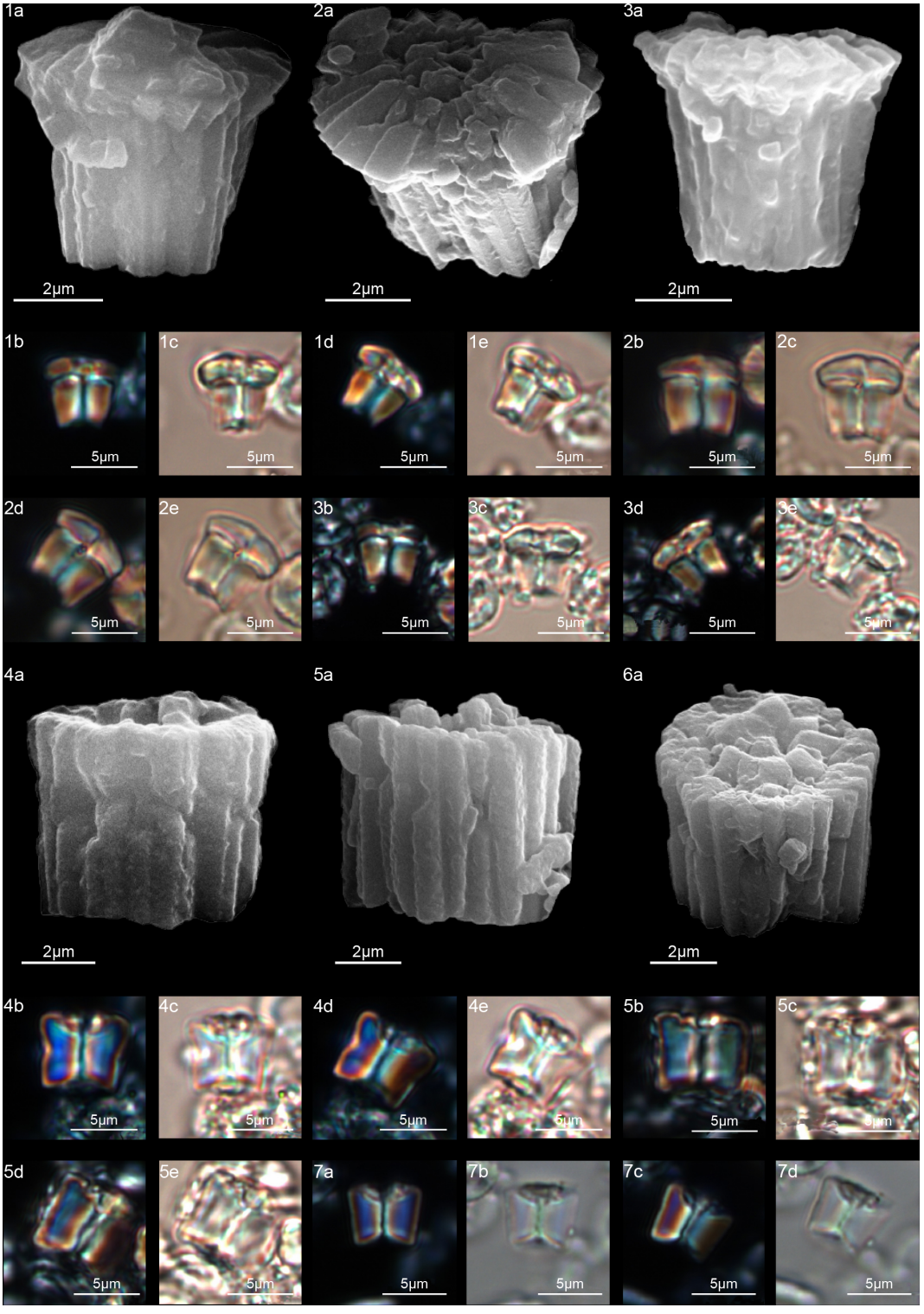

Figure 23. *Tectulithus stonehengei*. **(1)** Sample: 1262C 10-4, 131–132. **(1a)** SEM, **(1b, d)** XPL, **(1c, e)** PPL. **(2)** Sample: 1262C 10-3, 74–75. **(2a)** SEM, **(2b, d)** XPL, **(2c, e)** PPL. **(3)** Sample: 1209B 24-5, 8–9. **(3a)** SEM, **(3b, d)** XPL, **(3c, e)** PPL. *Fasciculithus billii*. **(4)** Sample: 1262C 10-4, 131–132. **(4a)** SEM, **(4b, d)** XPL, **(4c, e)** PPL. **(5)** Sample: 1209B 24-5, 8–9. **(5a)** SEM, **(5b, d)** XPL, **(5c, e)** PPL. **(6)** Sample: 1262C 10-3, 74–75. **(6a)** SEM. **(7)** 1262C 10-4, 131–132. **(7a, c)** XPL, **(7b, d)** PPL. See Table S1 for sample details.

Tectulithus pagodiformis n. sp.

(Fig. 21:1–3)

2010 *Fasciculithus billii* Perch-Nielsen, 1971; Dinarès-Turrel et al.: pl. III, figs. 13, 14.
2011 *Lithoptychius merloti* (Haq and Aubry, 1980) Aubry in Aubry et al., 2011; Aubry et al.: pl. 8, figs. 3a–d.
2011 *Lithoptychius janii* (Perch-Nielsen, 1971) Aubry in Aubry et al., 2011; Aubry et al.: pl. 8, figs. 2a–d.
2019 *Lithoptychius janii* (Perch-Nielsen, 1971) Aubry in Aubry et al., 2011; Metwally: pl. I, fig. 25.

Derivation of name

From pagoda, referring to the general shape of this nannolith.

Diagnosis

Specimens with a "pagoda" shape. The column has a distal concave surface in which a small tectum with a central knob lies inside the periphery of the column (Fig. 21:1, 2).

Holotype

Figure 21:1a–b (SEM) (Fig. 21:1c–f; LM).

Paratype

Figure 21:2.

Repository

Geological and Paleontological Museum, University of Florence. Holotype number: IGF 104726; sample number: IGF 104727-1. Paratype number: IGF 104727; sample number: IGF 104727-1.

Type locality

DSDP Site 356 (Sàn Paulo Plateau, Atlantic Ocean).

Type level

Sample DSDP 356Z-23R-1, 70–71.

Age

Selandian.

Description

This form has a column with a narrow waist, causing its sides to flare distally. The distal part of the column is convex and hosts the tectum, which is composed of curved elements that intertwine to form a central spike or a truncated cone in the middle (Fig. 21:1b). The diameter of the tectum is smaller than the column width and no opening is present. In the LM, an extinction line bisecting the column and tectum is visible.

Dimensions of the holotype

Total height 7 µm; column height 5 µm, proximal width 5.8 µm, distal width 7 µm; tectum height 2 µm, width 6.5 µm.

Occurrence of the holotype

Zone NP5; zone CNP7.

Remarks

Tectulithus pagodiformis differs from *T. janii* in having a more massive column with a concave distal surface and a tectum nestled inside the column and ending in a spike. *T. pagodiformis* differs from *F. vertebratoides* for the less curved outline of the column and the pointed calyptra.

Tectulithus pileatus (Bukry, 1973) n. comb.

(Fig. 21:4–6)

1973 *Fasciculithus pileatus* Bukry: p. 307, pl. 1, figs. 7–9, pl. 2, figs. 2, 3–5 (not fig. 1).
2011 *Lithoptychius pileatus* (Bukry, 1973) Aubry in Aubry et al., 2011; Aubry et al.: p. 273.
2012 *Lithoptychius pileatus* (Bukry, 1973) Aubry in Aubry et al., 2011; Monechi et al.: pl. 5, figs. 1–13.
2019 *Lithoptychius pileatus* (Bukry, 1973) Aubry in Aubry et al., 2011; Metwally: pl. I, fig. 26.

Measured dimensions

Total height 6.6–7 µm; column height 4.2–4.5 µm, proximal width 4.7–5.3 µm, distal width 6.2–7 µm; tectum height 2.4–2.6 µm, width 5.7–6.7 µm.

Biozone occurrence of the studied specimens

Upper zone NP4 to lower zone NP5; zone CNP7.

Emended description

SEM images of *T. pileatus* show specimens of a truncated cone-shaped column surmounted by a conical tectum. The latter is composed of radially arranged elements with anticlockwise imbrication. This species has been assigned to the genus *Tectulithus* on the basis of the presence of a conical cycle (tectum) made up of radial elements (Fig. 21, figs. 4–5). SEM photos show the tectum is restricted to the periphery of the column, as was suggested by Monechi et al. (2012). In the LM, the tectum has a convex lens-shaped cap.

Tectulithus pileatus differs from *T. janii* in having a convex lens-shaped tectum, which does not exceed the perimeter of the column. *Tectulithus merloti* differs from *T. pileatus*

in having a tectum that extends slightly beyond the column perimeter and in having a central opening.

Tectulithus stegastos (Aubry and Bord in Aubry et al., 2011) n. comb.

(Fig. 21:7–8)

2009 *Fasciculithus* sp. 4 Bernaola, et al.: fig. 5, E–H.
2010 *Fasciculithus* sp. Dinarès-Turrel et al.: pl. V, fig. 5.
2011 *Lithoptychius stegastos* Aubry and Bord in Aubry et al., 2011; Aubry et al.: pl. 6, figs. 1a–d, 2a–d, 3a, b, 4a–f, 5a–d.

Measured dimensions

Total height 3.8–4.2 µm; column height 3.3 µm, proximal width 4.7–5.3 µm, distal width 6.2–7 µm; tectum height 2.4–2.6 µm, width 5.7–6.7 µm.

Biozone occurrence of the studied specimens

Middle zone NP4; upper zone CNP5.

Emended description

Form with a column wider than it is tall, consisting of a few thick elements. The column has vertical and slightly flaring sides surmounted by a flat tectum made up of elements with a radial horizontal aspect (Fig. 21:7a). The tectum has the same diameter as or is slightly larger than the column, and it has a central depression that hosts a central canal.

The tectum overlaps the column and is entirely comprised inside the flat or slightly concave distal surface. In XPL, a sharp straight or slightly concave extinction line marks the contact between the column and the tectum.

Remarks

Tectulithus stegastos has been included in *Tectulithus* based on the presence of a thin and flat tectum. *Tectulithus stegastos* differs from *T. pileatus* in having a flat tectum, a shorter column and a wider central canal.

Tectulithus stonehengei (Haq and Aubry, 1980) n. comb.

(Fig. 23:1–3)

1980 *Fasciculithus stonehengei* Haq and Aubry: pl. 1, figs. 11–13.
2008 *Fasciculithus janii* Perch-Nielsen, 1971; Steurbaut and Sztrákos: pl. III, fig. 11.
2011 *Lithoptychius stonehengei* (Haq and Aubry, 1980) Aubry in Aubry et al., 2011; Aubry et al.: p. 273.
2012 *Fasciculithus janii* Perch-Nielsen, 1971; Monechi et al.: pl. 3, figs. 20, 24, 25.
2013 *Fasciculithus janii* Perch-Nielsen, 1971; Monechi et al.: pl. 1, figs. 21, 22.

Measured dimensions

Total height 4.8–6.4 µm; column height 3–4.1 µm, proximal width 3.2–4.5 µm, distal width 4.5–5.6 µm; tectum height 1.6–2.3 µm, width 5.6–6.4 µm.

Biozone occurrence of the studied specimens

Upper zone NP4 to lower zone NP5; zone CNP7.

Emended description

T. stonehengei has a column with a cylindrical outline composed of 16–18 vertical elements. The lower cycle of the tectum is composed of wedge-shaped elements that extend slightly past the perimeter of the column (Fig. 23:1–3). The upper tectum s.s. is formed of flat elements with a clockwise imbrication that form a wide central opening (Fig. 23:2a). No extinction line between the two cycles is visible. In the LM, the shape of the tectum is "rectangular". *Tectulithus stonehengei* differs from *T. merloti* in having a cylindrical column (with vertical sides) and a flatter tectum.

Fasciculithus (Bramlette and Sullivan, 1961) Aubry in Aubry et al., 2011

(Figs. 23–26)

Type species

Fasciculithus involutus, Bramlette and Sullivan, 1961.

Description

Fasciculithus consists of two structural units, the column and the calyptra. The column is the proximal unit, and it consists of wedge-shaped, radially arranged elements. In plain view, the column has a rosette-like outline. The column elements meet along the vertical axis, forming a central canal that goes right through the column (Fig. 24).

In late Paleocene specimens, regular depressions (fenestrae) on the column sides are common and are visible in both LM and SEM (see specimens from Bybell and Self-Trail, 1995, and Bown, 2010). The distal surface of the column is concave and hosts the calyptra, which is narrower than the periphery of the column and variable in shape and height. It consists of elements with a vertical (clockwise imbrication) or tilt disposition.

In the LM, there is no clear extinction line separating the column from the calyptra. A straight thick dark line bisecting the column and calyptra is visible.

Remarks

According to Aubry et al. (2011), *Fasciculithus* differs from *Gomphiolithus* in having two structural units (column and

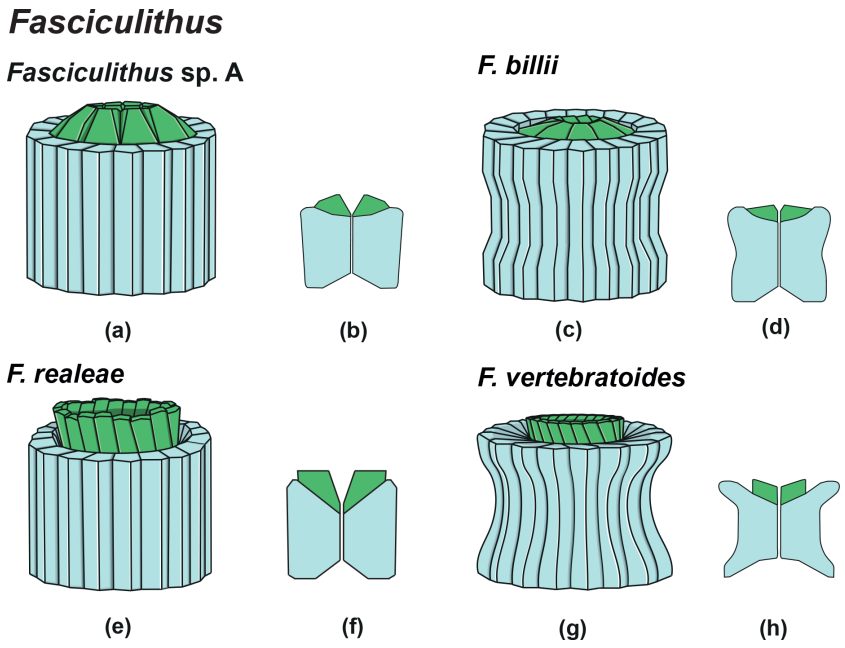

Figure 24. Overview of *Fasciculithus* column (light blue) and calyptra (green). Schematic drawing of the type species *Fasciculithus* sp. A. **(b)** Schematic cross section of *F. involutus*. **(c)** Schematic drawing of *F. billii*. **(d)** Schematic cross section of *F. billii*. **(e)** Schematic drawing of *F. vertebratoides*. **(f)** Schematic cross section of *F. vertebratoides*.

calyptra) and from *Lithoptychius* in the absence of the collaret. *Fasciculithus* differs from *Tectulithus* in having a calyptra composed of vertical or tilted wedge-shaped elements instead of a flat or conical tectum made up of radial elements with a clockwise arrangement.

Fasciculithus billii (Perch-Nielsen, 1971) emend.

(Fig. 23:4–7)

1971 *Fasciculithus billii* Perch-Nielsen: taf. 4, fig. 11; taf. 5, figs. 5–10; taf. 14, figs. 31–33.
2010 *Fasciculithus involutus* Bramlette and Sullivan, 1961; Dinarès-Turrel: pl. 3, fig. 15.
2011 *Lithoptychius billii* (Perch-Nielsen, 1971) Aurby in Aubry et al., 2011; Aubry et al.: p. 272.
2012 *Lithoptychius billii* Perch-Nielsen, 1971; Monechi et al.: pl. 5, figs. 14–25.

Emended diagnosis

Fasciculith shaped as a cotton reel with a small calyptra on the distal surface of the column.

Emended description

Fasciculithus billii consists of a cylindrical column, broadening at each end and surmounted by a small calyptra (Fig. 23:4–7). The distal part of the column is wider than the proximal part. The distal end varies from flat to slightly concave, with a calyptra in the central depression; the proximal end is concave. The calyptra consists of tilted elements, forming a wide central opening, and its height is variable. In side view, LM images show the true outline of the calyptra, which can be (Fig. 23:4b–7a) entirely included inside the column depression (Fig. 23:4a), although sometimes it can exceed the column depression (Fig. 23:5a).

Measured dimensions

Total height 5.1–7 µm; column height 4.2–6, proximal width 4.8–6.2 µm, distal width 5.7–6.9 µm; calyptra height 1.1–1.5 µm, width: 3.1–3.8 µm.

Biozone occurrence of the studied specimens

Upper zone NP4; zone CNP7.

Remarks

Fasciculithus billii was assigned to the genus *Lithoptychius* by Aubry et al. (2012) on the basis of the thickening observed at the distal end of the column of the holotype (Perch-Nielsen, 1971, pl. 5, fig. 8), which they considered a distinct unit (collaret). However, the thickening is present on both the distal and proximal ends of the column on the specimens imaged by Perch-Nielsen (1971). Additionally, our SEM photos show that the thickening cannot be considered a distinct unit (Fig. 23, figs. 4, 5).

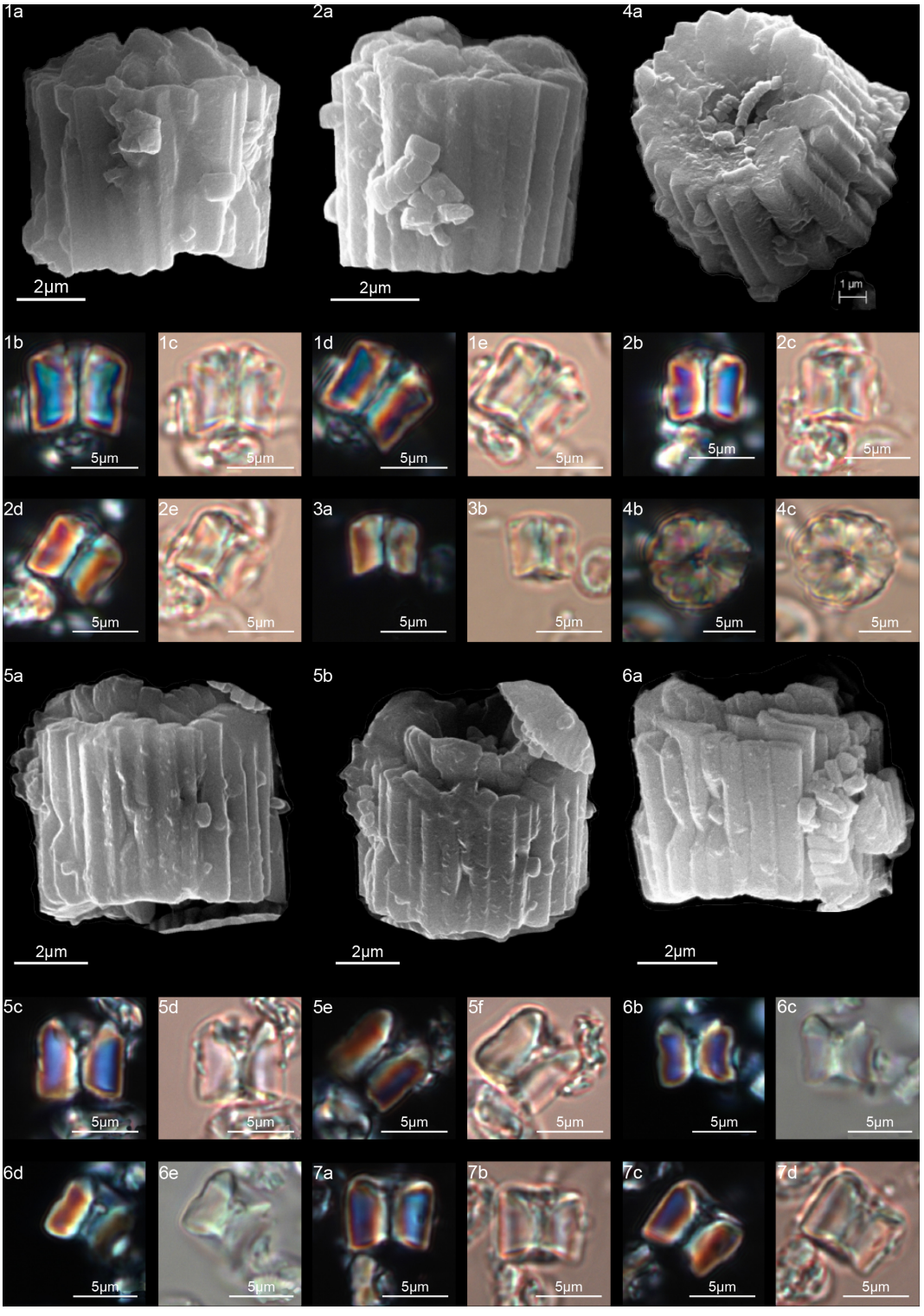

Figure 25. *Fasciculithus* sp. A. **(1)** Sample: 1262C 10-3, 74–75. **(1a)** SEM, **(1b, d)** XPL, **(1c, e)** PPL. **(2)** Sample: 1262C 10-3, 74–75. **(2a)** SEM, **(2b, d)** XPL, **(2c, e)** PPL. **(3)** Sample: 1262C 10-3, 74–75. **(3a)** XPL, **(3b)** PPL. **(4)** Sample: 1262C 10-3, 74–75. **(4a)** SEM, proximal view; **(4b)** XPL, **(4c)** PPL. *Fasciculithus realeae*. **(5)** Holotype (IGF 104728). Sample: 1209C-14-1, 56–67. **(5a, b)** SEM, **(5c, e)** XPL, **(5d, f)** PPL. **(6)** Paratype (IGF 104729). Sample: 1209C-14-1, 56–67. **(6a)** SEM, **(6b, d)** XPL, **(6c, e)** PPL. **(7)** Sample: 1209C-14-1, 56–67. **(7a, c)** XPL, **(7b, d)** PPL. See Table S1 for sample details.

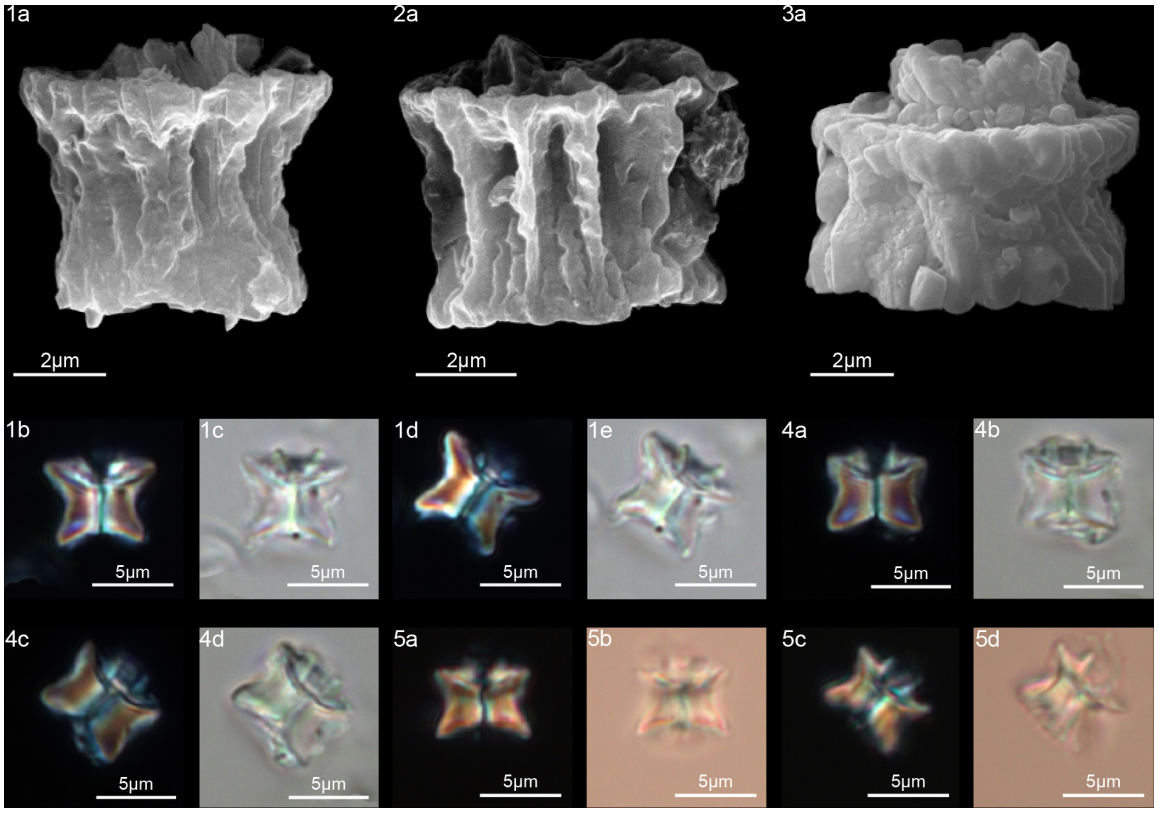

Figure 26. *Fasciculithus vertebratoides*. **(1)** Sample: 356Z 23R-1, 70–71. **(1a)** SEM, **(1b, d)** XPL, **(1c, e)** PPL. **(2)** Sample: 356-23R-1, 70–71. **(2a)** SEM. **(3)** Sample: 1262C 10-6, 23–24. **(3a)** SEM. **(4)** Sample: 119 37-4, 40–41. **(4a, c)** XPL, **(4b, d)** PPL. **(5)** Sample: 356Z 23R-1, 70–71. **(5a, c)** XPL, **(5b, d)** PPL. See Table S1 for sample details.

Fasciculithus realeae n. sp.

(Fig. 25:5–7)

Derivation of name

Named after Viviana Reale (Università degli Studi di Firenze, Italy), nannopaleontologist.

Diagnosis

Fasciculith with a massive column and a short and wide-open calyptra.

Holotype

Figure 25:5a.

Paratype

Figure 25:6a.

Repository

Geological and Paleontological Museum, University of Florence. Holotype inventory number: IGF 104728; sample number: IGF 104729-1. Paratype inventory number: IGF 104729; sample number: IGF 104724-1.

Type locality

ODP Site 1029, Shatsky Rise, western Pacific.

Type level

Sample ODP 1209-14-1, 56–57.

Age

Late Danian.

Description

Fasciculithus realeae has a column with parallel or slightly flaring sides and proximal and distal faces that are both deeply concave. The calyptra is reduced in height, and it is included in the distal depression of the column. Its sides flare in the distal direction, forming a wide opening. In SEM, the calyptra shows a scalloped profile, while in LM it is poorly visible.

An extinction line is not detectable between the calyptra and the column. A well-developed central canal passes through the column and calyptra.

Dimensions of the holotype

Total height: 6.3 µm; column: height: 5 µm; proximal width: 6.8 µm; distal width: 6.8 µm; calyptra: height: 1.3 µm; width: 4.3 µm.

Occurrence of the holotype

NP4 zone; upper CNP5 zone.

Remarks

Fasciculithus realeae differs from *F. billii* in having a calyptra made of vertical instead of tilted elements that exceed the column distal depression. *Fasciculithus realeae* differs from *Fasciculithus* sp. A in having a column with a deeply concave distal side and a flaring calyptra (Fig. 25:5b). In contrast, *Fasciculithus* sp. A in LM appears as distally convex with a distally bifurcated extinction line visible in *Fasciculithus realeae*.

Fasciculithus vertebratoides (Steurbaut and Sztrákos, 2008) emend.

(Fig. 26)

1971 *Fasciculithus janii* Perch-Nielsen, 1971; Perch-Nielsen: pl. 14, figs. 37–39 (not pl. 5, figs. 1–4).
1978 *Fasciculithus janii* Perch-Nielsen; Proto Decima et al.: pl. 12, figs. 1a–c.
1979 *Fasciculithus* cf. *F. billii* Perch-Nielsen, 1979: pl. 49, figs. 27–29.
1979 *Fasciculithus* aff. *F. richardii* – Okada and Thierstein: pl. 6, figs. 4a–b (not figs. 6a–b).
2008 *Fasciculithus vertebratoides* Steurbaut and Sztrákos: pl. III, figs. 1a–b, 3, 4, 5 (not figs. 2a–b), 21.
2010 *Fasciculithus vertebratoides* Steurbaut and Sztrákos, 2008; Dinarès-Turrel et al.: pl. III, figs. 11, 12.
2010 *Fasciculithus billii* Perch-Nielsen, 1971; Dinarès-Turrel et al.: pl. III, figs. 9, 10.
2011 *Lithoptychius vertebratoides* (Steurbaut and Sztrákos, 2008) Aubry in Aubry et al., 2011; Aubry et al.: p. 273.
2012 *Lithoptychius vertebratoides* (Steurbaut and Sztrákos, 2008) Aubry in Aubry et al., 2011; Monechi et al.: pl. 3, figs. 1, 2.
2016 *Fasciculithus vertebratoides* (Steurbaut and Sztrákos) Aubry in Aubry et al., 2011; Bown: pl. 8, figs. 13–16.
2019 *Lithoptychius ulii* (Perch-Nielsen, 1971) Aubry in Aubry et al., 2011; Metwally: pl. I, fig. 23.

Emended diagnosis

Fasciculith shaped like vertebrae in profile and consisting of a column and a calyptra.

Emended description

Fasciculith with a column characterized by longitudinal ridges and curved outline reminiscent of a vertebra, hourglass or egg timer (Steurbaut and Sztrákos, 2008). The elements show a thickening in the upper part of the distal end (Fig. 26). The distal end is deeply concave and surmounted by a calyptra. The calyptra is made up of a set of elements with clockwise imbrication with a scalloped profile. The calyptra has vertical sides and a wide central area. In the LM, an extinction line between the column and the calyptra is clearly visible.

Measured dimensions

Total height 5.3–6.7 µm; column height 4.3–5.2 µm, proximal width 5.4–7.6 µm, distal width 5.8–7.9 µm; calyptra: height 1–2 µm, width: 3–4.6 µm.

Biozone occurrence of the studied specimens

Upper zone NP4; zone CNP7.

Remarks

LM photos of specimens of *F. vertebratoides* at Site 119 (Fig. 26:2b–e) are similar to photos of *F. janii* of Perch-Nielsen (1971). However, *F. vertebratoides* differs from *T. janii* in the absence of a disk-shaped tectum that extends well beyond the column. *Fasciculithus vertebratoides* differs from *F. billii* in having a vertebra outline, a deep and wider distal depression, and a calyptra with vertical sides.

Fasciculithus sp. A Aubry, 2014

(Fig. 25:1–4)

2008 *Fasciculithus* sp. Steurbaut & Sztrákos, p. 26, pl. 2, fig. 22.
2012 *Fasciculithus involutus* Bramlette and Sullivan, 1961; Monechi et al.: pl. 6, figs. 1–16.
2013 *Fasciculithus involutus* Bramlette and Sullivan, 1961; Monechi et al.: pl. 1, fig. 23.
2014 *Fasciculithus* sp. A Aubry, p. 103.
2016 *Fasciculithus involutus* Bramlette and Sullivan, 1961; Bown: pl. 8, figs. 6–12.

Measured dimensions

Total height 4.8–7.1 µm; column height 3.9–5.4 µm, proximal width 4.9–6.7 µm, distal width 5.3–7.2 µm; calyptra height 0.9–1.7 µm, width: 4–5.4 µm.

Biozone occurrence of the studied specimens

In the upper part of zone NP4; zone CNP7.

Remarks

Fasciculithus composed of a column and a knob-shaped calyptra. The column has vertical sides, and it is composed of wedge-shaped elements with a smooth surface. The proximal and the distal sides are somewhat concave. The calyptra is narrower than the column, and it is made up of elements converging to the center, forming a small dome. A narrow central opening occurs (Fig. 25:4). In the LM, we do not observe an extinction line between the column and calyptra; the fasciculith appears as a single structural unit (Fig. 25:1, 2, 3). Thus, *Fasciculithus* sp. A appears as distally convex, giving a more rounded shape to the fasciculith. According to Steurbaut and Sztrákos (2008), *Fasciculithus* sp. A is characterized by a distally bifurcated extinction line visible in side view and in cross-polarized light (Fig. 25:1, 2, 3). In the LM, *Fasciculithus* sp. A differs from *F. billii* in having a column with vertical sides and a convex distal side. *Fasciculithus* sp. A differs from *F. tympaniformis* as this last shows a small knob calyptra resolvable in cross-polarized light as separated by extinction lines from the column. According to Monechi et al. (2012) *F. tympaniformis* is also characterized by an asymmetrical, distally curved extinction line.

Specimens belonging to *Fasciculithus* sp. A were previously attributed to early *F. involutus* (i.e., Monechi et al., 2012; Bown, 2016). The holotype specimen of *F. involutus* of Bramlette and Sullivan (1961) shows a column characterized by fenestrae. The occurrence of fenestrae thus represents a primary feature of *F. involutus*. The SEM photos from this study (Fig. 25:1–3) show that the observed specimens lack longitudinal ridges and fenestrae on the column that typically characterize *F. involutus*, as shown by Perch-Nielsen (taf. 4, figs. 1–10; taf. 7, fig. 5; Perch-Nielsen, 1971). For these reasons, the observed specimens were included in *Fasciculithus* sp. A of Aubry (2014).

Sample availability. Type materials and images for this study are stored at the Geological and Paleontological Museum and the Department of Earth Sciences of the University of Florence, Italy (Table S1 in the Supplement).

Code availability. The code for holotypes, paratypes and samples analyzed in this study is listed in Table 1 in the Supplement.

Data availability. The biostratigraphic information and the morphometric measurements taken for each specimen shown in this study are respectively available in Tables 2, S2 and S3–S7 of the Supplement. Data are also available upon request from the corresponding author.

Supplement. The supplement related to this article is available online at: https://doi.org/10.5194/jm-40-101-2021-supplement.

Author contributions. Data collection and sample analyses have been carried out by FM and CC under the supervision of SM. FM wrote the article and drafted the figures. All authors contributed to the writing and editing of the article.

Competing interests. The authors declare that they have no conflict of interest.

Disclaimer. Publisher's note: Copernicus Publications remains neutral with regard to jurisdictional claims in published maps and institutional affiliations.

Acknowledgements. This research used samples provided by the International Ocean Discovery Program (IODP). We thank Maurizio Ulivi of the M.E.M.A. laboratory for support with the SEM analyses. We would like to warmly thank the editor, Emanuela Mattioli, Jean Self-Trail and an anonymous reviewer for their detailed and constructive comments that considerably helped us to improve the paper. We are grateful to the editor-in-chief, Francesca Sangiorgi, for her kindness, suggestions and support.

Financial support. This research has been supported by the Italian Ministero dell'Università e della Ricerca MIUR (grant nos. 2010X3PP8J_005 and 2007W9B2WE_003 (Simonetta Monechi)).

Review statement. This paper was edited by Emanuela Mattioli and reviewed by Jean M. Self-Trail and one anonymous referee.

References

Agnini, C., Fornaciari, E., Raffi, I., Rio, D., Röhl, U., and Westerhold, T.: High-resolution nannofossil biochronology of middle Paleocene to early Eocene at ODP Site 1262: implications for calcareous nannoplankton evolution, Mar. Micropaleontol., 47, 215–248, https://doi.org/10.1016/j.marmicro.2007.05.003, 2007.

Agnini, C., Fornaciari, E., Raffi, I., Catanzariti, R., Pälike, H., Backman, J., and Rio, D.: Biozonation and biochronology of Paleogene calcareous nannofossils from low and middle latitudes, Newsl. Stratigr., 47, 131–181, https://doi.org/10.1127/0078-0421/2014/0042, 2014.

Angori, E. and Monechi, S.: High-resolution calcareous nannofossil biostratigraphy across the Paleocene/Eocene boundary at Caravaca (southern Spain), Isr. J. Earth Sci., 44, 197–206, 1996.

Angori, E., Bernaola, G., and Monechi, S.: Calcareous nannofossil assemblages and their response to the Paleocene-Eocene Thermal Maximum event at different latitudes: ODP Site 690 and Tethyan sections, Geol. Soc. Am. Spec. Pap., 424, 69–85, https://doi.org/10.1130/2007.2424(04), 2007.

Aubry, M.-P.: Handbook of Cenozoic Calcareous Nannoplankton, Book 3, Ortholithae (Pentaliths and Other), Heliolithae (Fasciculiths, Sphenoliths and Others), American Museum of Natural History Micropaleontology Press, New York, 279 pp., 1989.

Aubry, M.-P.: Handbook of Cenozoic calcareous nannoplankton Book 4, Heliolithae, Micropaleontology Press, Am. Mus. Nat. Hist., New York, 4, 1–381, 1990.

Aubry, M.-P.: Early Paleogene calcareous nannoplankton evolution: A tale of climatic amelioration, in: Late Paleocene-Early Eocene Climatic and Biotic Events in the Marine and Terrestrial Records, edited by: Aubry, M. P., Lucas, S., and Berggren, W. A., Columbia University Press, New York, 158–203, 1998.

Aubry, M.-P.: Cenozoic coccolithophores: Discoasterales (CC-B), in: Atlas of Micropaleontology series, Micropaleontology Press, New York, 431 pp., 2014.

Aubry, M.-P., Bord, D., and Rodriguez, O.: New taxa of the Order Discoasterales Hay 1977, Micropaleontology, 57, 269–287, 2011.

Aubry, M.-P., Rodriguez, O., Bord, D., Godfrey, L., Schmitz, B., and Knox, R. W. O'B.: The first radiation of fasciculiths: morphologic adaptations of the coccolithophores to oligotrophy, Austrian J. Earth Sci., 105, 29–38, 2012.

Bernaola, G., Martin-Rubio, M., and Baceta, J. I.: New high resolution calcareous nannofossil analysis across the D/S transition at the Zumaia section: comparison with South Tethys and Danish sections, Geol. Acta, 7, 79–92, https://doi.org/10.1344/105.000000272, 2009.

Bown, P. R.: Calcareous nannofossils from the Paleocene/Eocene Thermal Maximum interval of southern Tanzania (TDP Site 14), J. Nannoplankton Res., 31, 11–38, 2010.

Bown, P. R.: Paleocene calcareous nannofossils from Tanzania (TDP sites 19, 27 and 38), J. Nannoplankton Res., 36, 1–32, 2016.

Bramlette, M. N. and Sullivan, F. R.: Coccolithophorids and related nannoplankton of the early Tertiary in California, Micropaleontology, 7, 129–188, 1961.

Bukry, D.: Phytoplankton stratigraphy, Deep Sea Drilling Project Leg 20, Western Pacific Ocean, in: Initial Reports of the Deep Sea Drilling Project, Volume 20, edited by: Heezen, B. C., MacGregor, I. D., Foreman, H. P., Forristall, G., Hekel, H., Hesse, R., Hoskins, R. H., Jones, E. J. W., Kaneps, A. G., Krasheninnikov, V. A., Okada, H., Ruef, M. H., U.S. Government Printing Office, Washington, 307–317, https://doi.org/10.2973/dsdp.proc.20.114.1973, 1973.

Burkry, D. and Percival, S. F.: New Tertiary calcareous nannofossils, Tulane Studies in Geology and Paleontology, 8, 123–146, 1971.

Bybell, L. M. and Self-Trail, M.: Evolutionary, biostratigraphic and taxonomic study of calcareous nannofossils from a continuous Paleocene-Eocene boundary section in New Jersey, U.S. Geological Survey Professional Paper, 1554, 36, https://doi.org/10.3133/pp1554, 1995.

Criscione, J., Bord, D., Godfrey, L., and Aubry, M.-P.: Inferred pseudo-cryptic speciation in the coccolithophore species *Braarudosphaera bigelowii* (Gran and Braarud) during the early Paleocene (Danian), Mar. Micropaleontol., 137, 1–15, https://doi.org/10.1016/j.marmicro.2017.09.002, 2017.

Dinarès-Turell, J., Stoykova, K., Baceta, J. I., Ivanov, M., and Pujalte, V.: High-resolution intra- and interbasinal correlation of the Danian–Selandian transition (early Paleocene): the Bjala section (Bulgaria) and the Selandian GSSP at Zumaia (Spain), Palaeogeogr. Palaeocl., 297, 511–533, https://doi.org/10.1016/j.palaeo.2010.09.004, 2010.

Dinarès-Turell, J., Westerhold, T., Pujalte, V., Röhl, U., and Kroon, D.: Astronomical calibration of the Danian stage (Early Paleocene) revisited: Settling chronologies of sedimentary records across the Atlantic and Pacific Oceans, Earth Planet. Sc. Lett., 405, 119–131, https://doi.org/10.1016/j.epsl.2014.08.027, 2014.

Farouk, F. and Faris, M.: Calcareous nannofossil and foraminiferal bio-events of the Danian-Selandian transition of the Quseir area, northwestern Red Sea margin, Egypt, Micropalaeontology, 59, 201–222, 2013.

Fuqua, L. M., Bralower, T. J., Arthur, M. A., and Patzkowsky, M. E.: Evolution of calcareous nannoplankton and the recovery of marine food webs after the Cretaceous–Paleocene mass extinction, Palaios, 23, 185–194, https://doi.org/10.2110/palo.2007.p07-004r, 2008.

Haq, B. U. and Aubry, M.-P.: Early Cenozoic calcareous nannoplankton biostratigraphy and palaeobiogeography of North Africa and the Middle East and trans–Tethyan correlations, in: The geology of Libya, edited by Salem, M. J. and Busrewil, M. T., Academic Press, London, 1, 271–304, 1980.

Hay, W. W.: Calcareous Nannofossils, in: Oceanic Micropaleontology, edited by: Ramsay, A. T. S, Academic Press, London, 1055–1200, 1977.

Hay, W. W., DeConto, R., Wold, C. N., Wilson, K. M., Voigt, S., Schulz, M., Wold-Rossby, A., Dullo, W.-C., Ronov, A. B., Balukhovsky, A. N., and Soeding, E.: Alternative global Cretaceous paleogeog-raphy, in: The Evolution ofCretaceous Ocean/Climate Systems, edited by: Barrera, E. and Johnson, C., Geological Society of America Special Paper, 1–47, https://doi.org/10.1130/0-8137-2332-9.1, 1999.

Kasem, A. M., Wise, S., Faris, M., Farouk, S., and Zaharan, E.: Calcareous nannofossil biostratigraphy of the Paleocene at the Misheiti section, East Central Sinai, Egypt, Arab J. Geosci., 10, 455, https://doi.org/10.1007/s12517-017-3217-4, 2017.

Mahanipour, A., Paravandar, M., and Youssef, M.: Calcareous nannofossil biostratigraphy of the Late Cretaceous-early Paleocene interval in the Zagros basin (southeastern Tethys), Iran Alcheringa An Australasian Journal of Palaeontology, 45, 1–15, https://doi.org/10.1080/03115518.2021.1872702, 2021.

Martini, E.: Standard Tertiary and Quaternary calcareous nannoplankton zonation, in: Proceedings of the II Planktonic Conference Roma, 1970, edited by: Farinacci, A., Edizioni Tecnoscienza, Roma, 2, 739–785, 1971.

Metwally, A. A.: Characterization of the calcareous nannofossil assemblages across the Latest Danian Event (LDE) at Wadi El-Maheer, northern Eastern Desert, Egypt, J. African Earth Sci., 156, 58–67, 2019.

Miniati, F., Monechi, S., and Cappelli, C.: The Late Danian Event at Site 1209: A rapid diversification of calcareous nannofossils, Rendiconti online Soc. Geol. Ital., 31, 149–150, https://doi.org/10.3301/ROL.2014.94, 2014.

Miniati, F., Cappelli, C., and Monechi, S.: New data on the structure of early fasciculithus from a combined LM and SEM study, in: INA15 abstracts, Bohole, Philippines, 7–16 March 2015, 59 pp., 2015.

Monechi, S., Reale, V., Bernaola, G., and Balestra, B.: Taxonomic review of early Paleocene fasciculiths, Micropaleontology, 58, 351–365, 2012.

Monechi, S., Reale, V., Bernaola, G., and Balestra, B.: The Danian/Selandian boundary at Site 1262 (South Atlantic) and in the Tethyan region: Biomagnetostratigraphy, evolutionary trends in fasciculiths and environmental effects of the Latest Danian Event, Mar. Micropaleontol., 98, 28–40, https://doi.org/10.1016/j.marmicro.2012.11.002, 2013.

Moshkovitz, S.: A new method for observing the same nannofossil specimens both by light microscope and scanning electron microscope and preservation of types, Isr. J. Earth Sci., 23, 145–147, 1974.

Okada, H. and Bukry, D.: Supplementary modification and introduction of code numbers to the low-latitude coccolith biostratigraphic zonation (Bukry, 1973; 1975), Marine Micropaleontol., 5, 321–325, https://doi.org/10.1016/0377-8398(80)90016-X, 1980.

Okada, H. and Thierstein, H. R.: Calcareous nannoplankton Leg 43 Deep Sea Drilling Project, in: Initial Reports of the Deep Sea Drilling Project, edited by: Tucholke, B. E., Vogt, P. R., Murdmaa, I. O., Rothe, P., Houghton, R. L., Galehouse, J., Kaneps, A., McNulty Jr., C. L., Okanda, H., Kendrick, J. W., Demars, K. R., and McCave, I. N., U.S. Government Printing Office Washington, 43, 507–543, https://doi.org/10.2973/dsdp.proc.43.117.1979, 1979.

Pavšic, J.: Nannoplankton from the Upper Cretaceous and Paleocene beds in the Gorica region, Geologicky Razprovy Porocila, 20, 33–57, 1977.

Perch-Nielsen, K.: Einige neue Coccolithen aus dem Paleozän der Bucht von Biskaya, B. Geol. Soc. Denmark, 2, 347–361, 1971.

Perch-Nielsen, K.: Albian to Pleistocene calcareous nannofossils from the western South Atlantic, DSDP Leg 39, in: Initial Reports of the Deep Sea Drilling Project, edited by: Supko, P. R., Perch-Nielsen, K., Neprochnov, Y. P., Zimmerman, H. B., McCoy F., Kumar, N., Thiede J., Bonatti, E., Fodor, R., Boersma, A., Dinkelman, M. G., and Carlson, R. L., U.S. Government Printing Office, Washington, 39, 699–823, https://doi.org/10.2973/dsdp.proc.39.131.1977, 1977.

Perch-Nielsen, K.: Calcareous nannofossils at the Cretaceous/Tertiary boundary in Tunisia, in: Cretaceous/Tertiary Boundary Event Symposium, edited by: Christensen, W. K. and Birkelund, T., 2, 238–243, University of Copenhagen, Copenhagen, Denmark, 1979.

Perch-Nielsen, K.: Les coccolithes du Paléocène près El Kef, Tunisie, et leurs ancêtres. Cahiers de Micropaléontologie, 3, 7–23, 1981.

Perch-Nielsen, K.: Cenozoic calcareous nannofossils, in: Plankton Stratigraphy, edited by: Bolli, H. M., Saunders, J. B., and Perch-Nielsen, K., Cambridge University Press, Cambridge, 427–554, 1985.

Prins, B.: Speculations on relations, evolution, and stratigraphic distribution of discoasters, in: Proceedings of the II Planktonic Conference, Roma, 1970, edited by: Farinacci, A., Edizioni Tecnoscienza, Roma, 2, 1017–1037, 1971.

Proto Decima, F., Medizza, F., and Todesco, L.: Southeastern Atlantic Leg 40 calcareous nannofossils, in: Initial Reports of the Deep Sea Drilling Project, edited by: Bolli, H. M., Ryan, W. B. F., McKnight, B. K., Kagami, H., Melguen, M., Siesser, W. G., Natland, J. H., Longoria, J. F., Proto Decima, F., Foresman, J. B., and Hottman, W. E., U.S. Government Printing Office, Washington, 40, 571–634, https://doi.org/10.2973/dsdp.proc.40.112.1978, 1978.

Romein, A. J. T.: Lineages in early Paleogene calcareous nannoplankton, Utrecht Micropaleontological Bulletins, 22, Utrecht University, Utrecht, Netherlands, 1–230, 1979.

Schindelin, J., Arganda-Carreras, I., Frise, E., Kaynig, V., Longair, M., Pietzsch, T., Preibisch, S., Rueden,C., Saalfeld, S., Schmid, B., Tinevez, J.-Y., White, D. J., Hartenstein, V., Eliceiri, K., Tomancak, P., and Cardona, A.: an open-source platform for biological-image analysis, Nat. Methods, 9, 676–682, https://doi.org/10.1038/nmeth.2019, 2012.

Schmitz, B., Pujalte, V., Molina, E., Monechi, S., Orue-Etxebarria, X., Speijer, R. P., Alegret, L., Apellaniz, E., Arenillas, I., Aubry, M. P., Baceta, J. I., Berggren, W. A., Bernaola, G., Caballero, F., Clemmensen, A., Dinarès-Turell, J., Dupuis, C., Heilman-Clausen, C., Hilario Orus, A., Knox, R., Martin-Rubio, M., Ortiz, S., Payros, A., Petrizzo, M. R., Von Salis, K., Sprong, J., Steurbaut, E., and Thomsen, E.: The global stratotype sections and points for the bases of the Selandian (middle Paleocene) and Thanetian (upper Paleocene) stages at Zumaia, Spain, Episodes, 34, 220–243, 2011.

Steurbaut, E. and Sztrákos, K.: Danian/Selandian boundary criteria and North Sea Basin-Tethys correlations based on calcareous nannofossil and foraminiferal trends in SW France, Mar. Micropaleontol., 67, 1–29, https://doi.org/10.1016/j.marmicro.2007.08.004,2008.

Varol, O.: Palaeocene calcareous nannofossil biostratigraphy, in: Nannofossils and their applications, edited by: Crux, J. A., Van Heck, S. E., British Micropalaeontological Society Series, Ellis Horwood Limited, Chichester, 267–310, 1989.

Westerhold, T., Röhl, U., Raffi, I., Fornaciari, E., Monechi, S., Reale, V., Bowles, J., and Evans, H. F.: Astronomical calibration of the Paleocene Time, Palaeogeogr. Palaeocl., 257, 377–403, https://doi.org/10.1016/j.palaeo.2007.09.016, 2008.

Westerhold, T., Röhl, U., Donner, B., McCarren, H. K., and Zachos, J.: A complete high-resolution Paleocene benthic stable isotope record for the central Pacific (ODP Site 1209), Paleoceanography, 26, PA2216, https://doi.org/10.1029/2010PA002092, 2011.

Young, J. R., Bergen, J. A., Bown, P. R., Burnett, J. A., Fiorentino, A., Jordan, R. W., Kleijne, A., van Niel, B. E., Romein, A. J. T., and Von Salis, K.: Guidelines for coccolith and calcareous nannofossil terminology, Palaeontology, 40, 875–912, 1997.

Youssef, M.: High resolution calcareous nannofossil biostratigraphy and paleo-ecology across the Latest Danian Event (LDE) in central Eastern Desert, Egypt, Mar. Micropaleontol., 72, 111–128, https://doi.org/10.1016/j.marmicro.2009.03.007, 2009.